1. Report No.	2. Government Accession No.	3. Recipient's Catalog No.
SWUTC/12/476660-00025-1		

4. Title and Subtitle	5. Report Date
LABORATORY EVALUATION OF FRICTION LOSS AND COMPACTABILITY OF ASPHALT MIXTURES	April 2012
	6. Performing Organization Code
7. Author(s)	8. Performing Organization Report No.
Emad Kassem, Eyad Masad, Ahmed Awed, and Dallas Little	Report 476660-00025-1
9. Performing Organization Name and Address	10. Work Unit No. (TRAIS)
Texas Transportation Institute The Texas A&M University System College Station, Texas 77843-3135	11. Contract or Grant No. DTRT07-G-0006
12. Sponsoring Agency Name and Address	13. Type of Report and Period Covered
Southwest Region University Transportation Center Texas Transportation Institute Texas A&M University System College Station, Texas 77843-3135	Technical Report: September 2010–December 2011
	14. Sponsoring Agency Code

15. Supplementary Notes

Supported by a grant from the U.S. Department of Transportation, University Transportation Centers Program

16. Abstract

This study aimed to develop prediction models for friction loss and laboratory compaction of asphalt mixtures. In addition, the study evaluated the effect of compaction level and compaction method of skid resistance and the internal structure of asphalt mixtures. The predictive model for friction loss was developed based on parameters that describe aggregate texture and angularity before and after polishing, aggregate gradation, and polishing cycles in the laboratory. Squared-shape slabs of asphalt mixtures were prepared in the laboratory using a linear kneading compactor and polished using a wheel-polishing device. The frictional characteristics were measured after different intervals of polishing cycles. Mixtures with coarser aggregate gradation were found to have better skid resistance than those with fine aggregate gradation. The friction loss model was found to correlate very well with the experimental measurements.

The predictive model for laboratory compaction of asphalt mixtures was developed based on parameters that describe aggregate shape characteristics, aggregate gradation, binder content, and binder properties at compaction temperatures. The researchers executed intensive laboratory experiments to quantify the effect of these parameters on the compaction of asphalt mixture in the laboratory. Two models that describe slope and intercept of the laboratory compaction curves of asphalt mixtures were developed. These models showed strong correlations between the predicted values and the measured ones. These models provide essential inputs to quantify the compaction effort needed to compact asphalt mixtures.

In the last phase of this study, the researchers evaluated the effect of compaction level and compaction method on skid resistance and internal structure of asphalt pavements. The vibratory roller was found to yield a smoother surface than the static roller. In addition, the results confirmed that the vibratory roller was more effective in reducing the air voids than the static roller. Moreover, the test sections compacted using the vibratory roller had more uniform air void distribution compared to the test sections compacted using the static roller.

17. Key Words	18. Distribution Statement
Asphalt Mixtures, Skid, Friction, Compaction, Texture, Angularity, Micro-Deval, AIMS, Abrasion, Polishing, X-Ray CT	No restrictions. This document is available to the public through NTIS: National Technical Information Service Alexandria, Virginia 22312

19. Security Classif. (of this report)	20. Security Classif. (of this page)	21. No. of Pages	22. Price
Unclassified	Unclassified	97	

LABORATORY EVALUATION OF FRICTION LOSS AND COMPACTABILITY OF ASPHALT MIXTURES

by

Emad Kassem
Associate Research Scientist

Eyad Masad
Research Engineer

Ahmed Awed
Graduate Research Assistant

and

Dallas Little
Senior Research Fellow

Research Report SWUTC/12/476660-00025-1

Southwest Region University Transportation Center
Texas Transportation Institute
The Texas A&M University System
College Station, Texas 77843-3135

April 2012

DISCLAIMER

The contents of this report reflect the views of the authors, who are responsible for the facts and the accuracy of the information presented herein. This document is disseminated under the sponsorship of the Department of Transportation, University Transportation Centers Program in the interest of information exchange. The U.S. Government assumes no liability for the contents or use thereof. This report is not intended for construction, bidding, or permits purposes.

ACKNOWLEDGMENTS

The authors recognize that support was provided by a grant from the U.S. Department of Transportation, University Transportation Centers Program to the Southwest Region University Transportation Center. The authors would also like to thank Dr. Magdy Mikhail from the Texas Department of Transportation for serving as a project monitor for this study.

EXECUTIVE SUMMARY

This study aimed to develop prediction models for friction loss and laboratory compaction of asphalt mixtures. In addition, the study evaluated the effect of compaction level and compaction method of skid resistance and the internal structure of asphalt mixtures. A predictive model for friction loss of asphalt mixtures was developed based on inputs that described aggregate texture and angularity before and after polishing, aggregate gradation, and polishing cycles in the laboratory. The researchers found that asphalt mixtures with coarser aggregate gradation had better skid resistance than those with finer aggregate gradation. Moreover, aggregates with good resistance to abrasion and polishing had better skid resistance compared to aggregates with poor resistance to abrasion and polishing. The predictive model was found to correlate very well with the experimental measurements in the laboratory.

A predictive model for laboratory compaction of asphalt mixtures was developed based on parameters that described aggregate shape characteristics, aggregate gradation, binder content, and binder properties at compaction temperatures. The researchers executed intensive laboratory experiments to quantify the effect of these parameters on the compaction of asphalt mixtures in the laboratory. Two models that described slope and intercept of the laboratory compaction curves of asphalt mixtures were developed. The developed models showed strong correlations between the predicted values and the measured ones. These methods provide essential inputs to quantify the effort needed to compact asphalt mixtures.

Finally, the researchers evaluated the effect of compaction level and compaction method on skid resistance of asphalt pavements. In addition, they utilized the X-ray Computed Tomography to study the influence of compaction method and level of compaction on the internal structure of asphalt mixtures. The researchers found that the international friction index decreased with the number of passes for all the test sections, with a steeper change for the test sections compacted using the vibratory roller. The vibratory roller was found to yield a smoother surface than the static roller. In addition, the vibratory roller was more effective in reducing the air voids with the number of passes compared to the static roller. Moreover, the test sections compacted using the vibratory roller had more uniform air void distribution compared to test sections compacted using the static roller.

TABLE OF CONTENTS

LIST OF FIGURES

Page

LIST OF TABLES

Page

CHAPTER 1: INTRODUCTION

OVERVIEW

A safe, reliable and efficient road system is essential for public safety and is necessary to support the U.S. economy. Approximately 94 percent of the paved roads in the United States are surfaced with asphalt. Every year, the American Society of Civil Engineers (ASCE) publishes a report card on U.S. infrastructure. According to the 2009 report, 14,000 U.S. citizens out of 41,059 were killed in motor vehicle crashes due to the poor road and highway conditions. In addition, more than 2,491,000 people were injured in vehicle crashes. Several nationwide studies have demonstrated that 15 to 18 percent of the traffic crashes occur on wet pavements (Smith 976; Davis et al. 2002; FHWA 1990). The pavement friction is one of the primary factors that affect the performance of the asphalt pavements in wet conditions. In addition, poor compaction of asphalt pavements has been associated with premature permanent deformation rutting, excessive aging, and moisture damage.

OBJECTIVES

The objectives of this study were as follows:

1. Study the change in the frictional characteristics (texture and angularity) of the aggregates due to abrasion.
2. Employ methods to characterize pavement frictional properties.
3. Develop a predictive analytical model for skid loss of asphalt pavements using the frictional characteristics and gradation of aggregates.
4. Develop a predictive statistical model for compaction of asphalt mixtures using the Superpave gyratory compactor using the frictional characteristics and gradation of aggregates, binder properties, and mix volumetric properties.
5. Study the effect of field compaction method and level of compaction on skid resistance of asphalt pavement.
6. Evaluate the effect of asphalt mixture type (coarse vs. fine and hot mix asphalt [HMA] vs. warm mix asphalt [WMA]) on skid resistance of asphalt pavement.
7. Study the effect of compaction method and level of compaction on the internal structure of asphalt mixtures.

WORK PLAN

This study consisted of three phases and eight tasks. In the first phase of this study, the researchers evaluated the fundamental properties of the asphalt mixture constituents. The shape characteristics of aggregates (texture, angularity) were measured using the Aggregate Imaging Measurement System (AIMS) and Micro-Deval test. The viscosity of the binders at the compaction temperatures was determined using a rotational viscometer. In the second phase, extensive skid resistance laboratory experiments were conducted on slabs of asphalt mixtures. In addition, laboratory specimens were prepared and the compaction curves were obtained for these specimens. In the third phase of this study, the researchers developed predictive models for skid resistance and compactability based on the properties measured in the first phase and the collected experimental data in the second phase. Following are detailed descriptions of each phase.

Phase I

Phase I had three tasks, as follows:

- Task 1: Literature Search—The researchers conducted a literature search to collect relevant information and review publications on the subject with a focus on methods for measuring pavement surface friction in the laboratory, measuring aggregate characteristics (texture, angularity), and measuring aggregate resistance to polishing, as well as previous efforts for developing models for friction loss and compaction of asphalt mixtures.
- Task 2: Selection and Acquiring Test Materials—The researchers identified three aggregates that have different shape characteristics (different texture and angularity). This selection was based on a database that the researchers developed in the past. Two asphalt binders with different rheological properties were evaluated: modified PG 76-22 binder and unmodified PG 67-22 binder.
- Task 3: Measurements of Aggregate and Asphalt Binder Properties—The shape characteristics of aggregates were measured using the AIMS test before and after polishing in the Micro-Deval apparatus. The purpose of conducting these tests was to determine the microtexture of the aggregates and evaluate its resistance to abrasion and polishing. In addition, the viscosity of the binders at the compaction temperatures was measured using the Brookfield Rotational Viscometer. The purpose of this test

was to determine the effect of the viscosity of the binder at the compaction temperature on the workability of the asphalt mixtures during the laboratory compaction.

Phase II

Phase II had three tasks, as follows:

- Task 4: Preparation of Asphalt Mixture Slabs—The kneading compactor was used to compact square-shaped asphalt mixture slabs (20 inches by 20 inches) with 2 inches height. These slabs were prepared using aggregates with different shape characteristics and aggregate gradations. The researchers used three different types of aggregates (limestone 1, limestone 2, and sandstone), and four different aggregate gradations (Texas Department of Transportation [TxDOT] Type F, TxDOT Type C, stone mix asphalt [SMA], and permeable friction course [PFC]). In addition, the researchers studied the frictional characteristics of some field test sections that were recently constructed to examine the effect of compaction method and level of compaction on skid resistance of asphalt pavements. These test sections were constructed at the Riverside Campus of Texas A&M University as part of another study funded by the Texas Department of Transportation.
- Task 5: Preparation of Asphalt Mixture Specimens—The Superpave gyratory compactor (SGC) was used to prepare cylindrical laboratory specimens with a height of 2.5 inches and a diameter of 6 inches. The mixtures that were prepared in Task 4 were also used to produce the test specimens in Task 5. The purpose of this task was to evaluate the effect of mixture design, aggregate characteristics, binder content, and binder properties on the compactability represented in the compaction curves from the SGC.
- Task 6: Polishing Test Slabs and Measuring Surface Frictional Properties—The laboratory asphalt mixture slabs were polished using a wheel-polishing device that was recently acquired by the Texas Transportation Institute. The wheel-polishing device was used to simulate the polishing at the surface under traffic. The dynamic friction tester (DFT) and circular texture meter (CTMeter) were utilized to study the frictional characteristics of the test slabs at different polishing stages. The DFT was

used to measure coefficient of friction on the surface, while the CTMeter was employed for measuring the mean profile depth of the surface.

Phase III

Phase III consisted of two tasks, as follows:

- Task 7: Development of Predictive Models for Friction Loss and Compactability—Predictive models for surface friction loss and laboratory compaction of asphalt mixtures were developed using the generated experimental data in Phases I and II. These data included frictional characteristics, aggregate characteristics, binder properties, and mixture design. The predictive friction model can be used to select the proper combination of aggregate source and mixture design to produce asphalt pavements with adequate skid resistance.
- Task 8: Document the Findings—The researchers documented the findings of this study in this final report. The final report gives a complete description of the problem, research approach, experimental methods, results, and conclusions.

REPORT ORGANIZATION

This report has five chapters. Chapter 1 presents a brief background and the work plan. Chapter 2 discusses the preparation of asphalt mixture slabs, the polishing procedure, and the development of the friction loss model. Chapter 3 documents the development of a predictive model for laboratory compaction of asphalt mixtures. Chapter 4 presents the effort by the authors to evaluate the influence of the compaction method, level of compaction, and mixture type of skid resistance of asphalt mixture. A summary of the findings of this study and conclusions are presented in Chapter 5.

CHAPTER 2: DEVELOPMENT OF A PREDICTIVE MODEL FOR SKID LOSS OF ASPHALT PAVEMENTS

OVERVIEW

Skid resistance is a key factor that affects the performance of asphalt pavements. Nationwide studies have demonstrated that 15 to 18 percent of traffic crashes occur on wet pavements. In wet conditions, the water acts as a lubricant between the pavement surface and the tires and hence reduces friction. The skid resistance of roads is related to microtexture and macrotexture of the pavement surface (Dahir 1979). The macrotexture of the pavement surface is related to mixture design, aggregate gradation, and compaction level, while the microtexture is related to the texture and shape characteristics of aggregates (Kandhal and Parker 1998; Crouch et al. 1995). This part of the study focused on the development of a predictive model for friction loss of asphalt pavements using frictional characteristics and gradation of utilized aggregates.

OBJECTIVES

This part of the study had the following objectives:

1. Study the change in the frictional characteristics (texture and angularity) of the aggregates due to abrasion.
2. Employ methods to characterize pavement frictional properties.
3. Develop a predictive analytical model for skid loss of asphalt pavements using the frictional characteristics and gradation of the aggregates.

RESEARCH TASKS

The researchers carried out the following tasks in order to achieve the above objectives:

1. Identify a number of aggregates with different frictional characteristics in terms of texture and angularity to study the influence of microtexture on skid resistance.
2. Develop mixture designs using different aggregate gradations in order to study the effect of the macrotexture of skid resistance.
3. Prepare square-shaped laboratory asphalt mixture slabs (20 inches by 20 inches) using a linear kneading compactor.
4. Polish the test slabs using a wheel-polishing device.

5. Measure the surface frictional properties of the test slabs. The CTMeter was used to measure the mean profile depth (MPD), while the DFT was used to measure the coefficient of friction at different speeds.
6. Use the AIMS to study the frictional characteristics (texture and angularity) of the aggregates before and after the Micro-Deval abrasion test.
7. Develop a predictive model for friction loss using the frictional characteristics of aggregates.

BACKGROUND

Pavement Surface Characterization

The safety of a pavement surface is affected by surface texture and friction (Mahone 1975). In wet conditions, the water acts as a lubricant between the pavement surface and the tires, and that reduces friction. The skid resistance of roads is related to microtexture and macrotexture of the pavement surface (Dahir 1979). The macrotexture of the pavement surface is related to mixture design, aggregate gradation, and compaction level, while the microtexture is related to the texture and shape characteristics of aggregates (Crouch 1995; Kandhal and Parker 1998).

Pavement texture is a road surface property that describes the interaction between the road surface and vehicles tires. Pavement texture is classified into four different categories based on element wavelength. Table 2-1 shows the classification of the pavement texture (Henry 2000).

Table 2-1. Classification of Pavement Texture (Henry 2000)

Texture Classification	Relative Wavelengths
Microtexture	$\lambda < 0.5$ mm
Macrotexture	0.5 mm $< \lambda <$ 50 mm
Megatexture	50 mm $< \lambda <$ 500 mm
Roughness/Smoothness	500 mm $< \lambda <$ 50 m

Microtexture and macrotexture greatly influence the skid resistance on road surfaces. Figure 2-1 illustrates the difference between microtexture and macrotexture (Henry 2000). Macrotexture of the pavement provides good drainage of water from the pavement surface; however, it contributes to the hysteresis component of the pavement friction. Microtexture of the pavement provides the direct contact between the tires and road surface and contributes to the adhesion part of the pavement friction. Pavement with a rough texture provides better skid resistance; however, it may increase noise, vibration, and tire wear (Ivey et al. 1992).

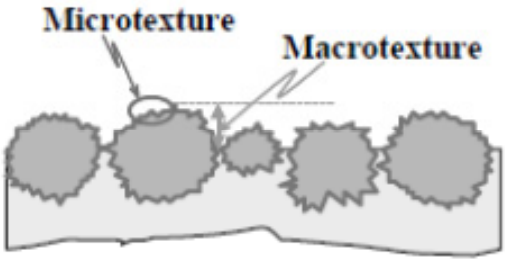

Figure 2-3. Microtexture and Macrotexture (Henry 2000)

The asphalt mixture consists of different aggregate sizes. The large aggregate sizes contribute to the macrotexture of the pavement surface. The pavement macrotexture can be measured using the CTMeter. The CTMeter (Figure 2-2a) consists of a mounted arm that ends with a laser sensor. This arm rotates in a circle with a 284 mm diameter. The laser sensor collects 1024 data samples in one round, which get divided into eight equal segments. These data are used to calculate the MPD of the pavement. The MPD for each segment is calculated based on the peak profile level in each segment and the average profile level for the entire circumference. Then, the calculated MPD of the eight segments is averaged and presented as the MPD of the pavement surface (American Society for Testing and Materials [ASTM] 2009a).

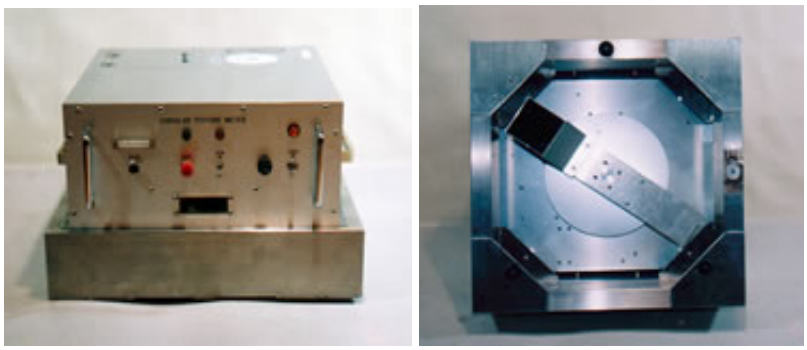

(a) CTMeter

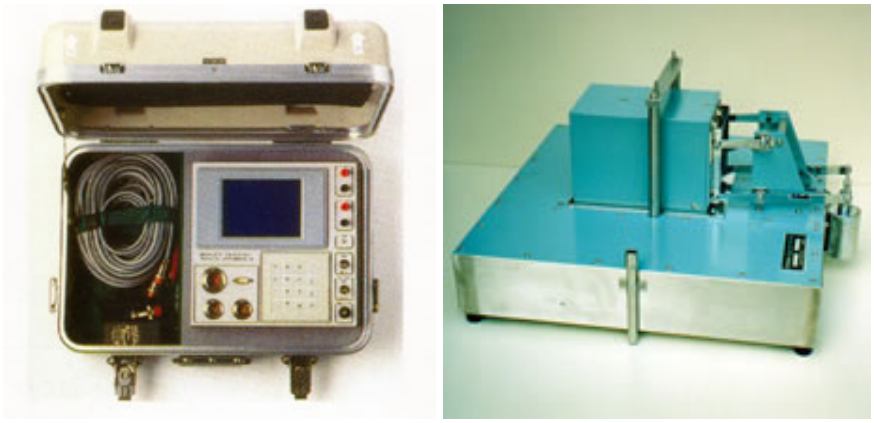

(b) DFT

Figure 2-4. Pictures of CTMeter and DFT

The microtexture of the pavement is the surface roughness at the microscopic level. The microtexture is not measured directly in the field; nevertheless, it can be estimated using the friction measurement at low speeds by the DFT. The mechanism of the DFT is based on calculating the coefficient of friction at different speeds in wet conditions. The coefficient of friction is measured based on the friction between the wetted surface of the pavement and three rubber pads attached to a circular disk. This disk rotates freely while suspended over the pavement until it reaches 100 km/hr. Then, it is lowered to make contact with the pavement surface while it is wet. The rotational speed of the circular disk is decreased until it stops completely because of the induced frictional forces in the rubber pads. The coefficient of friction at 20 km/hr is considered an indication of the pavement microtexture (ASTM 2009b).

Aggregate Characteristics

Aggregate gradation and shape are major characteristics in influencing the nature of asphalt mixtures. The ability of the aggregates to resist the polishing action by traffic is the most significant aggregate characteristic to skid resistance of pavement surfaces. This is greatly confined to the angularity and wear resistance of coarse aggregates. The use of hard, polish-resistant, and irregularly shaped coarse aggregate maintains a good level of skid resistance (Bloem 1971). Hogervorst (1974) explained that skid resistance changes with vehicle speed, and it depends on both microtexture and macrotexture (Figure 2-3). The results of this study showed that the skid resistance decreased with an increase in vehicle speed, and pavements with a coarse and rough surface provided better skid resistance compared to the ones with a fine and polished surface.

Aggregates are different in their mineralogy and get polished at a different rate with the traffic (McDaniel and Coree 2003). There are several methods for measuring the aggregate polishing resistance; however, the results from these methods are influenced by other factors that are not related to their frictional properties. A new technique for measuring the aggregate polishing resistance was developed at Texas A&M University (Masad et al. 2006; Mahmoud and Masad 2007). This method consists of measuring the aggregate texture using AIMS before and after abrasion in the Micro-Deval apparatus. This method was found to be very useful in studying the resistance of aggregates to the skid when they are used in pavements (Masad et al. 2009). Masad et al. (2009) conducted a study to evaluate the effect of aggregate properties and mixture design on the skid resistance of asphalt pavement. The results demonstrated that the aggregate texture and mixture design were found to be the most influential factors on skid resistance.

EXPERIMENTAL DESIGN

The researchers conducted a full factorial experiment that included three types of aggregates and four different asphalt mixture designs. The aggregates included limestone 1 (soft aggregate), limestone 2 (intermediate aggregate), and sandstone (hard aggregate). These aggregates were acquired from different locations in Texas. The asphalt mixture designs included a fine dense-graded mixture (Type F), coarse dense-graded mixture (Type C), SMA mixture, and PFC asphalt mixture (TxDOT 2004). An unmodified binder (PG 67-22) was utilized in this experiment. A total of 12 asphalt mixtures and 24 test slabs were evaluated. Two

square-shaped slabs from each mixture were prepared and tested. Figure 2-4 shows the experimental design. Table 2-2 presents the mix design and aggregate gradation for the 12 mixes evaluated in this study. The mixture designs were developed according to the Superpave mix design procedure (Asphalt Institute 2007).

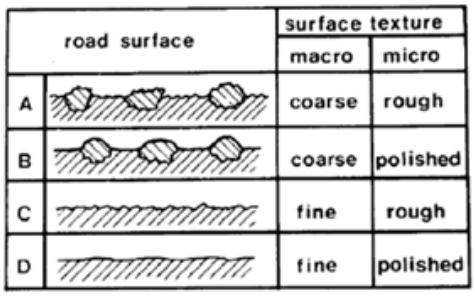

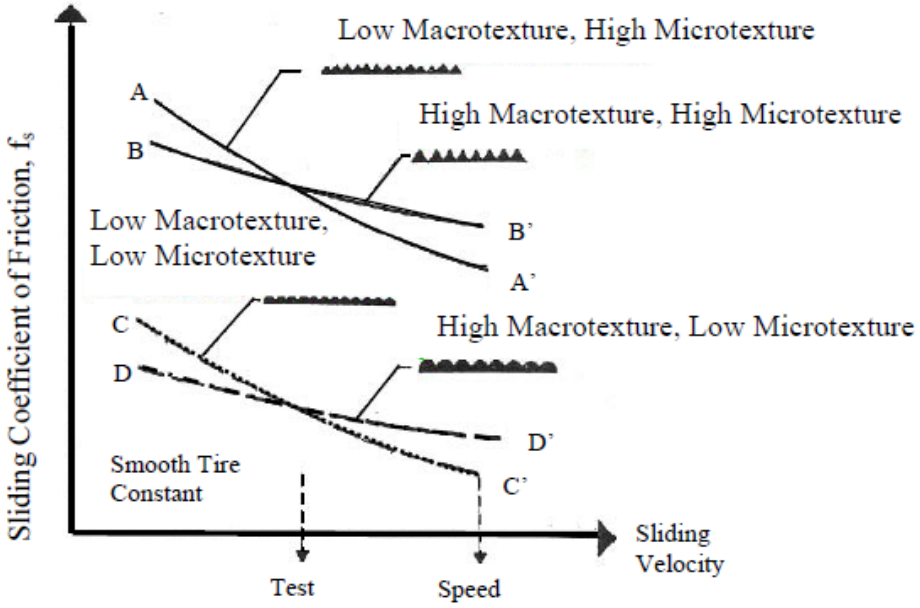

Figure 2-5. The Effect of Microtexture/Macrotexture on Pavement Friction (Hogervorst 1974; Noyce et al. 2005)

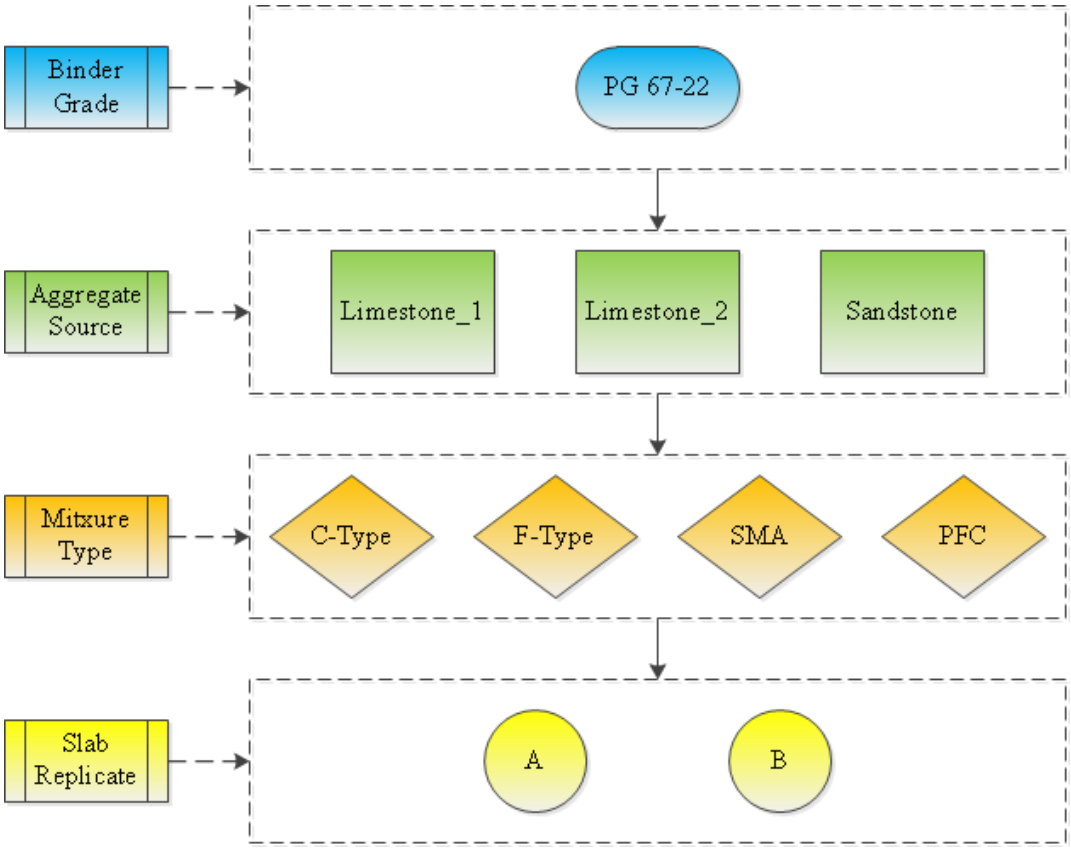

Figure 2-6. Experimental Design

Table 2-2. Mix Design

Aggregate Source	Limestone_1				Limestone_2				Sandstone			
Mixture Type	C-Type	F-Type	SMA	PFC	C-Type	F-Type	SMA	PFC	C-Type	F-Type	SMA	PFC
G_{mm}	2.399	2.382	2.382	2.402	2.454	2.426	2.467	2.440	2.406	2.397	2.380	2.361
Binder Content, %	5.1	5.7	5.4	4.4	4.5	5.2	5.2	4.5	5.6	6.0	6.3	6.8
Sieve Size, mm	Cumulative % Passing											
25.0	100	100	100	100	100	100	100	100	100	100	100	100
19.0	100	100	100	100	99.6	100.0	99.2	99.0	100	100	100	100
9.50	80.8	100	59.7	43.8	74.0	94.9	49.1	36.1	83.5	100	74.0	49.2
4.75	57.0	85.6	31.6	16.4	58.7	80.4	31.8	17.1	55.1	81.9	30.0	16.2
2.36	33.3	38.4	18.9	3.1	36.8	50.4	21.7	8.8	32.3	38.5	19.3	8.5
0.60	14.1	15.4	14.3	2.0	17.5	23.7	15.6	4.1	16.0	12.7	15.2	5.7
0.30	11.0	11.9	12.2	2.0	8.7	11.5	12.1	2.4	8.8	8.5	12.3	4.3
0.075	6.5	7.0	9.7	1.8	2.8	3.5	9.6	1.5	2.5	4.1	9.4	2.8

ANALYSIS OF AGGREGATE RESISTANCE TO DEGRADATION

The Micro-Deval test was used in this study to measure the abrasion resistance and durability of coarse aggregates (American Association of State Highway and Transportation Officials [AASHTO], 2002). Figure 2-5a shows the Micro-Deval apparatus, while Figure 2-5b shows the abrasion container and steel balls used in the test.

(a) Micro-Deval Apparatus (b) Abrasion Container and Steel Balls

Figure 2-7. Micro-Deval Test

This test was performed in the presence of water, and the test procedure is summarized as follows:

- A representative mass (A) of each type of aggregate of 1500 ± 5 g was sampled according to Table 2-3.
- The aggregate sample was placed in the container with 5000 ± 5 g of steel balls, and 2.0 ± 0.05 liters of tap water were added.
- The container was placed in the Micro-Deval machine and left for two hours before testing.
- The test was started and run at 100 ± 5 rpm for 105 ± 1 minutes.
- After 105 minutes, the aggregate sample was poured and washed over 1.18 mm sieve.
- The mass of aggregate retained on the 1.18 mm sieve was recorded (B).

- The abrasion loss was calculated using Equation (2-1):

$$Percent\ Loss = \frac{A - B}{A} \times 100 \quad (2\text{-}1)$$

Table 2-3. Micro-Deval Aggregate Sample

Passing	**Retained**	**Mass**
12.5 mm	9.5 mm	750 g
9.5 mm	6.35 mm	375 g
6.35 mm	4.75 mm	375 g

The researchers ran this test for 105 minutes as well as 180 minutes to study the degradation with time. Figure 2-6 shows the Micro-Deval abrasion loss for different aggregate samples. The percent loss was calculated after 105 minutes in the Micro-Deval (AMD 105) and after 180 minutes in the Micro-Deval (AMD 180). The results in Figure 2-6 show that sandstone had the lowest weight loss, which indicates good resistance to degradation, while limestone 1 had the highest weight loss, which indicates poor resistance to degradation. Limestone 2 had average weight loss with moderate degradation resistance. A comprehensive study by Kandhal and Parker (1998) concluded that weight loss of 18 percent after 105 minutes is a good threshold to separate good aggregates from poor aggregates in terms of the resistance to abrasion. According to this criterion, limestone 1 is expected to have poor abrasion resistance, while sandstone will have good abrasion resistance. Limestone 2 is expected to have moderate abrasion resistance since its weight loss was about 17 percent after 105 minutes.

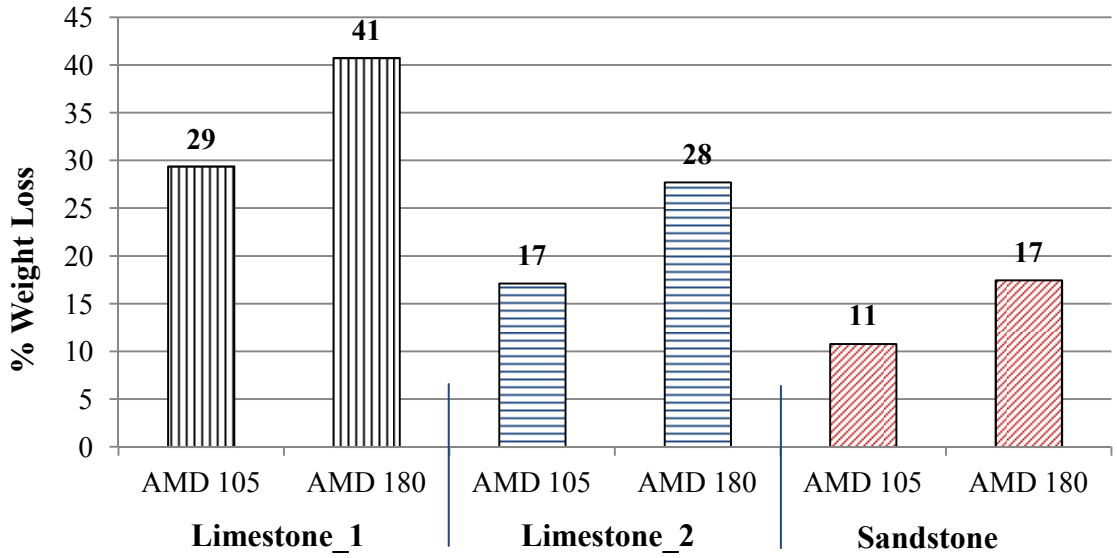

Figure 2-8. Micro-Deval Weight Loss after 105 Minutes and 180 Minutes

ANALYSIS OF AGGREGATE SHAPE CHARACTERISTICS

AIMS was used in this study to quantify the texture, form, and angularity of the tested aggregates. The AIMS shown in Figure 2-7 is an automated system that determines aggregate characteristics through image processing and analysis methods. The system consists of a bottom light, top light, camera unit, and aggregate measurement tray (Figure 2-7b). Different trays are used for different aggregates sizes, and the trays are designed to place the aggregates within the camera field of view. The aggregate samples are distributed on the load tray, as Figure 2-7b shows. The AIMS software presents aggregate shape measurements of the form, angularity, and surface texture (Figure 2-8). The aggregate angularity is qualified by measuring the irregularity of a particle surface from black and white images. The texture index is determined by analyzing grayscale images captured by AIMS using the wavelet analysis method. The shape of the aggregate is determined by two-dimensional form, sphericity, and flat/elongated ratio. The reader is referred to Al-Rousan (2004) for more information about AIMS.

(a) AIMS System (b) Aggregate Distribution

Figure 2-9. Aggregate Image Measurement System

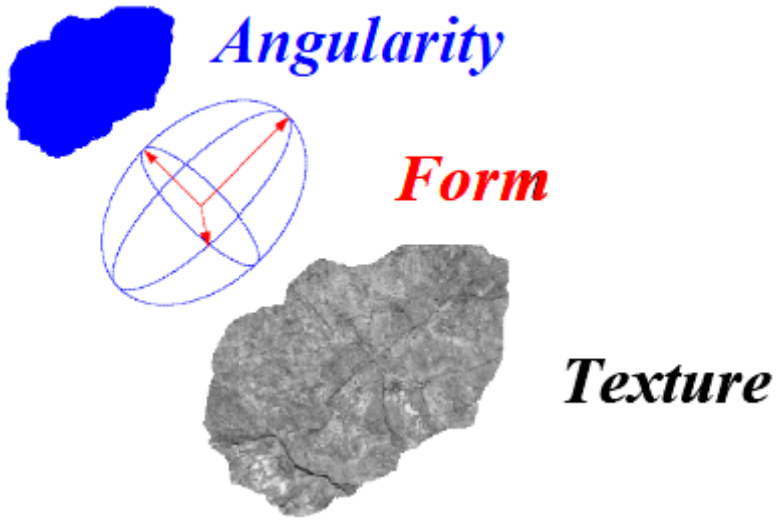

Figure 2-10. Analysis Properties (Pine Instrument Company 2011)

The researchers used the AIMS to study the aggregate shape characteristics before and after the Micro-Deval test. They studied the shape characteristics for three different sizes from each type of aggregate. These sizes are given in Table 2-3. Each size had slightly different texture indexes and angularity index distributions. Figures 2-9, 2-10, and 2-11 show the average texture index distribution for limestone 1, limestone 2, and sandstone, respectively. The average texture index distribution decreased as a result of abrasion in the Micro-Deval. The sandstone had a rough texture compared to limestone 1 and limestone 2. Limestone 1 had the lowest texture, corresponding to a smooth texture. Limestone 2 had a low-to-medium texture before the Micro-Deval test, but it became comparable to limestone 1 with a low texture after the Micro-

Deval test. Figure 2-12 shows the weighted-average values of the texture index of each type of aggregate (limestone 1, limestone 2, and sandstone) and for each mixture (Type F, Type C, SMA, and PFC). For a given aggregate type, different mixtures had slightly different values of texture index and angularity index. This is due to the fact that these mixtures have different aggregate gradation (Table 2-2) with different fractions of the evaluated aggregate sizes (Table 2-3). Same aggregates with different sizes differ in texture index and angularity index distributions. The procedure for calculating the weighted-average values for texture and angularity index is described by the AASHTO (2010).

Figures 2-13, 2-14, and 2-15 show the angularity index distribution for limestone 1, limestone 2, and sandstone, respectively. Figure 2-16 shows the weighted-average values of the angularity index of each type of aggregate and for each mixture. Figure 2-16 illustrates that these aggregates had a comparable angularity index before the Micro-Deval test; however, they had a different angularity index after the Micro-Deval test. Sandstone had the highest angularity followed by limestone 2 and limestone 1 after 105 and 180 minutes in the Micro-Deval test. These results are consistent with the findings of the Micro-Deval weight loss test (Figure 2-6), where sandstone was found to have good resistance to degradation, while limestone 1 had poor resistance to degradation.

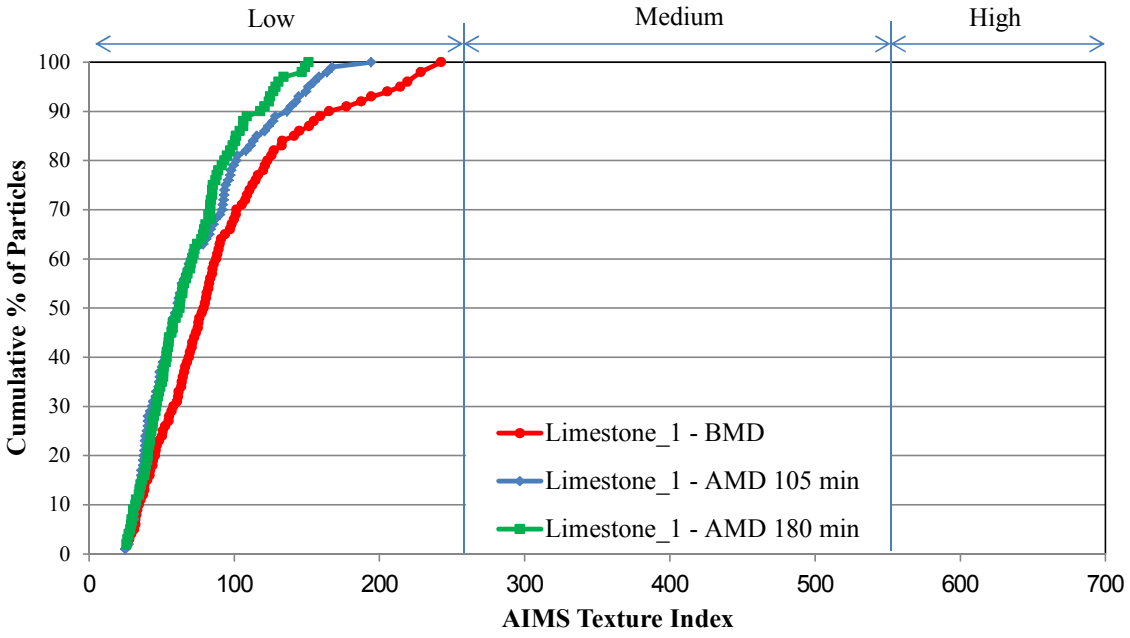

Figure 2-11. AIMS Texture Distribution for Limestone 1 Aggregate

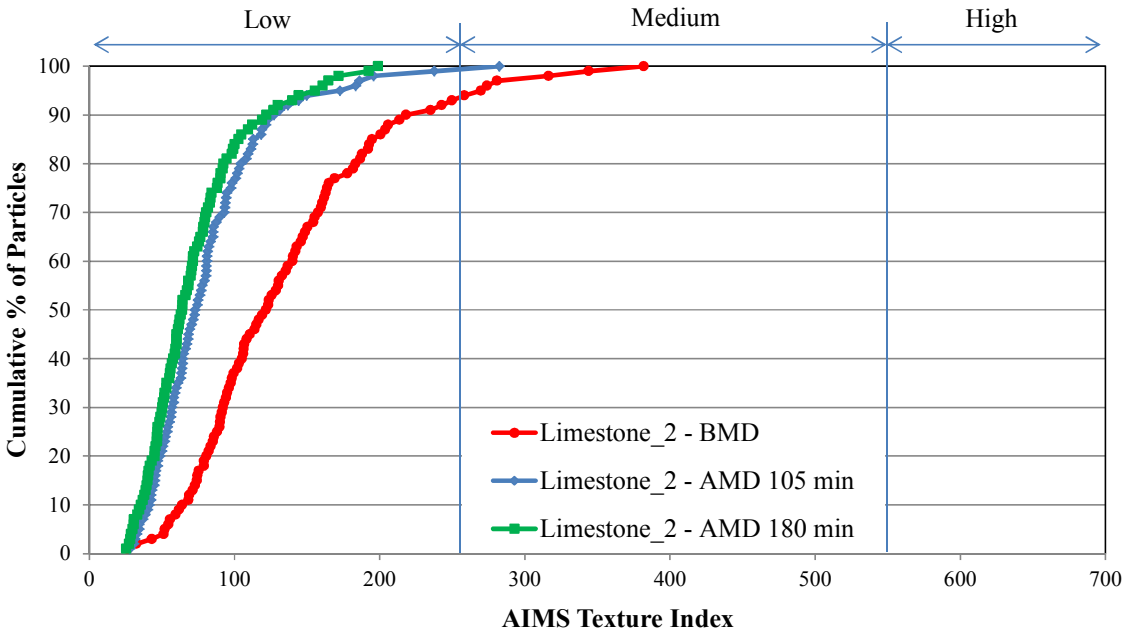

Figure 2-12. AIMS Texture Distribution for Limestone 2 Aggregate

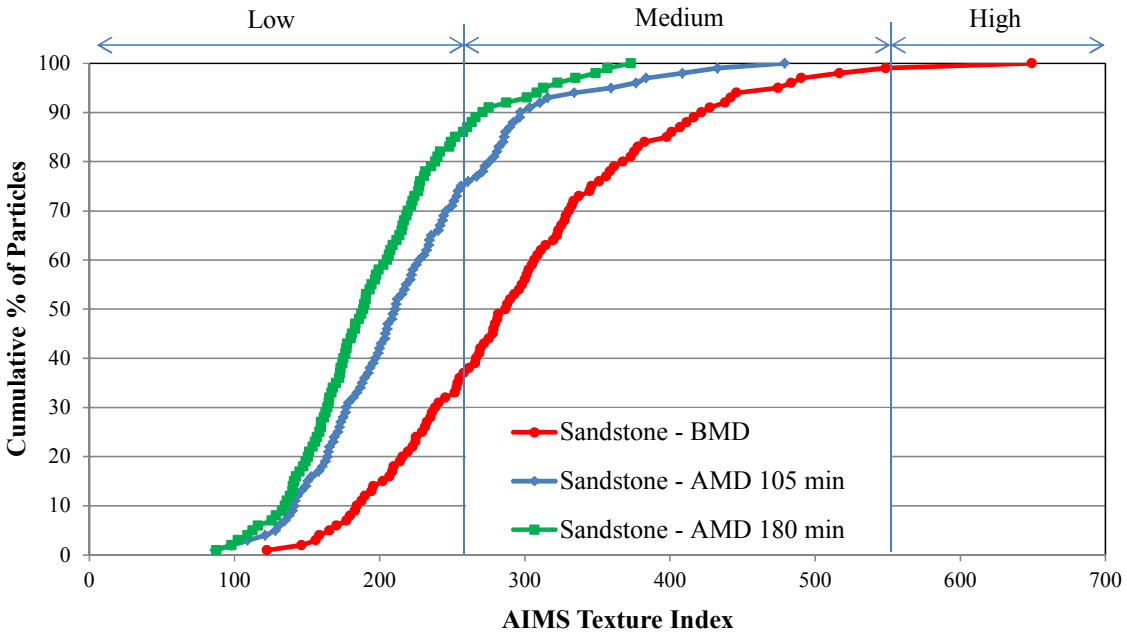

Figure 2-13. AIMS Texture Distribution for Sandstone Aggregate

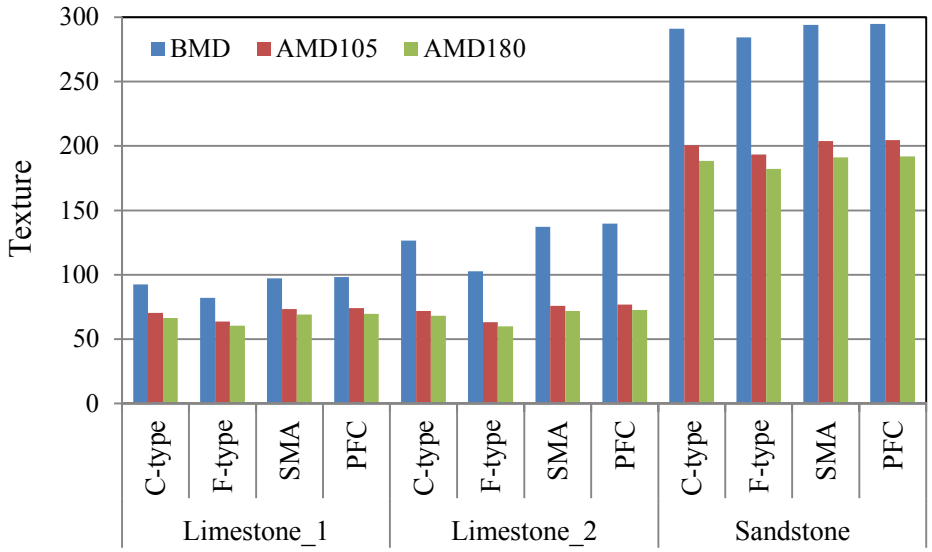

Figure 2-14. Weighted-Average Texture Index for Different Mixtures

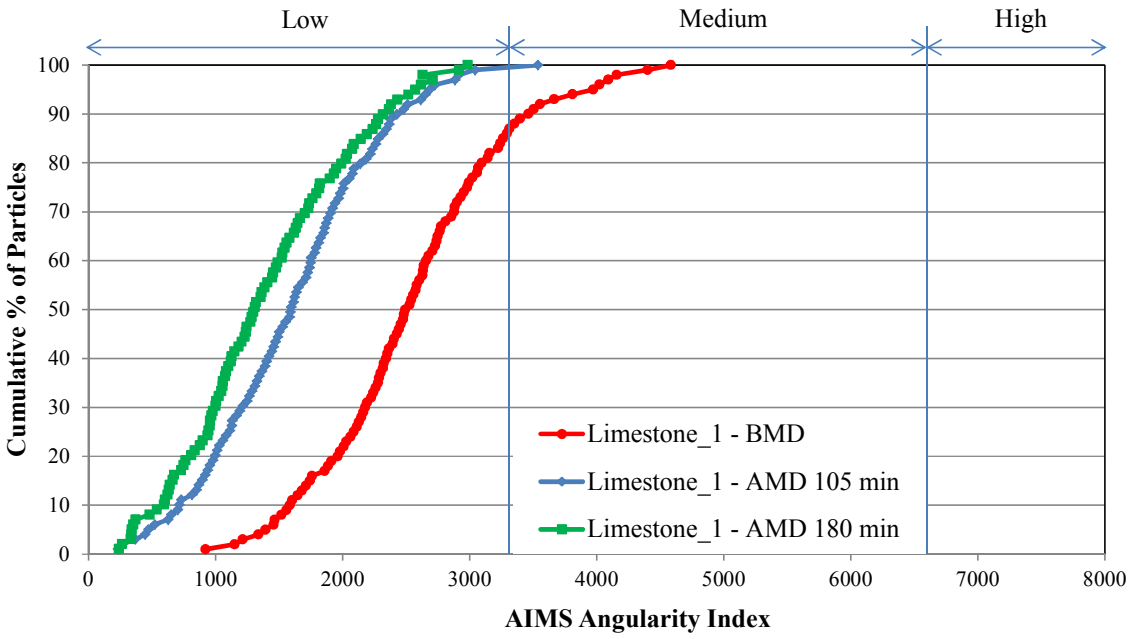

Figure 2-15. AIMS Angularity Distribution for Limestone 1 Aggregate

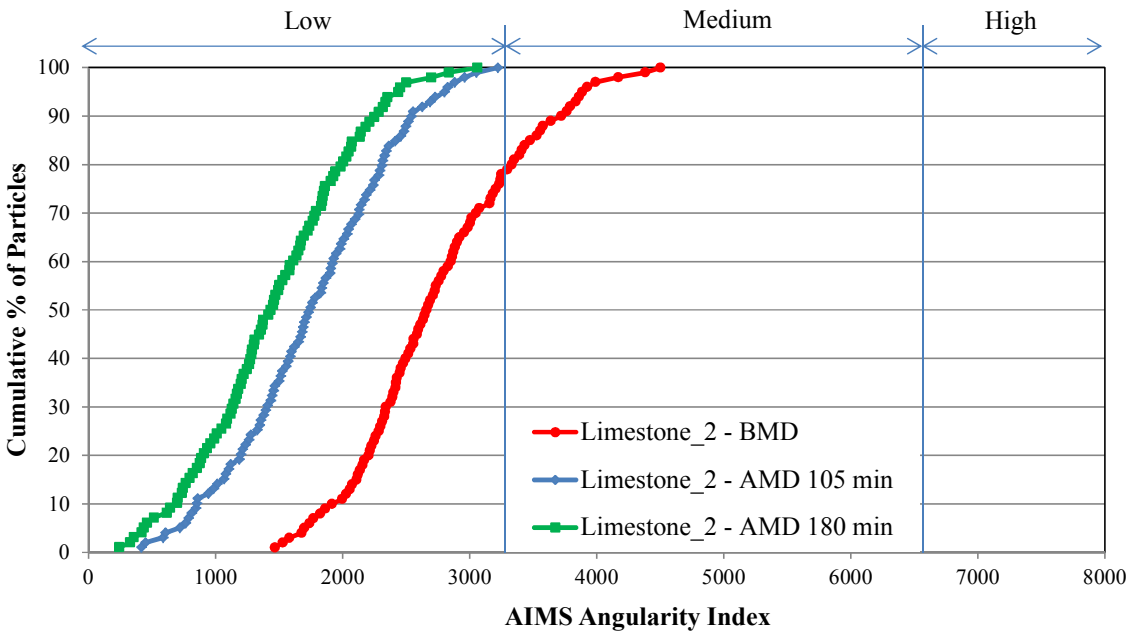

Figure 2-16. AIMS Angularity Distribution for Limestone 2 Aggregate

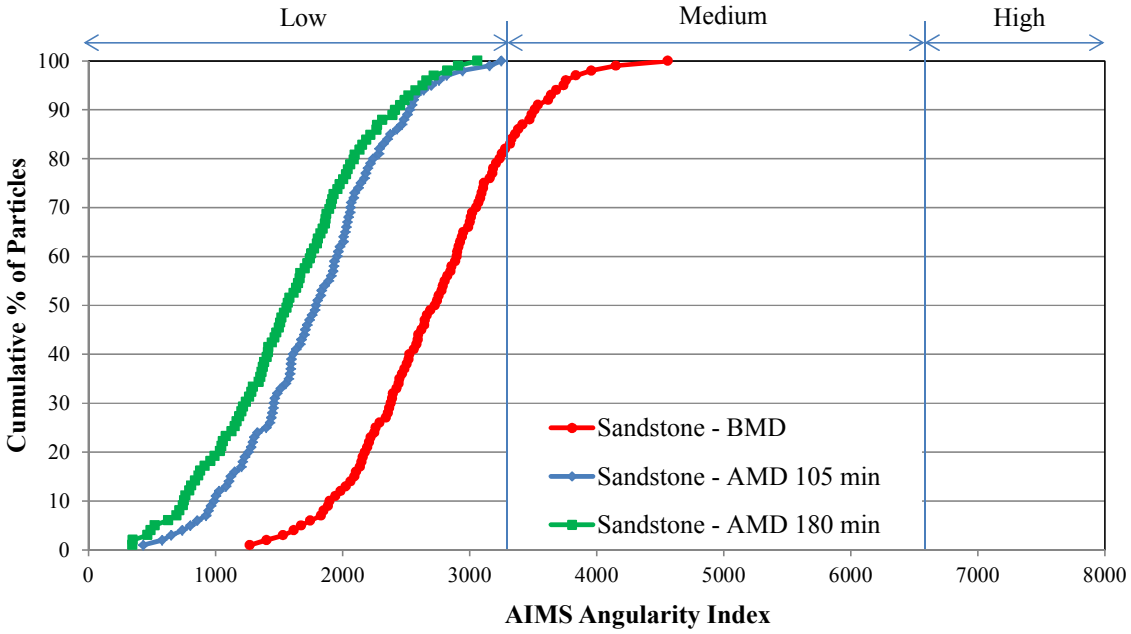

Figure 2-17. AIMS Angularity Distribution for Sandstone Aggregate

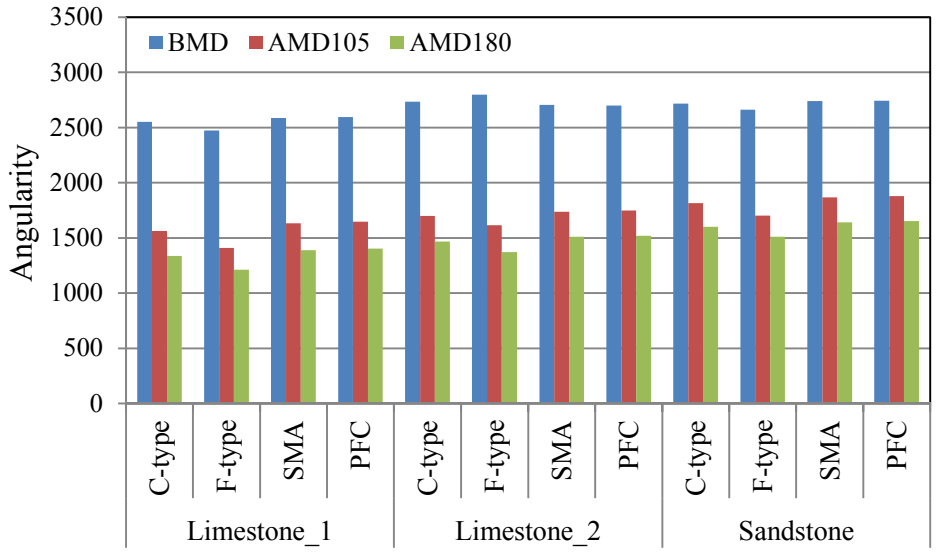

Figure 2-18. Weighted-Average Angularity Index for Different Mixtures

TEST SLAB PREPARATION

Square-shaped test slabs were prepared in the laboratory. Twelve different mixtures were evaluated, and two replicate test slabs were prepared from each mixture. A total of 24 test slabs were prepared and tested in this study. About 30 kg of loose mixtures was required for preparing one test slab. The mixing and compaction temperatures were 143°C and 121°C, respectively. A linear kneading compactor was used to compact the test slabs. The mold of the linear kneading compactor was slightly modified to accommodate the 20 inch square-shaped slabs. The thickness of the test slabs was 2 inches. The size of the test slabs was sufficient for polishing and using the CTMeter and DFT, as discussed later in this chapter. Figure 2-17 shows the compaction procedure, which is described below:

- Loose mixtures were placed in the compaction mold at the predetermined compaction temperature (Figure 2-17a). The mold was heated to the same compaction temperature.
- The loose mixtures were spread evenly (Figure 2-17b), and a separation paper was placed on top of the loose mixtures.
- A number of thin steel plates were placed vertically above the mixtures and perpendicular to the direction of movement of the mold (Figure 2-17c).

- The top surface of the mixtures was completely covered with the steel plates, as Figure 2-17d shows.
- The compaction roller was lowered and the steel plates were rolled (Figure 2-17e). The compaction roller was kept still while the mold moved during compaction (Figures 2-17e and 2-17f).

(a) Placing HMA Mixtures

(b) Spreading HMA Mixtures

(c) Steel Plates

(d) Covering the Top Surface with Steel Plates

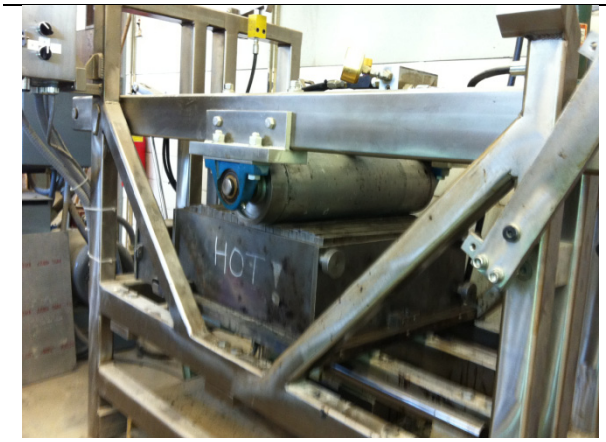

(e) Lowering the Compaction Roller

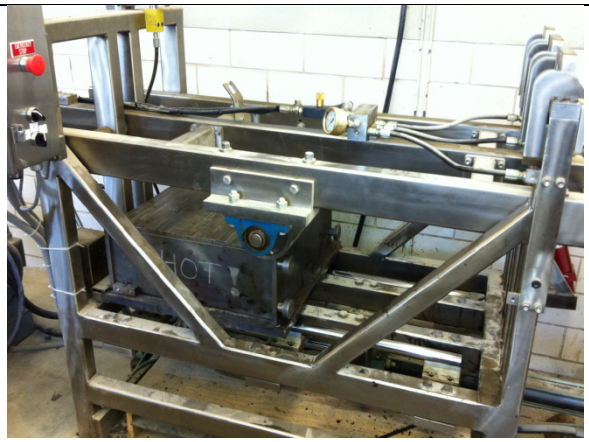

(f) Rolling Process

Figure 2-19. Compaction Process Using Linear Kneading Compactor

POLISHING OF THE LABORATORY TEST SLABS

A three-wheel-polishing device was used to polish the test slabs (Figure 2-18). The polisher consists of three pneumatic rubber wheels attached to a turntable. The turntable is loaded with several circular loading plates of 10 lb each. The weight of the wheel assembly is 72.3 lb. In this study, the total applied load on the pneumatic rubber wheels was 105 lb, and the tire pressure was maintained at 50 psi. The tire print width was about 0.9 inch (2.3 mm), and the wheels rotated around a circle that was 11.2 inches (284 mm) in diameter. The pneumatic rubber wheels polished the asphalt mixture test slabs similar to the polishing that occurs in the field under traffic. The polisher has a water spray system to simulate wet conditions, reduce the wear of the rubber wheels, and wash away the fine aggregates at the surface, allowing more polishing to occur. Vollor and Hanson (2006) give more information about the asphalt mixture polisher. In this study, the test slabs were polished to 5000, 10,000, 30,000, 50,000, and 100,000 cycles.

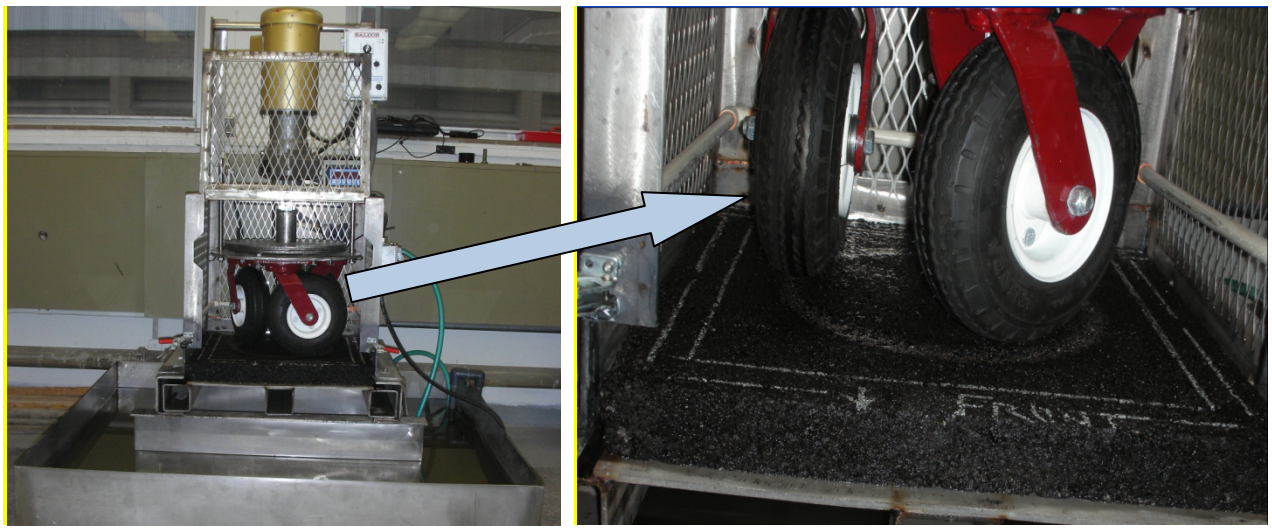

(a) Polishing Machine (b) Pneumatic Rubber Wheels

Figure 2-20. Laboratory Polishing Machine

ANALYSIS OF SKID RESISTANCE

The CTMeter and DFT were used to measure the MPD and the coefficient of friction at 20 km/hr (DFT_{20}), respectively, after each application of polishing cycles. Then the international friction index (IFI) was calculated. Figures 2-19 to 2-21 show the MPD of the test slabs measured using the CTMeter according to the ASTM procedure (ASTM 2009a). Coarse

mixtures such as PFC have high MPD values compared to fine mixtures such as Type F. The MPD is a measure of the macrotexture; thus, it depends on how fine or coarse the gradation is. There was a slight change in the MPD during polishing. Generally, the MPD increased slightly with the number of polishing cycles. Such small increase could be due to washing the fine aggregates and asphalt binder film coating the aggregates at the surface of the test slabs. Figures 2-22 to 2-24 show the DFT_{20} values for the test slabs measured using the DFT according to the ASTM procedure (ASTM 2009b). The DFT_{20} is considered an indication of the pavement microtexture. The DFT_{20} decreased with the number of polishing cycles due to abrasion and polishing of aggregates at the surface. The sandstone test slabs had higher DFT_{20} values than the ones made with limestone 1 and limestone 2 aggregates. High DFT_{20} is an indication of rough microtexture. The AIMS results showed that the sandstone aggregates had rough microtexture compared to limestone 1 and 2 (Figures 2-12), which agree with the DFT results. Figure 2-24 shows that the DFT_{20} for the sandstone test slabs had a slight change with the number of polishing cycles compared to a significant drop in the test slabs made with limestone 1 and limestone 2, as Figures 2-22 and 2-23 illustrate. The Micro-Deval test results showed that sandstone had good resistance to abrasion and degradation (Figure 2-6), which explains the small drop in the DFT_{20} for the sandstone test slabs compared to limestone 1 and limestone 2 test slabs.

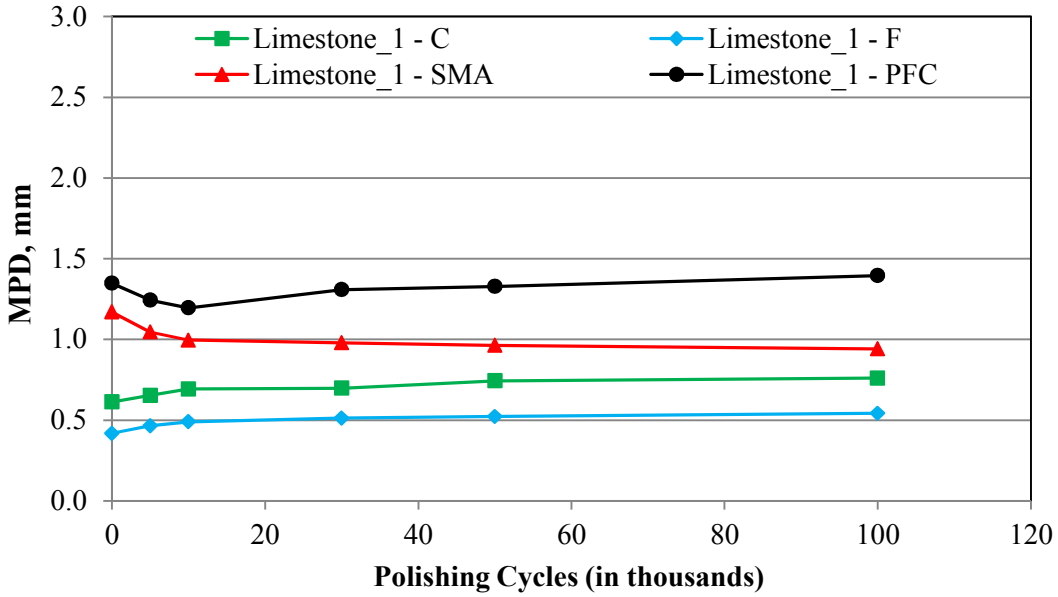

Figure 2-21. MPD with Polishing Cycles for Limestone 1 Test Slabs

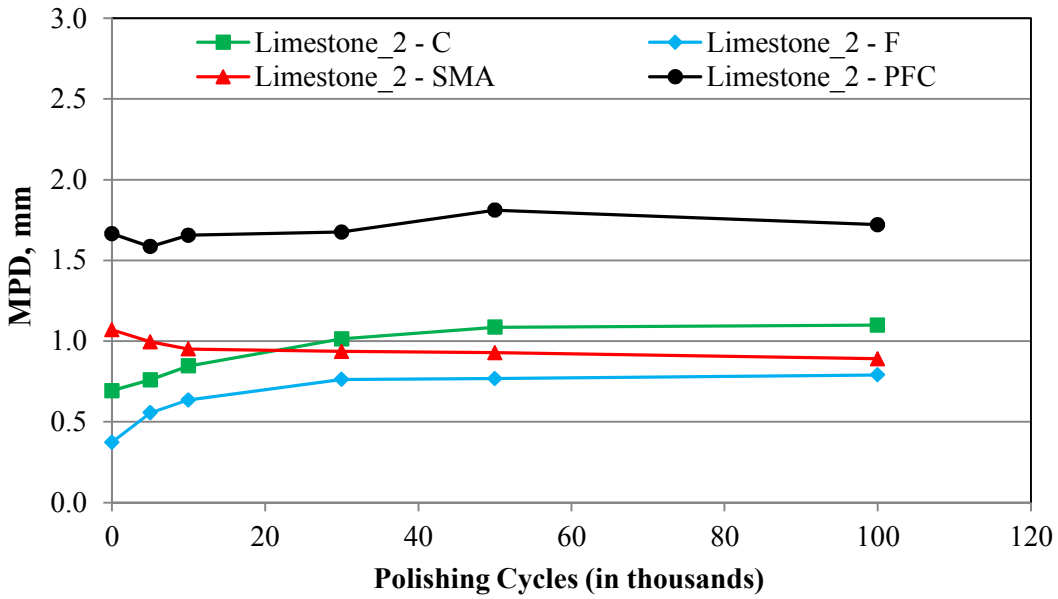

Figure 2-22. MPD with Polishing Cycles for Limestone 2 Test Slabs

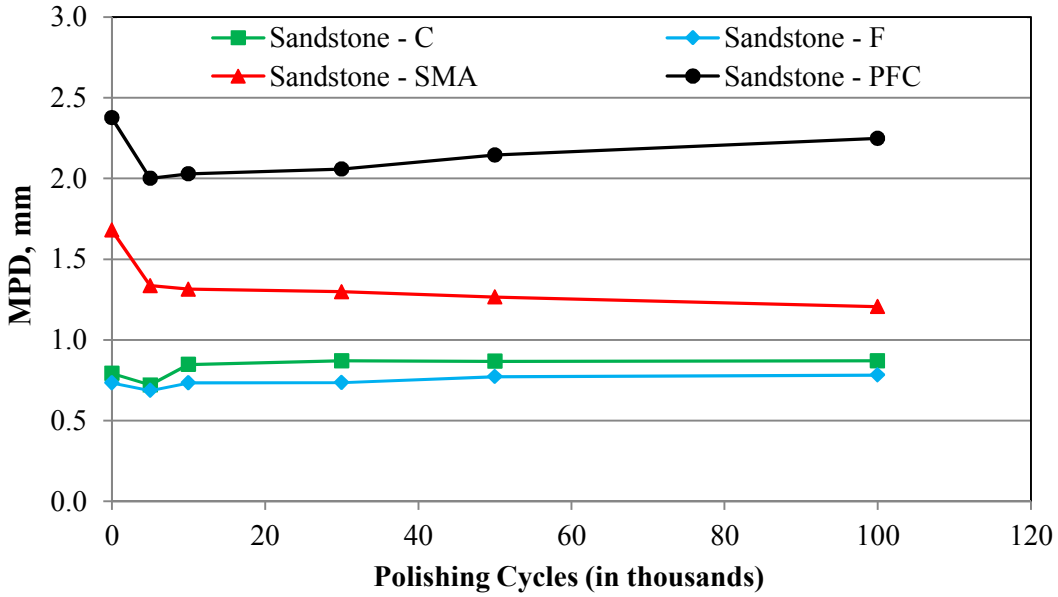

Figure 2-23. MPD with Polishing Cycles for Sandstone Test Slabs

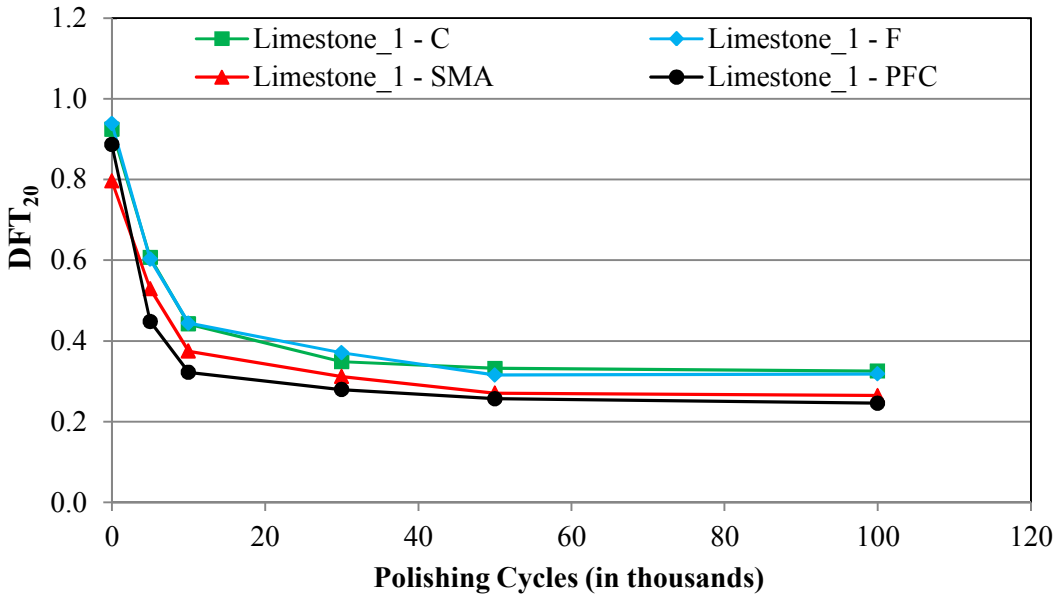

Figure 2-24. DFT_{20} with Polishing Cycles for Limestone 1 Test Slabs

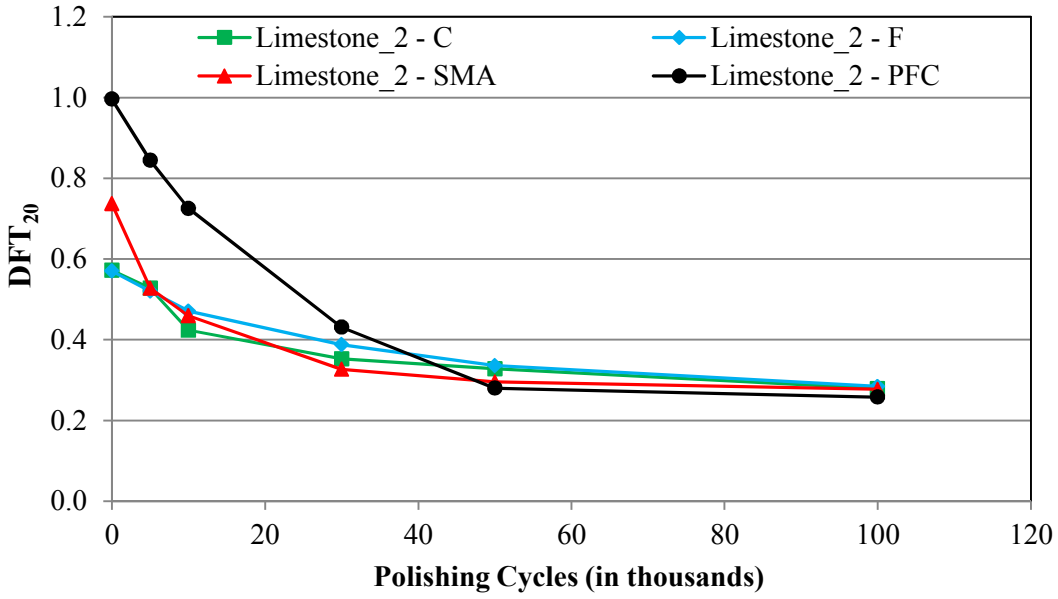

Figure 2-25. DFT_{20} with Polishing Cycles for Limestone 2 Test Slabs

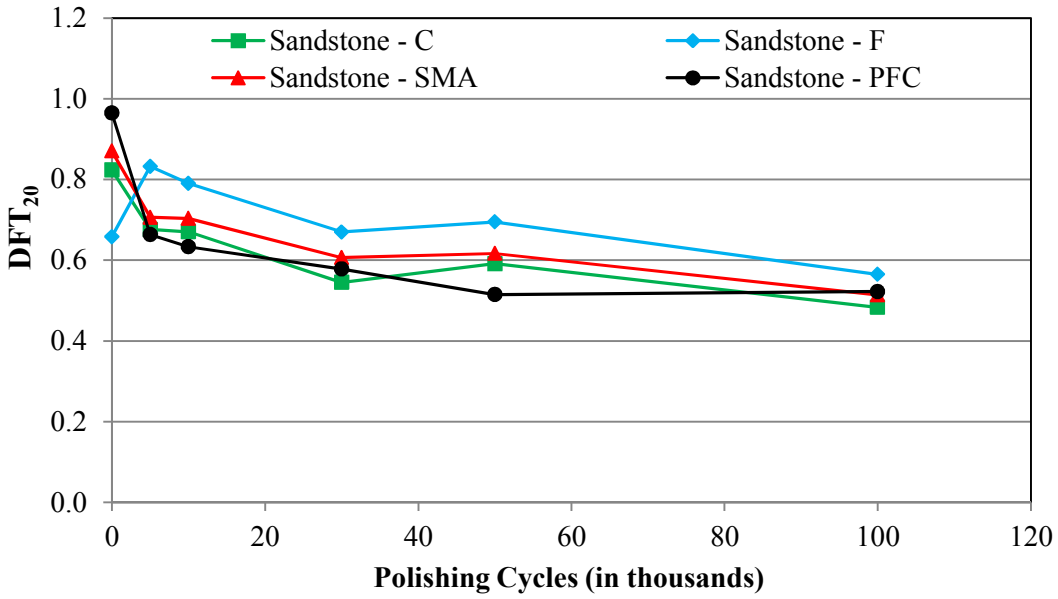

Figure 2-26. DFT_{20} with Polishing Cycles for Sandstone Test Slabs

The skid resistance was quantified by the IFI. The IFI is a universal method for characterization of pavement surface and harmonization of different friction measuring equipment (Wambold et al. 1995; Henry et al. 2000; Masad, Rezaei et al. 2010). The IFI is calculated using texture and friction measurements taken using different test methods. In this study, the IFI was calculated using the MPD and DFT_{20} measured using the CTMeter and DFT, respectively. Equations (2-2) and (2-3) calculate the IFI using MPD and DFT_{20} measurements according to ASTM E 1911.

$$IFI = 0.081 + 0.732 DFT_{20} \exp\left(\frac{-40}{S_p}\right) \quad (2\text{-}2)$$

$$S_p = 14.2 + 89.7 MPD \quad (2\text{-}3)$$

Figures 2-25, 2-26, and 2-27 show the IFI versus the polishing cycles for the test slabs prepared using limestone 1 and limestone 2, and sandstone, respectively. Mixtures with coarser aggregate gradation (PFC and SMA) had higher IFI, better skid resistance, than those with finer aggregate gradation (Type F and Type C). The sandstone test slabs had higher IFI compared to limestone 1 and limestone 2 test slabs at the corresponding number of cycles. The IFI for the limestone 1 test slabs was comparable to the IFI for limestone 2 test slabs; however, the IFI for the limestone 1 test slabs dropped faster compared to test slabs made with limestone 2. For

limestone 1 test slabs, the IFI reached the terminal value after only 30,000 polishing cycles. These results are in agreement with the Micro-Deval test, where the sandstone was determined to have good resistance to abrasion and degradation, while limestone 1 and limestone 2 were determined to have poor and moderate resistance to abrasion and degradation, respectively.

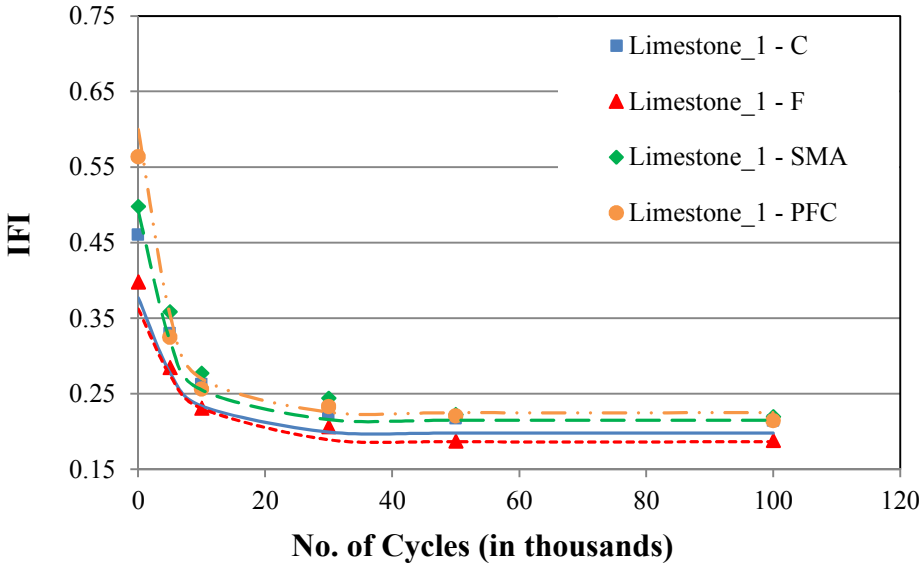

Note: data points represent experimental measurements and lines represent predictive model.

Figure 2-27. IFI vs. Polishing Cycles for Limestone 1 Test Slabs

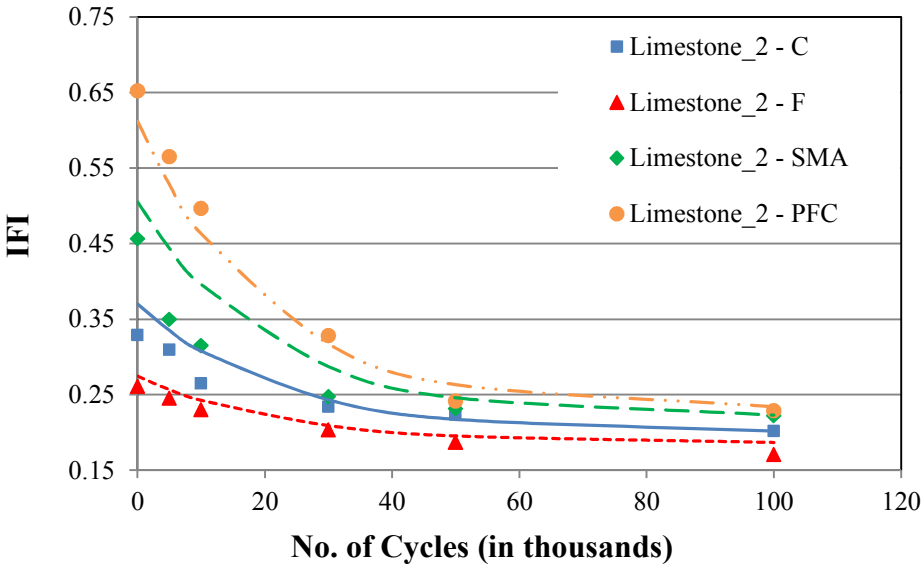

Note: data points represent experimental measurements and lines represent predictive model.

Figure 2-28. IFI vs. Polishing Cycles for Limestone 2 Test Slabs

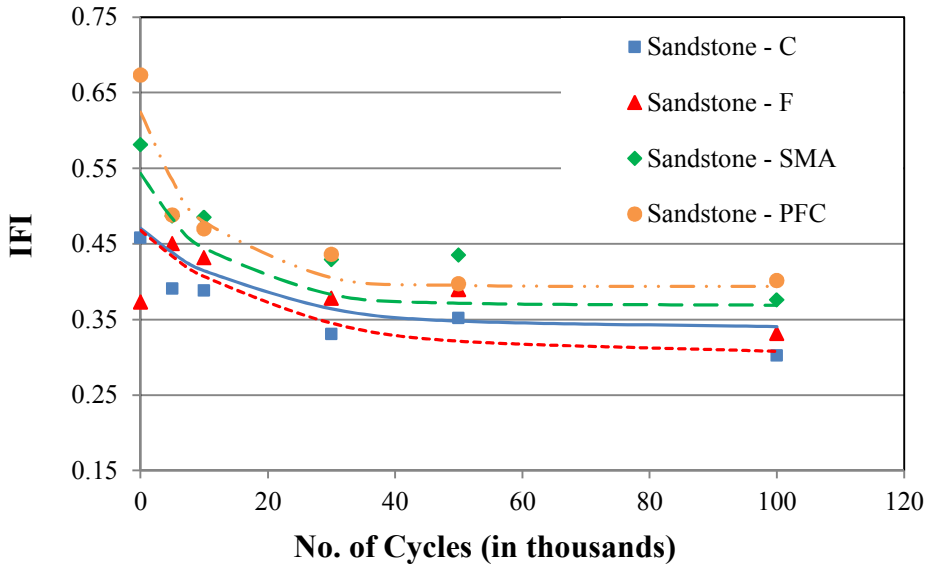

Note: data points represent experimental measurements and lines represent predictive model.

Figure 2-29. IFI vs. Polishing Cycles for Sandstone Test Slabs

DEVELOPMENT OF A PREDICTIVE MODEL FOR SKID RESISTANCE

Masad, Rezaei et al. (2010) developed a method to predict pavement skid resistance with time. This method is based on inputs that describe aggregate texture before and after polishing, gradation of asphalt mixture, and traffic. The researchers validated and modified the developed method by Masad, Rezaei et al. (2010) with the laboratory measurements obtained in this study. The researchers used the proposed procedure by Masad, Rezaei et al. (2010) for measuring aggregate texture and its resistance to polishing. However, the researchers also evaluated the change in angularity due to polishing and abrasion. Figure 2-28 illustrates the procedure followed for measuring aggregate texture and angularity and its resistance to polishing and abrasion. The AIMS test was used to measure the aggregate texture and angularity before and after the Micro-Deval test. Luce (2006) found that the texture and angularity of the aggregates decrease with the time of the Micro-Deval test. Figure 2-29 shows an example of change in texture for different aggregates versus polishing time in the Micro-Deval test (Masad et al. 2005). Masad et al. (2006) found that the loss of texture can be described using only three data points taken before the Micro-Deval test and after 105 minutes and 180 minutes of the Micro-Deval test. The researchers in this study conducted the AIMS test before the Micro-Deval test

and after 105 minutes and 180 minutes of the Micro-Deval test, as discussed earlier. An example of the change in the texture with time is given in Figure 2-30. Mahmoud (2005) found that the change in the texture with time can be described by Equation (2-4):

$$TX(t) = a_{TX} + b_{TX} * e^{(-c_{TX} * t)} \quad (2\text{-}4)$$

where a_{TX} , b_{TX} , and c_{TX} are regression constants, while *t* is the polishing time in the Micro-Deval test. Figure 2-30 shows an example of these regression constants.

The researchers in this study found that the equation proposed by Mahmoud (2005) to describe the texture loss can also be used to describe the loss of aggregate angularity, as given in Equation (2-5):

$$GA(t) = a_{GA} + b_{GA} * e^{(-c_{GA} * t)} \quad (2\text{-}5)$$

where a_{GA} , b_{GA} , and c_{GA} are regression constants, while *t* is the polishing time in the Micro-Deval test. Figure 2-31 shows an example of these regression constants for the change in angularity.

Macrotexture affects skid resistance, and hence the researchers developed a method to quantify the aggregate gradation. Masad, Rezaei et al. (2010) found that the aggregate gradation can be described by the cumulative two-parameter Weibull distribution, as presented in Equation (2-6):

$$F(x;\lambda,k) = 1 - e^{-\left(x/\lambda\right)^k} \quad (2\text{-}6)$$

where *x* is the aggregate size in millimeters, and λ and κ are the scale and shape parameters of the Weibull distribution, respectively. Figure 2-32 illustrates the effect of the aggregate gradation on the parameters of the Weibull distribution function.

Finally, the researchers used Equation (2-7) to quantify the change in the calculated IFI with the polishing cycles based on the MPD and DFT_{20} measurements following Masad, Rezaei et al. (2010):

$$IFI(N) = a_{mix} + b_{mix} * e^{(-c_{mix} * N)} \quad (2\text{-}7)$$

where a_{mix} , $a_{mix} + b_{mix}$, and c_{mix} are the terminal, initial, and rate of change in IFI, respectively, while *N* is the polishing cycles in thousands using the polisher. These regression parameters can be obtained using nonlinear regression analysis. Figure 2-33 shows an example of the change in IFI with polishing cycles and the regression constants.

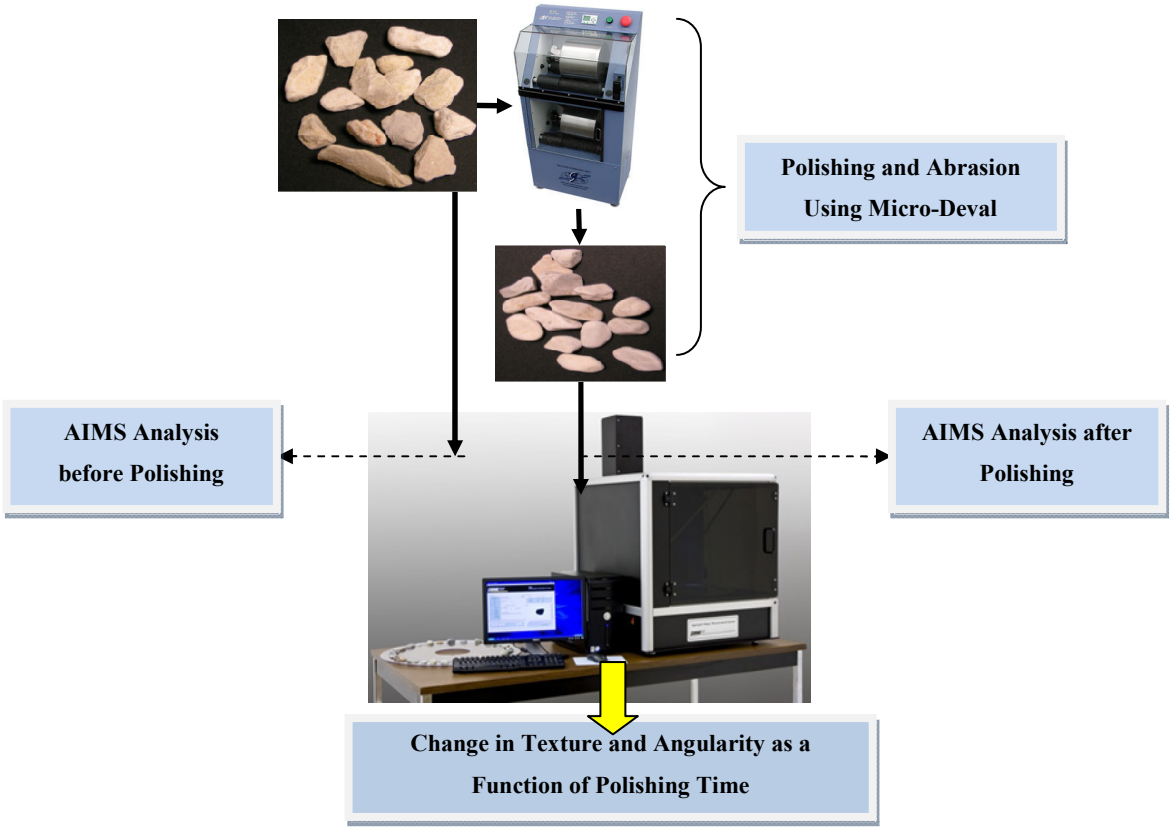

Figure 2-30. Procedure for Measuring Aggregate Texture and its Resistance to Polishing

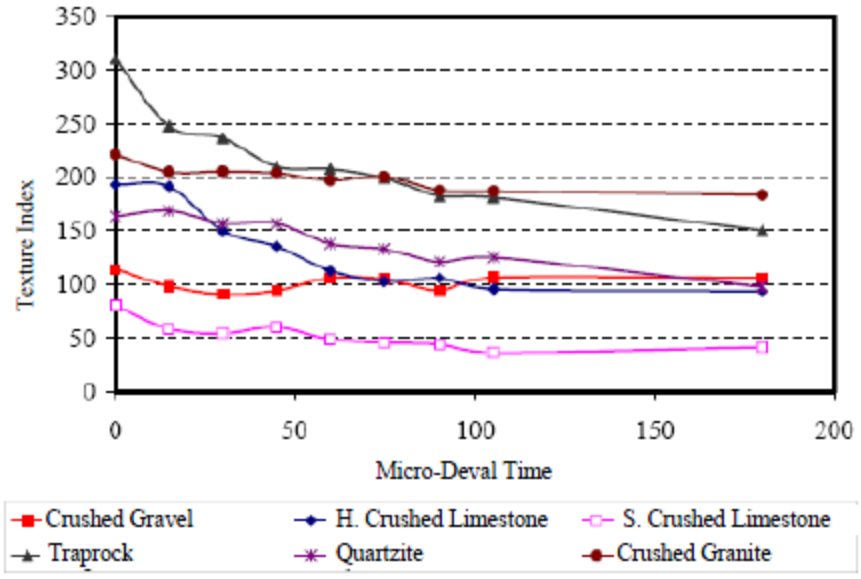

Figure 2-31. Aggregate Texture vs. Time of the Micro-Deval Test (Masad et al. 2005)

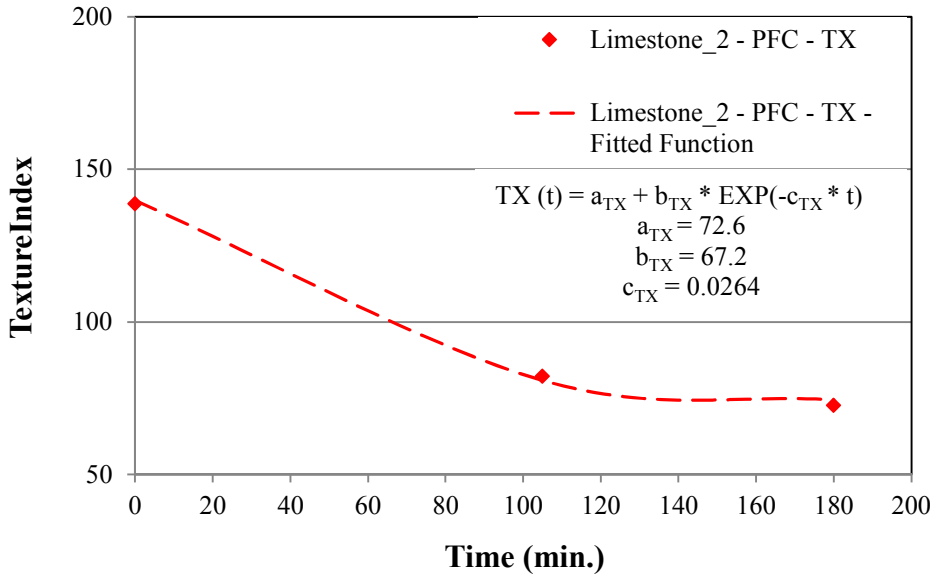

Figure 2-32. Aggregate Texture vs. Micro-Deval Time

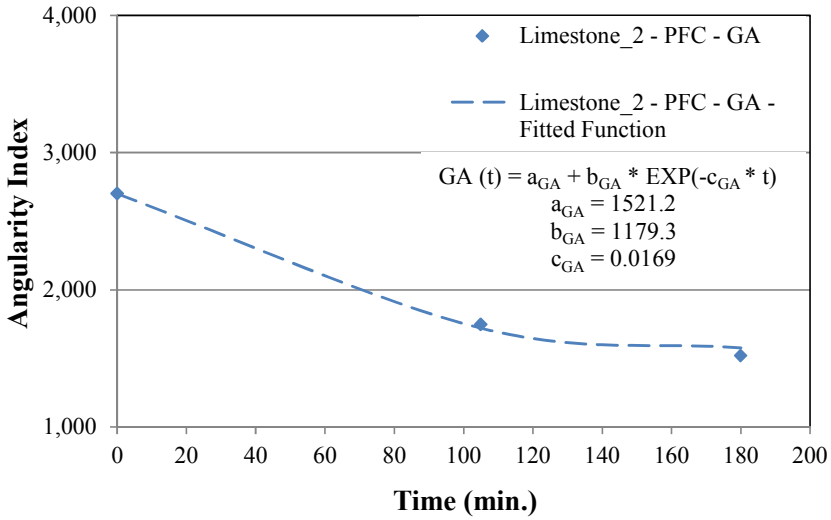

Figure 2-33. Aggregate Angularity vs. Micro-Deval Time

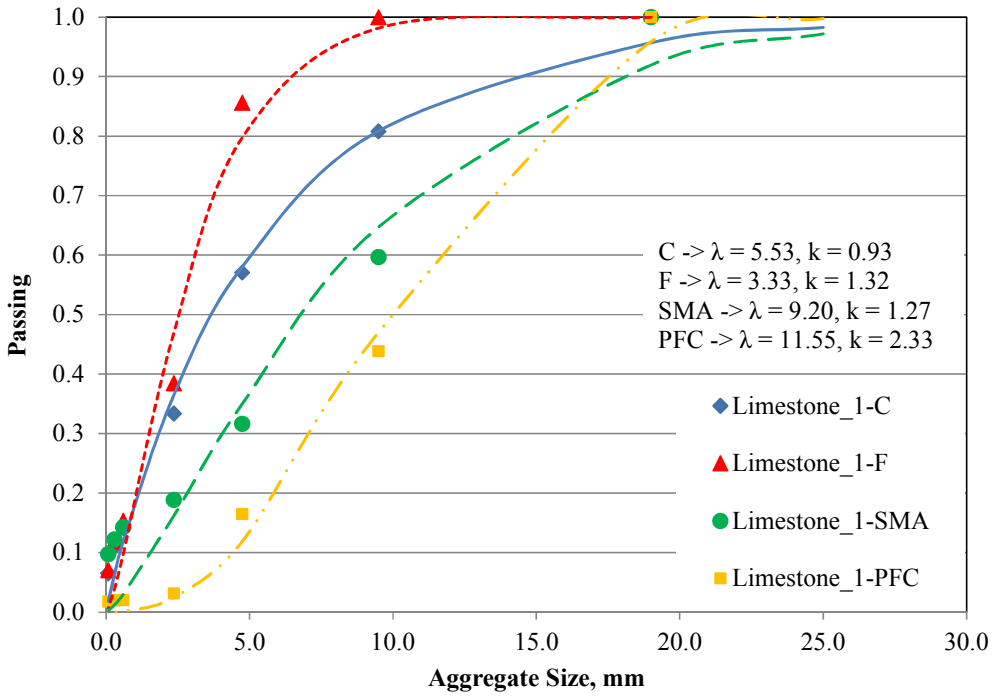

Figure 2-34. Weibull Distribution for Different Aggregate Gradations

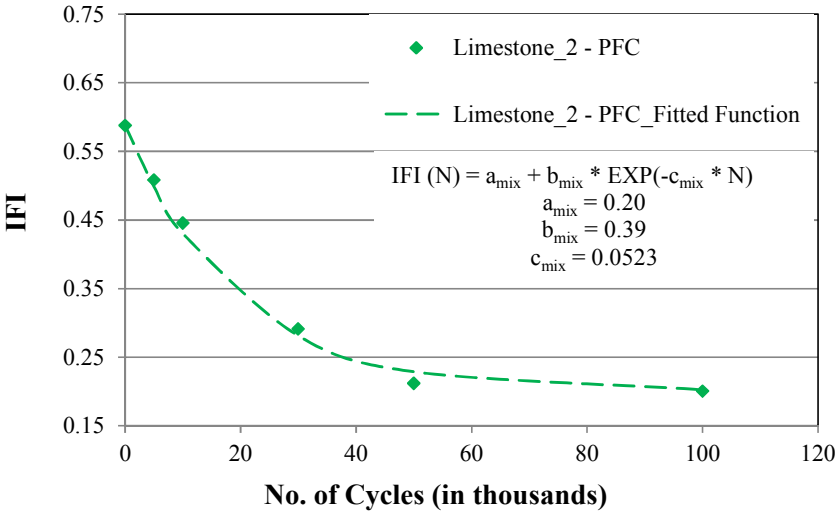

Figure 2-35. IFI vs. Polishing Cycles

Masad, Rezaei et al. (2010) correlated the coefficients of IFI (Equation [2-7]) to the aggregate texture coefficients (Equation [2-4]) and Weibull distribution parameters that describe the aggregate gradations (Equation [2-6]). The researchers in this study used the same parameters to describe the texture and gradation, but they also included the aggregate angularity coefficients

(Equation [2-5]). They included the aggregate angularity in the statistical models that predict the IFI coefficients with number of polishing cycles. Equations (2-8), (2-9), and (2-10) describe the IFI coefficients, a_{mix} , $a_{mix} + b_{mix}$, and c_{mix}, respectively.

$$a_{mix} = \frac{47.493 + \lambda}{307.071 - 0.003(AMD)^2} \tag{2-8}$$

$$(a_{mix} + b_{mix}) = 0.308 * \ln\left(\frac{1.438 * (a_{TX} + b_{TX}) + 46.893 * \lambda + 333.491 * k}{2.420 * (a_{GA} + b_{GA})}\right) + 1.008 \tag{2-9}$$

$$c_{mix} = 0.052 + 2.284 * 10^{-14} * e^{\left(0.523 / c_{TX}\right)} + 2.008 * 10^{-47} * e^{\left(1.708 / c_{GA}\right)} \tag{2-10}$$

where *AMD* is the aggregate texture after the 105 minutes of the Micro-Deval test; a_{TX} , b_{TX} , and c_{TX} are regression constants of the texture equation (Equation [2-4]); a_{GA} , b_{GA} , and c_{GA} are regression constants of the angularity equation (Equation [2-5]); and λ and κ are the scale and shape parameters of the Weibull distribution (Equation [2-6]).

Figures 2-34 to 2-36 show the predicted model parameters versus the measured ones. Figures 2-25 to 2-27 showed the measured IFI for the test slabs and model predictions. Figure 2-37 shows all the experimental IFI measurements presented in Figures 2-25 through 2-27, plotted against the predicted IFI at the same polishing cycles. It can be seen that the developed IFI model was able to capture the loss of the IFI measured in the laboratory. The predicted IFI correlated very well with the IFI measured in the laboratory. Figure 2-38 summarizes the IFI model parameters. The IFI model parameters (Equations [2-8] through [2-10]) are modified equations from Masad, Rezaei et al. (2010). The authors found that a better correlation was achieved between the predicted and measured IFI when they added parameters to describe the loss in aggregate angularity.

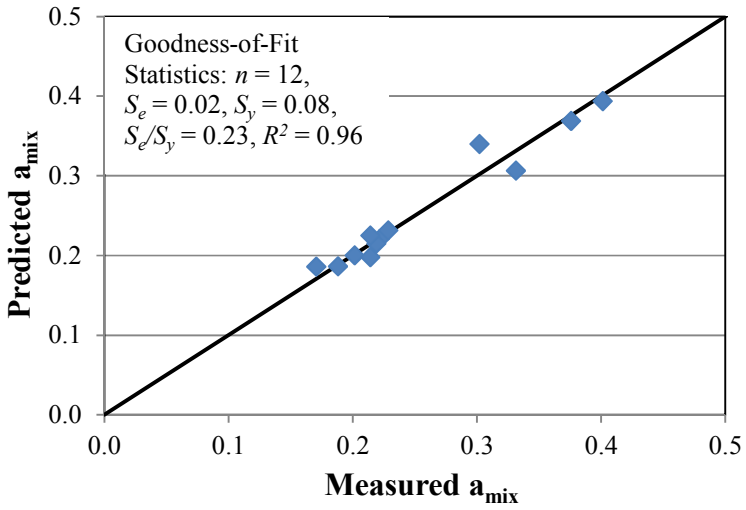

Figure 2-36. Predicted Terminal IFI (a_{mix}) vs. Predicted Terminal IFI

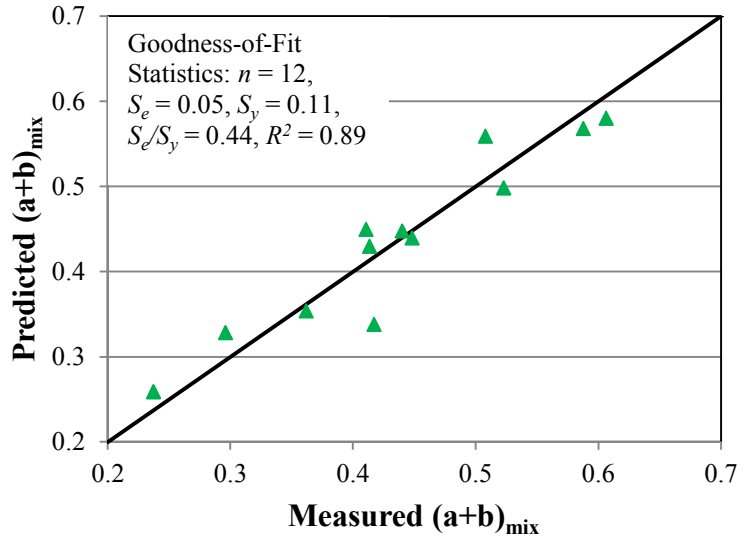

Figure 2-37. Predicted Initial IFI (a_{mix}+b_{mix}) vs. Predicted Initial IFI

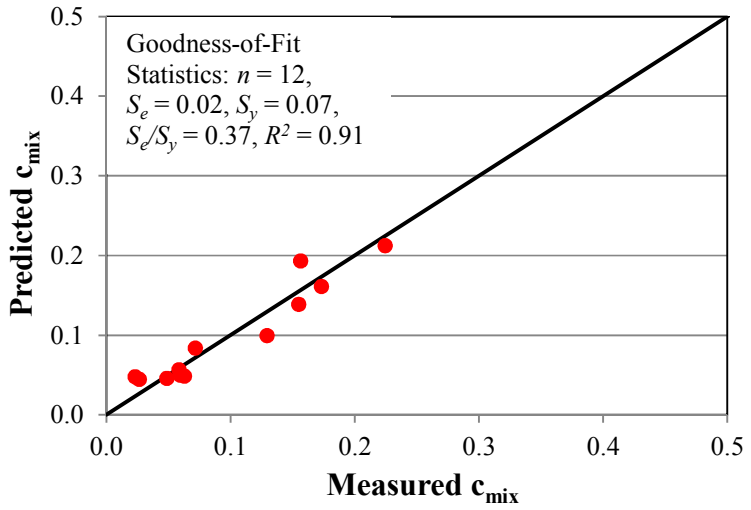

Figure 2-38. Predicted IFI Rate Change (c_{mix}) vs. Measured IFI Rate Change

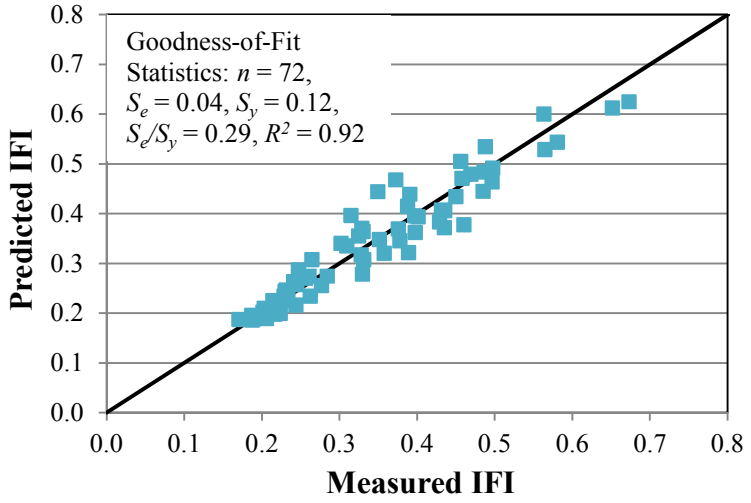

Figure 2-39. Predicted IFI vs. Measured IFI

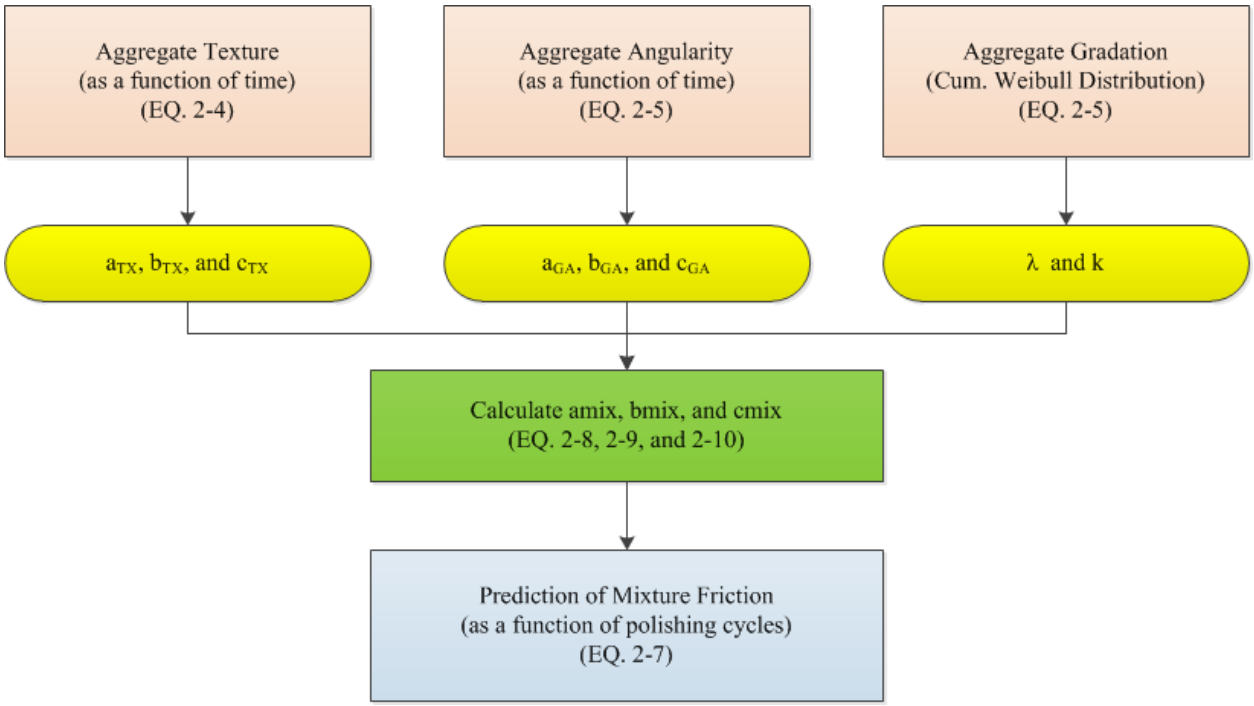

Figure 2-40. Components of the Friction Loss Model

CONCLUSIONS

In this part of the study, the researchers evaluated the influence of the aggregate shape characteristics (texture and angularity) and aggregate gradation on the surface friction of asphalt pavements. In addition, a predictive model was developed for friction loss of laboratory asphalt mixture test slabs. The main findings from this part of the study can be summarized as follows:

- The Micro-Deval was used to evaluate the abrasion and degradation resistance of the tested aggregates. The results showed that sandstone had good resistance to abrasion and degradation, while limestone 1 and limestone 2 had poor and moderate resistance to abrasion and degradation, respectively.
- The AIMS system was used to study the aggregate shape characteristics of test aggregates. The AIMS results revealed that the sandstone aggregates had rough microtexture compared to limestone 1 and 2.
- The three-wheel polisher was found to be a good tool to polish the top surface of asphalt mixture slabs.
- The coarse mixtures had higher MPD values compared to the fine mixtures.

- The AIMS results revealed that the sandstone aggregates had rough microtexture compared to limestone 1 and 2.
- The DFT_{20} decreased with the number of polishing cycles due to the abrasion and polishing of the aggregates. The sandstone test slabs had higher DFT_{20} values than the ones made with limestone 1 and limestone 2 aggregates. High DFT_{20} value is an indication of rough microtexture. The results were in agreement with the AIMS results.
- Mixtures with coarser aggregate gradation (PFC and SMA) had higher IFI, better skid resistance, than those with finer aggregate gradation (Type C and Type F). Aggregates with good resistance to abrasion and polishing had also better skid resistance compared to aggregates with poor resistance to abrasion and polishing.
- A predictive model for asphalt mixture friction loss was developed as a function of polishing cycles in the laboratory. This model was based on inputs that describe aggregate texture and angularity before and after the Micro-Deval abrasion test and gradation of asphalt mixtures. The model correlated well the experimental measurements in the laboratory.

CHAPTER 3: DEVELOPMENT OF A PREDICTIVE MODEL FOR LABORATORY COMPACTION OF ASPHALT MIXTURES

OVERVIEW

Compaction has significant influence on the performance of asphalt mixtures. Insufficient compaction leads to premature permanent deformation, excessive aging, and moisture damage (U.S. Army Corps of Engineers 2000). Compaction is the process by which the volume of asphalt mixtures is reduced, resulting in an increase in unit weight of the mixture and interlock among aggregate particles. Achieving proper density is vital for building long-lasting HMA pavements that resist distress; however, achieving specified density levels can be challenging, as some mixes require greater compactive effort than others. Compactability is the term used to quantify the effort needed to compact HMA to certain density levels. This part of the study focused on the development of a predictive model to quantify the compaction effort to compact HMA in the laboratory.

OBJECTIVE

The objective of this part of the study was to develop a predictive model for compactability of asphalt mixtures. This model was based on parameters that described aggregate shape characteristics, aggregate gradation, binder content, and binder properties at compaction temperatures. This objective was achieved through executing intensive laboratory experiments to quantify the effect of these parameters on the compaction of asphalt mixtures in the laboratory.

LITERATURE REVIEW

Several laboratory-measured parameters have been suggested as indicators of HMA compactability (National Center for Asphalt Technology [NCAT] 2011; Roberts et al. 1991). Researchers attempted to examine the use of laboratory-measured parameters for asphalt mixtures and their components as indicators of HMA compactability and resistance to permanent deformation. Bahia et al. (1998) quantified the densification characteristics of asphalt mixtures through developing an index called the Compaction Energy Index (CEI). The CEI is determined from the Servopac gyratory compactor as the area beneath the compaction curve from the eighth gyration to 92 percent of G_{mm}. They found that low CEI corresponded to less effort needed to

compact a given mixture. CEI is reasoned to be similar to the work applied by rollers to compact asphalt mixtures to the desired density during construction. The Bailey method (Pine 2004) presented parameters that defined the shape of the gradation curve to quantify compaction. Three parameters were used: CA, FA_c, and FA_f, which defined the shape of the coarse aggregate portion of the gradation, the shape of the coarse portion of the fine aggregate, and the shape of the fine portion of the fine aggregate, respectively. Each parameter was used to represent the packing characteristics of its belonging fraction of the combined blend. It was found that when the CA ratio increased, the mixtures were difficult to compact, whereas a decrease in the FA_c ratio decreased the compactability of the overall fine fraction and increased the compactability of the mixture. Leiva and West (2008) conducted a study to relate laboratory compaction to filed compaction. They examined several laboratory parameters that affect the compaction of asphalt mixtures. These parameters included the CEI, Bailey method ratios, compaction slope, locking point, and number of gyrations required to reach 92 percent of the maximum specific gravity. They concluded that all these characteristics were valuable in explaining compactability in the laboratory. Their results emphasized that gradation type, aggregate type, and aggregate size are the most significant variables to explain compactability of HMA specimens using the SGC. Muras (2010) conducted a research study to develop a correlation between HMA properties and compaction parameters. The purpose of this study was to predict compactability in the laboratory. Several mixtures including different gradation, aggregate, and asphalt binder characteristics were included. A correlation was found between the mixture properties and the compaction parameters. The analysis showed that the binder content in the asphalt mixture and the slope of the aggregate gradation curve are important in determining the compactability of the asphalt mixture.

FACTORS AFFECTING COMPACTION

Compacting asphalt mixtures is affected by several factors that include properties of the mixture components, environmental conditions, method of compaction, and work site conditions (U.S. Army Corps of Engineers 2000). The required compaction effort increases with an increase in aggregate angularity, size, and hardness. The grade and amount of asphalt binder also influence the compaction process. A mixture produced with too little asphalt is stiff and usually requires more compaction effort than a mixture with high asphalt binder content. The

temperatures of the air and mixture are also important factors that influence compaction (U.S. Army Corps of Engineers 2000).

BASIC MIX PARAMETERS

Mixture Properties

The aggregate gradation is a property of the mixture depending on its type. The mixture type, namely aggregate gradation, has a significant effect on the compactability (Pine 2004; Leiva and West 2008; Masad, Koneru et al. 2010). A cumulative two-parameter Weibull distribution was used to fit the gradation distribution between the standard aggregate size and cumulative percent passing. The cumulative two-parameter Weibull function has the form of:

$$F(x;k,\lambda) = 1 - e^{-\left(x/\lambda\right)^k} \tag{3-1}$$

where F is the dependent variable (cumulative percent passing in decimals), x is the independent variable (aggregate size in millimeters), and λ and k are the model parameters known as shape and scale, respectively. Figure 3-1 shows the effect of shape and scale parameters on the Weibull distribution function.

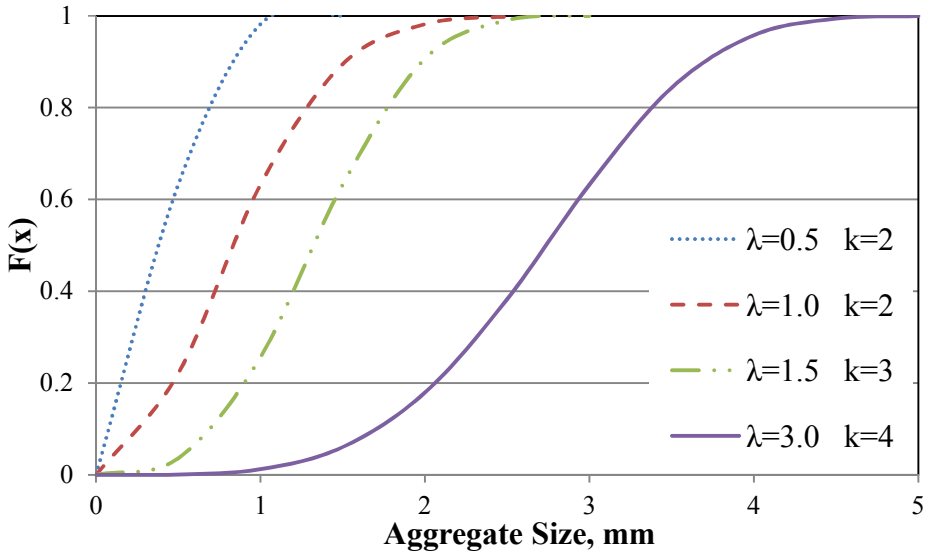

Figure 3-2. Example of Weibull Distribution Functions

Aggregate Properties

The aggregate shape characteristics are properties related to the aggregate source and type. The aggregate shape characteristics control the ease of asphalt mixture compactability (U.S. Army Corps of Engineers 2000; Leiva and West 2008). The aggregate shape characteristics can be measured using AIMS, as shown in Figure 2-7. Aggregate gradient angularity and texture have the most significant effect on the compactability of asphalt mixtures among the aggregate shape characteristics (Masad, Koneru et al. 2010). First, gradient angularity applies to both fine and coarse aggregate sizes and describes variations at the particle boundary that influence the overall shape. The gradient angularity quantifies changes along a particle boundary, with higher gradient values indicating a more angular shape. Gradient angularity has a relative scale of 0 to 10,000, with a perfect circle having a small non-zero value. The gradient angularity is analyzed by quantifying the change in the gradient on a particle boundary and is related to the sharpness of the corners of two-dimensional images of aggregate particles. Second, texture describes the relative smoothness or roughness of aggregate particles' surfaces. The AIMS texture applies to coarse aggregate sizes only and describes surface microtexture features less than approximately 0.5 mm in size, which are too small to affect the overall shape. Texture has a relative scale of 0 to 1000 with a smooth polished surface approaching a value of zero (Pine Instrument Company 2011).

Binder Properties

The properties of asphalt binders have a great influence on the ease of compactability (Leiva and West 2008). Binder can affect the asphalt mixture compactability through its content in the mixture. Also, the binder viscosity at the compaction temperature varies based on the binder grade.

LABORATORY EXPERIMENTS

Asphalt Mixture Overview

The researchers conducted a full factorial experiment that included three types of aggregates, four different asphalt mixture designs, two asphalt binders, and three different binder contents. Three aggregates were used: limestone 1 (soft aggregate), limestone 2 (intermediate aggregate), and sandstone (hard aggregate). Four different mixture designs were developed: fine dense-graded mixture (Type F), coarse dense-graded mixture (Type C), SMA mixture, and PFC

asphalt mixture (TxDOT 2004). Two asphalt binders were utilized in the experiments: unmodified binder (PG 67-22) and modified binder (PG 76-22). Three different binder contents were considered: optimum asphalt content (OAC%) and optimum asphalt content ± 0.5 percent (OAC±0.5%). Two replicates (A and B) were prepared at a given combination. Figure 3-2 shows the full factorial experimental design. The total number of specimens that were prepared in this part of the study was 144 specimens: two binders multiplied by three aggregates multiplied by four mixture types multiplied by three binder contents multiplied by two replicates. Table 3-1 shows the job mix formula (JMF) of these 12 mixtures at OAC percent. The JMF summarizes the aggregate gradation and OAC percentage for each mixture.

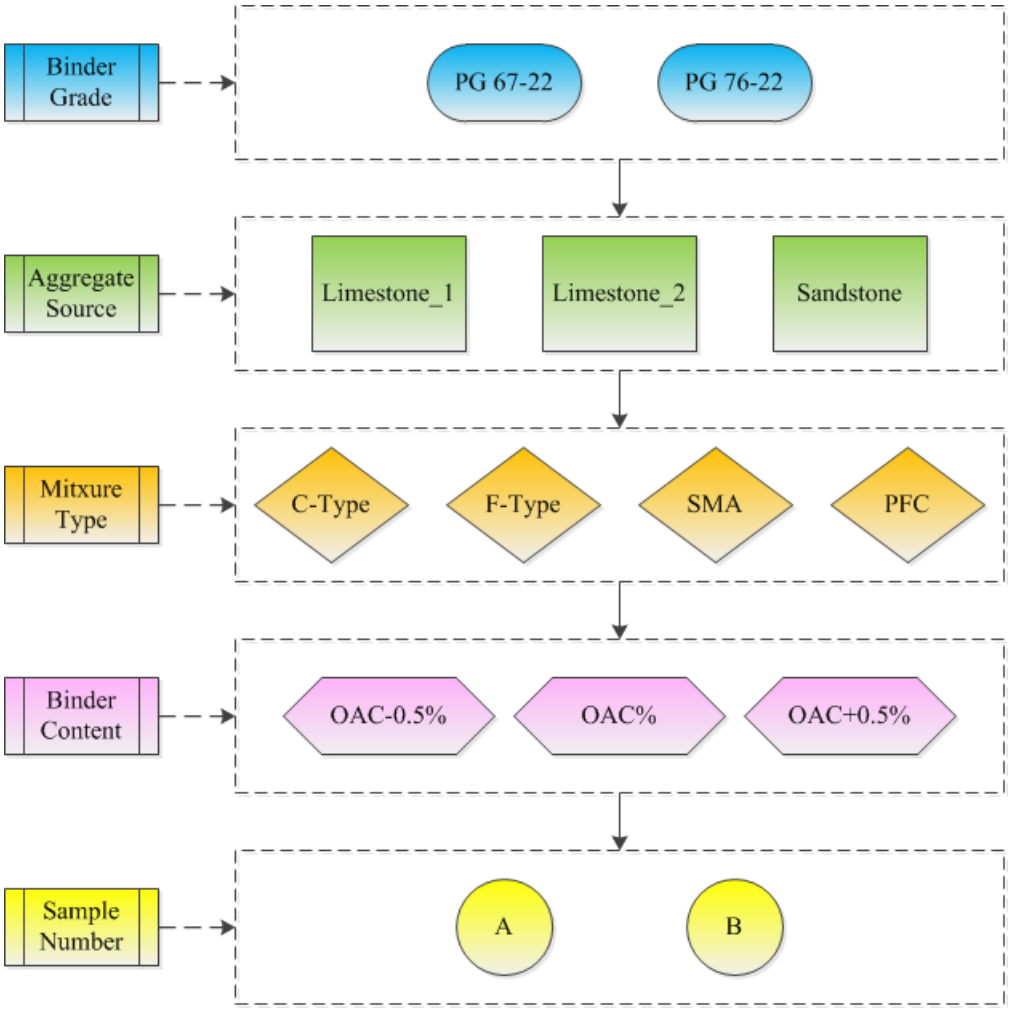

Figure 3-3. Full Factorial Matrix of Asphalt Mixture Properties

Table 3-1. Job Mix Formula for the Investigated Laboratory Mixtures

Aggregate Source	Limestone_1				Limestone_2				Sandstone			
Mixture Type	C-Type	F-Type	SMA	PFC	C-Type	F-Type	SMA	PFC	C-Type	F-Type	SMA	PFC
G_{mm}	2.399	2.382	2.382	2.402	2.454	2.426	2.467	2.440	2.406	2.397	2.380	2.361
OAC % (by Mix Wt.)	5.1	5.7	5.4	4.4	4.5	5.2	5.2	4.5	5.6	6.0	6.3	6.8
Sieve Size, mm	Cumulative % Passing											
25.0	100	100	100	100	100	100	100	100	100	100	100	100
19.0	100	100	100	100	99.6	100.0	99.2	99.0	100	100	100	100
9.50	80.8	100	59.7	43.8	74.0	94.9	49.1	36.1	83.5	100	74.0	49.2
4.75	57.0	85.6	31.6	16.4	58.7	80.4	31.8	17.1	55.1	81.9	30.0	16.2
2.36	33.3	38.4	18.9	3.1	36.8	50.4	21.7	8.8	32.3	38.5	19.3	8.5
0.60	14.1	15.4	14.3	2.0	17.5	23.7	15.6	4.1	16.0	12.7	15.2	5.7
0.30	11.0	11.9	12.2	2.0	8.7	11.5	12.1	2.4	8.8	8.5	12.3	4.3
0.075	6.5	7.0	9.7	1.8	2.8	3.5	9.6	1.5	2.5	4.1	9.4	2.8

Determination of Compactability Model Parameters

The researchers developed a model for laboratory compaction prediction based on parameters that describe aggregate shape characteristics, aggregate gradation, binder content, and binder properties at compaction temperatures. This section discusses these parameters.

Aggregate Gradation

The researchers focused on the methods used to describe the aggregate gradation in Chapter 2. The aggregate gradation distribution was determined using the cumulative two-parameter Weibull function, as shown in Equation (3-1). Table 3-2 presents the scale and shape parameters of the Weibull distribution function.

Table 3-2. Scale and Shape Parameters of Weibull Distribution Function

Gradation Parameters	Limestone_1				Limestone_2				Sandstone			
	C-Type	F-Type	SMA	PFC	C-Type	F-Type	SMA	PFC	C-Type	F-Type	SMA	PFC
λ	5.55	3.33	9.28	11.55	5.62	3.03	10.00	12.35	5.55	3.49	8.10	11.03
K	0.919	1.321	1.233	2.328	0.842	0.910	1.199	2.351	0.973	1.412	1.385	2.136

Aggregate Characterization

The surface texture (TX) and gradient angularity (GA) were the aggregate shape characteristics of interest. The determination of aggregate source and source blend shape characteristics were based upon the procedure given by the AASHTO (2010). This standard was used to characterize the combined shape values for an aggregate source from the individual

particle shape properties using gradation analysis and shape properties determined by means of digital image analysis. The characterization of the coarse portion of the aggregate distribution was done by using the sieve sizes of 9.5 mm, 6.35 mm, and 4.75 mm, while 2.36 mm, 0.6 mm, and 0.3 mm were the sieves used to characterize the fine portion of the aggregate distribution. A hundred particles per each size were scanned to get the shape characteristics using the AIMS. After getting the means of the shape characteristics of interest (TX and GA), AASHTO designation PP64-10 procedures (AASHTO 2010) were used to calculate the combined shape values for the whole mixture. Table 3-3 includes the combined values for TX and GA for each aggregate source based on the gradation analysis of each asphalt mixture.

Table 3-3. Combined Texture and Gradient Angularity Values for the Laboratory Mixtures

Aggregate Source	Limestone_1				Limestone_2				Sandstone			
Mixture Type	C-type	F-type	SMA	PFC	C-type	F-type	SMA	PFC	C-type	F-type	SMA	PFC
TX	92.5	82.0	97.1	98.2	126.7	102.7	137.3	139.8	291.2	284.5	294.2	294.9
GA	2552.7	2474.5	2587.4	2595.5	2735.5	2799.0	2707.0	2700.5	2716.2	2664.0	2739.5	2744.9

Binder Characterization

Binder characterization was performed using the Brookfield Rotational Viscometer according to AASHTO TP48-97 (AASHTO 2006). In this study, two binder grades were used: PG 67-22 and PG 76-22. Before testing, the binders were short-term aged (Rolling Thin Film Oven [RTFO] condition) to simulate the aging during mixing and compacting asphalt mixtures in the field. The viscosity of both binders was tested and measured at two temperatures: 135°C and 163°C. Figure 3-3 shows the Brookfield viscosity-temperature relationships for the two investigated binders. Table 3-4 shows the specified mixing and compaction temperatures and the viscosity (in Pa.s) at compaction temperature for the investigated binders.

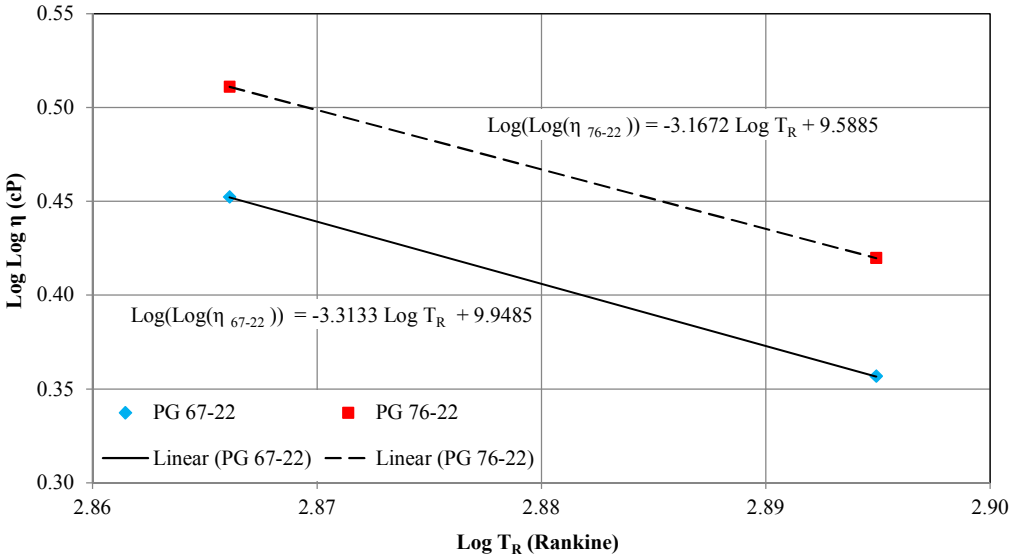

Figure 3-4. Brookfield Viscosity-Temperature Relationships of the Investigated Binders

Table 3-4. The Viscosity of Binders at Compaction Temperatures

PG	Mixing Temperature, °F (°C)	Compaction Temperature, °F (°C)	η (Pa.s) @ Comp. Temp.
67-22	290 (143)	250 (121)	1.504
76-22	325 (163)	300 (149)	0.826

Specimen Preparation

For each asphalt mixture, aggregate and asphalt binder were blended according to the JMF given in Table 3-1. Two replicates were prepared per each mixture with the dimensions of 150 mm (6.0 inches) in diameter and 62.5 mm (2.5 inches) in height. The SGC was used for compacting the test specimens in accordance with AASHTO PP 60-09 (AASHTO 2009). The SGC applied a pressure of 600 kPa on the specimen at an angle of 1.25° to the mold assembly. Figure 3-4 shows four different asphalt mixture samples made using limestone 1 aggregate at OAC. The researchers prepared eight more specimens using limestone 2 aggregate and PG 76-22 at OAC but at different compaction temperatures. Two replicates of Type C mixture were mixed at 130°C, while another two replicates of Type C mixture were mixed at 170°C to include a wide range of viscosity values. Similarly, four specimens of SMA mixture were mixed at the same two temperatures. The viscosity of the PG 76-22 at 130° was 2.356 Pa.s, while its viscosity at 170°C was 0.316 Pa.s.

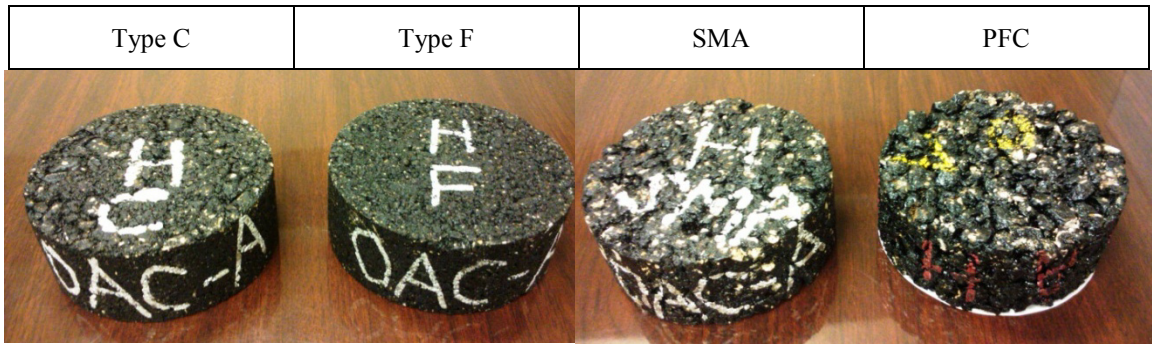

Figure 3-5. Examples of Different Asphalt Mixture Samples

COMPACTABILITY CHARACTERIZATION

The SGC used in the study had the ability to save a text file with the compaction data for each test specimen upon completion of compaction. Each file contained general data about the test including date, time, sample diameter, gyration rate, vertical stress, gyration angle, weight of material, and theoretical maximum specific gravity. The text files also contained information about each gyration in the compaction process including gyration number, sample height, and shear stress. The researchers used the data that documented the change in height with number of gyrations.

Following compaction of the two replicates for each mixture, some loose material was used for determining the theoretical maximum specific gravity (G_{mm}) (ASTM 2011). Once each laboratory molded sample had sufficiently cooled, its bulk specific gravity (G_{mb}) was measured using the CoreLok® machine (AASHTO 2004). The final G_{mb} was used to correct the calculated bulk specific gravities by the SGC at each gyration, whereas the G_{mm} was used to calculate the density or air void content ($\%AV$) of the compacted samples. Equations (3-2) through (3-5) show how the air void content can be calculated from the sample height at each gyration:

$$V = \left(\frac{\pi D^2}{4}\right) * h \tag{3-2}$$

$$\rho_{uncorr} = \frac{W}{V} \tag{3-3}$$

$$\rho_{corr.} = \rho_{uncorr.} * \left(\frac{G_{mb\,final}}{\rho_{uncorr._{final}}}\right) \tag{3-4}$$

$$AV\% = 100 * \left(1 - \frac{\rho_{corr.}}{G_{mm}} \right) \quad (3\text{-}5)$$

where V is the sample volume in cc, D is the sample diameter in cm, h is the sample height in cm, W is the sample weight in g, ρ_{uncorr} is the uncorrected bulk specific gravity at each gyration, ρ_{corr} is the corrected bulk specific gravity at each gyration, $G_{mb\,final}$ is the measured bulk specific gravity using the CoreLok machine, $\rho_{uncorr\,final}$ is the uncorrected bulk specific gravity at last gyration, G_{mm} is the measured theoretical maximum specific gravity, and $AV\%$ is the percent of the air void content at each gyration. The change in percent air void versus number of gyrations can be described using Equation (3-6). Figure 3-5 shows an example of the relationship between number of gyrations and corrected air void content.

$$AV\% = a * LN(No.of\ Gyrations) + b \quad (3\text{-}6)$$

where a and b are the slope and intercept of the relationship, respectively.

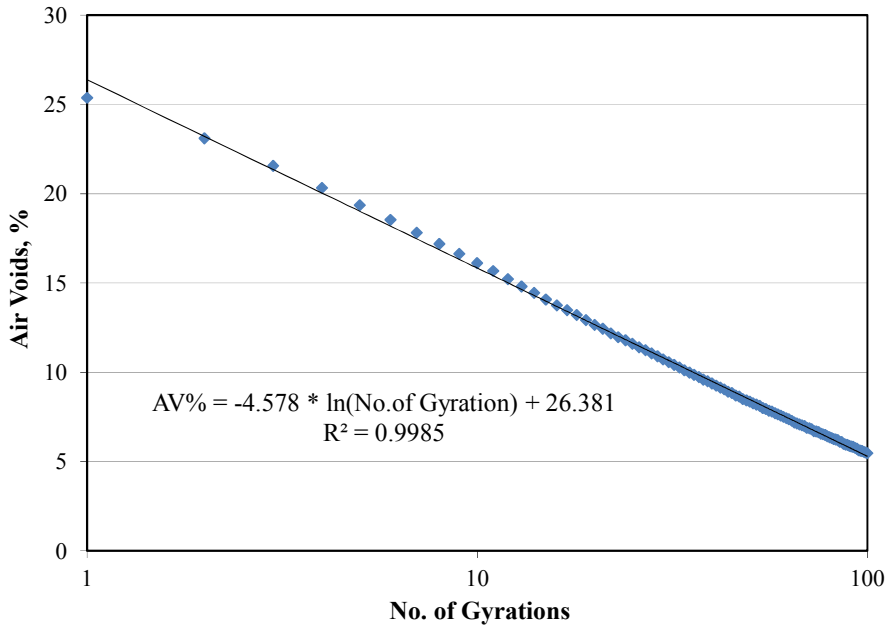

Figure 3-6. An Example of a Compaction Curve

DEVELOPMENT OF COMPACTABILITY MODELS

The compaction curves for the laboratory specimens were generated as described earlier. Figure 3-6 shows the compaction curves for different mixtures, while Figure 3-7 shows

compaction curves for two replicates of different asphalt mixtures. Figure 3-8 shows the compaction for some asphalt mixtures at different asphalt contents, while Figure 3-9 shows compaction curves for two replicates of the same asphalt mixture at different asphalt contents. The results showed clearly that the mixture type and the asphalt content have great influence on the slope and intercept values of compaction curves.

A multiple linear regression analysis was conducted using the SPSS statistical software to predict both slope and intercept of the compaction curve for asphalt mixtures. Different models were developed to describe slope and intercept. The analysis included the parameters that describe the properties of aggregates and binders: gradation shape parameter, λ; gradation scale parameter, K; aggregate angularity, GA; aggregate texture, TX; asphalt content, P_b; and binder viscosity in Pa.s, η.

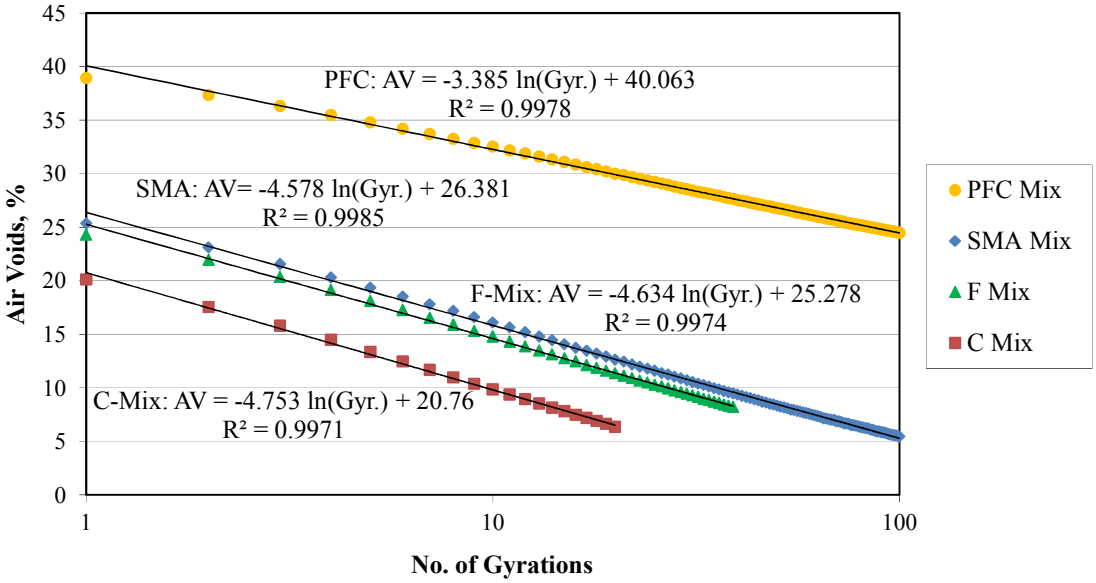

Figure 3-7. Example of Compaction Curves for Different Mix Types

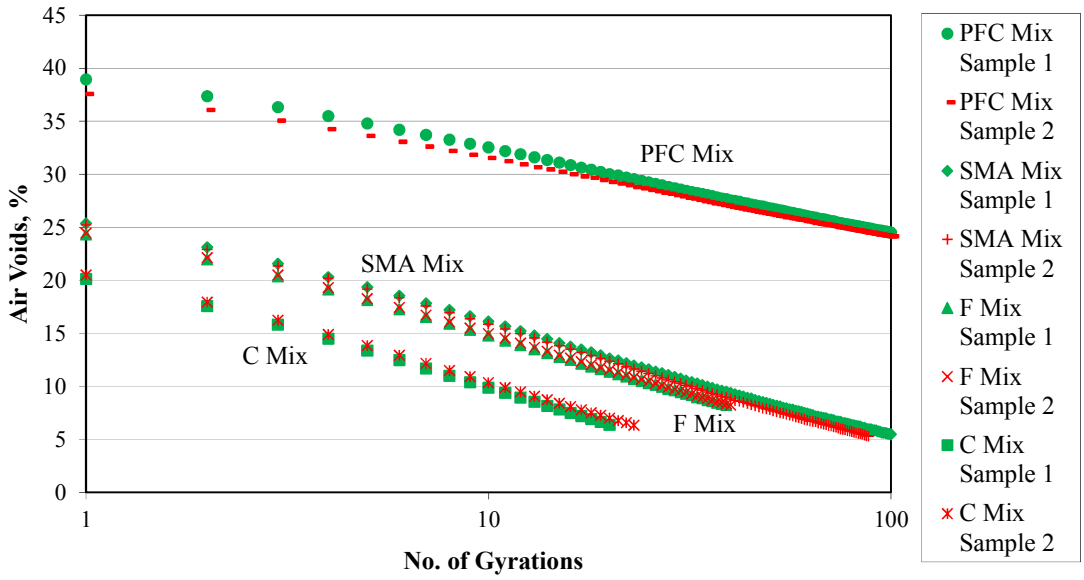

Figure 3-8. Example of Two Replicate Compaction Curves for Different Mix Types

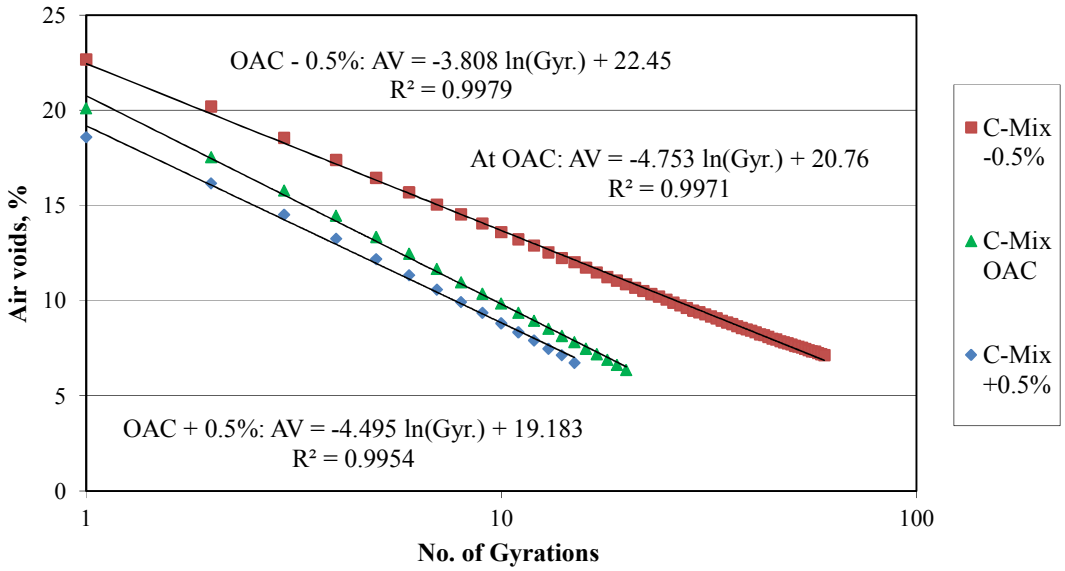

Figure 3-9. Example of Compaction Curves for Samples Having Different Asphalt Content

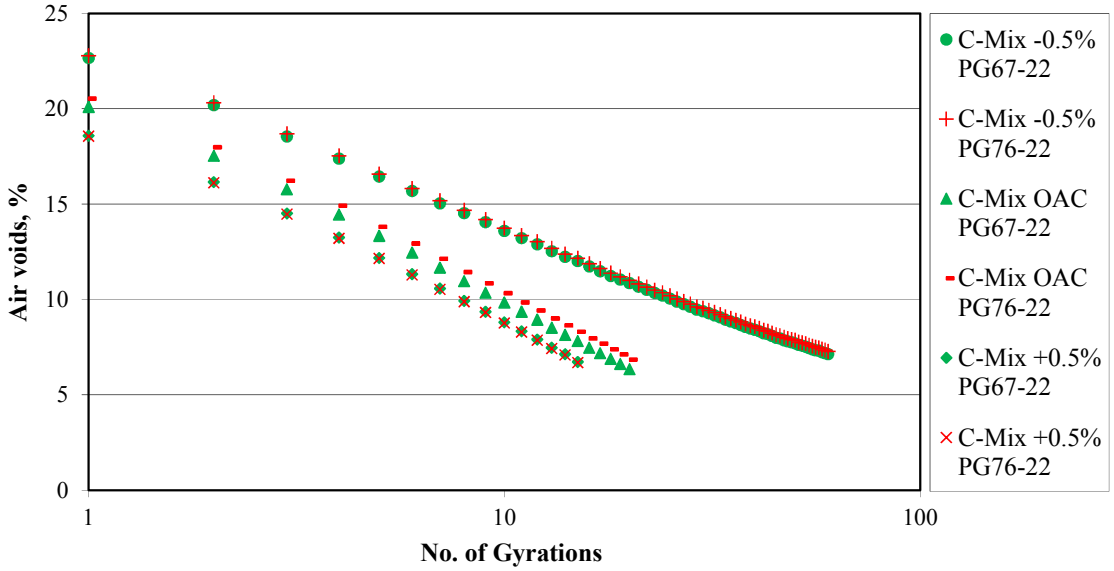

Figure 3-10. Example of Two Replicate Compaction Curves for Samples Having Different Asphalt Content

Slope Model

After comprehensive analysis, the researchers concluded that the best model for predicting slope is a linear mixed model, as given in Equation (3-7). This model included the following parameters: λ, k, GA, TX, and P_b.

$$a = -15.128 + 1.116*\lambda - 1.792*K + 0.0044*GA + 0.0108*TX + 0.1337*\lambda*K - 0.0004*\lambda*GA - 0.0011*\lambda*TX + 0.2545*K*P_b - 0.0002*GA*P_b \quad (3\text{-}7)$$

where a = slope of the compaction curve, λ = gradation shape parameter, K = gradation scale parameter, GA = aggregate angularity, TX = aggregate texture, and P_b = asphalt content.

To assess the performance of the investigated predictive procedures, the correlation of the predictive and measured values was evaluated using goodness-of-fit statistics. The criteria were based on the coefficient of determination (R^2) and the standard error divided by the standard deviation of measured slope values about the mean measured (S_e/S_y). The R^2 is simply the square of the correlation coefficient between the measured and predicted slope (higher R^2 indicates higher accuracy). The S_e/S_y is an indicator of the relative improvement in accuracy; thus, smaller value points out better accuracy. Figure 3-10 shows predicted versus measured slope values with

very good correlation ($R^2 = 0.90$, $S_e/S_y = 0.33$) based on 152 data points. Table 3-5 shows descriptive statistics for the parameters used in the slope model.

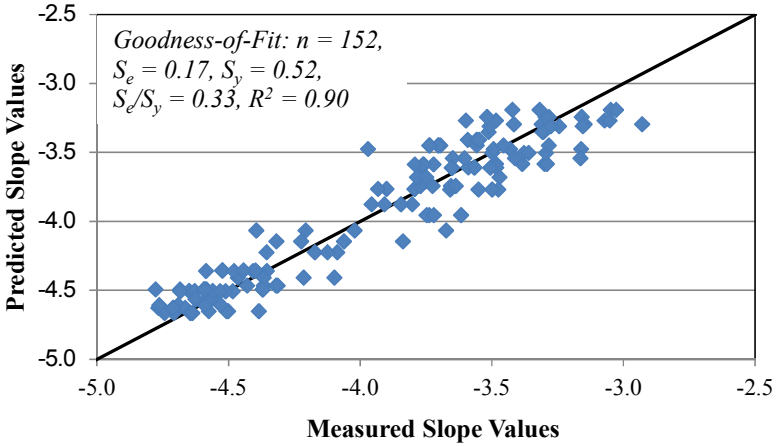

Figure 3-11. Predicted vs. Measured Slope Values

Table 3-5. Descriptive Statistics of Slope Model

Property	Count	Mean	Standard Deviation	Coefficient of Variation
a	152	-3.9	0.52	-13.3%
λ	152	7.4	3.24	43.6%
k	152	1.4	0.55	38.4%
GA	152	3022.2	178.05	5.9%
TX	152	171.8	88.97	51.8%
P_b	152	5.4	0.87	16.1%

Researchers performed an analysis of variance (ANOVA) to determine which parameters in the slope model significantly affected predicted slope. Table 3-6 provides the ANOVA results of the predicted slope. The results show that all the included factors had a significant effect on the predicted slope at a level of significance $\alpha = 5\%$ (P-values ≤ 0.05). Figure 3-11 shows the residuals versus the predicted slope values. The residual plot should look completely random without any pattern to provide a good indication of the nature of the relationship. The residual plot for the predicted slope values looks random without any pattern.

Table 3-6. ANOVA for Slope Model Parameters

Source	Numerator DF	Denominator DF	F-Statistic	P-value	Significant at α = 5%
Intercept	1	152	157.53	3.03E-25	Yes
λ	1	152	66.56	1.19E-13	Yes
k	1	152	45.05	3.58E-10	Yes
GA	1	152	169.32	1.74E-26	Yes
TX	1	152	321.13	2.60E-39	Yes
λ * k	1	152	54.31	1.02E-11	Yes
λ * GA	1	152	113.29	4.06E-20	Yes
λ * TX	1	152	148.64	2.81E-24	Yes
k* P_b	1	152	55.03	7.81E-12	Yes
GA * P_b	1	152	89.85	4.92E-17	Yes

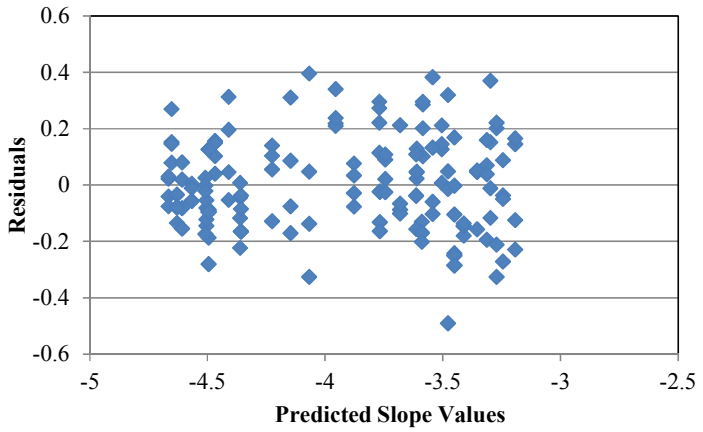

Figure 3-12. Residual Plot of Slope Model

Intercept Model

The best model for predicting intercept was found to be a linear mixed model, as given in Equation (3-8). The intercept model included the following parameters: λ, k, GA, TX, P_b, and η.

$$b = 16.387 + 7.017^{*}\lambda + 18.042^{*}K - 16.135^{*}P_b + 17.687^{*}\eta - 1.1897^{*}\lambda^{*}K - 0.0018^{*}\lambda^{*}GA - 0.0061^{*}\lambda^{*}TX + 0.5853^{*}\lambda^{*}\eta + 0.0382^{*}K^{*}TX - 2.672^{*}K^{*}\eta + 0.0046^{*}GA^{*}P_b - 0.0064^{*}GA^{*}\eta \quad (3\text{-}8)$$

where b = intercept of the compaction curve, λ = gradation shape parameter, K = gradation scale parameter, GA = aggregate angularity, TX = aggregate texture, P_b = asphalt content, and η = binder viscosity in Pa.s.

To assess the performance of the investigated predictive procedures, the correlation of the predictive and measured values was evaluated using goodness-of-fit statistics. Figure 3-12 shows predicted versus measured intercept values with very good correlation ($R^2 = 0.94$, $S_e/S_y = 0.25$) based on 152 data points. Table 3-7 shows descriptive statistics for the parameters used in the intercept model.

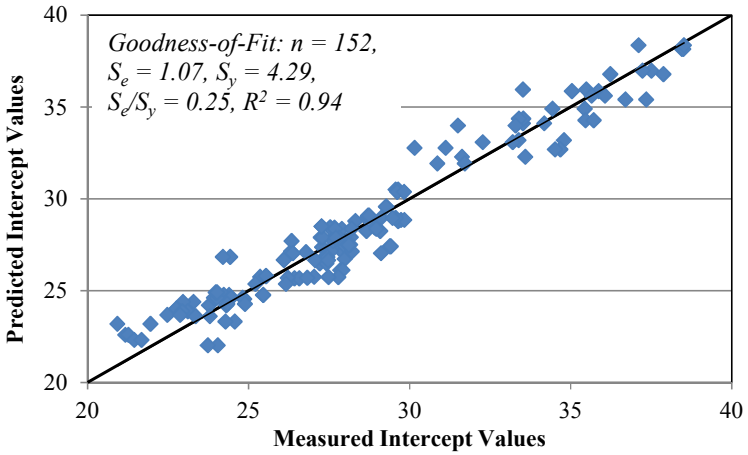

Figure 3-13. Measured vs. Predicted Intercept Values

Table 3-7. Descriptive Statistics of Intercept Model

Property	Count	Mean	Standard Deviation	Coefficient of Variation
b	152	28.5	4.29	15.1%
λ	152	7.4	3.24	43.6%
k	152	1.4	0.55	38.4%
GA	152	3022.2	178.05	5.9%
TX	152	171.8	88.97	51.8%
P_b	152	5.4	0.87	16.1%
η	152	1.2	0.41	34.7%

An ANOVA was performed to determine which factors of the intercept model significantly affected the predicted intercept. Table 3-8 provides the ANOVA results of the

predicted intercept. The results show that all the included factors had a significant effect on the predicted intercept at a level of significance $\alpha = 5\%$ (P-values ≤ 0.05). Figure 3-13 shows the residuals versus the predicted intercept values. The residual plot should look completely random without any pattern to provide a good indication of the nature of the relationship. The residual plot for the predicted intercept values seems to fall into two parts (left and right), but it is still acceptable due to the investigated intercept value ranges.

Table 3-8. ANOVA for Intercept Model Parameters

Source	Numerator DF	Denominator DF	F-Statistic	P-value	Significant at $\alpha = 5\%$
Intercept	1	152	87.23	1.14E-16	Yes
λ	1	152	89.09	6.25E-17	Yes
k	1	152	140.33	2.40E-23	Yes
P_b	1	152	135.52	8.56E-23	Yes
η	1	152	17.57	4.68E-05	Yes
λ * k	1	152	101.84	1.20E-18	Yes
λ * GA	1	152	84.19	3.03E-16	Yes
λ * TX	1	152	110.18	1.00E-19	Yes
λ * η	1	152	31.25	1.02E-07	Yes
k * TX	1	152	150.00	1.99E-24	Yes
k * η	1	152	15.27	1.40E-04	Yes
GA * P_b	1	152	104.48	5.41E-19	Yes
GA * η	1	152	23.39	3.22E-06	Yes

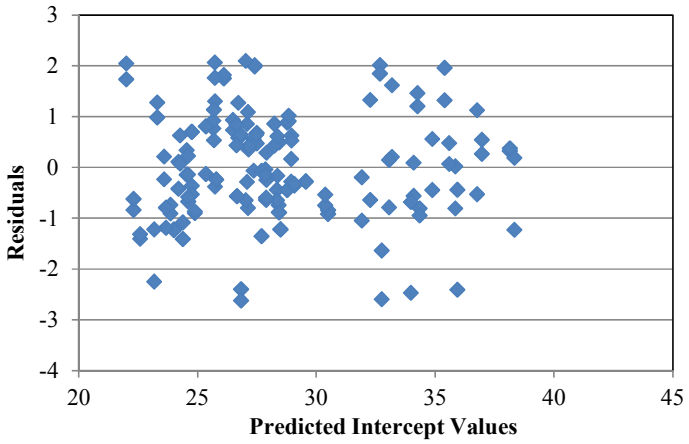

Figure 3-14. Residual Plot of Intercept Model

SENSITIVITY ANALYSIS

The predictive models developed and expressed by Equations (3-7) and (3-8) are rational relative to all variables. The sensitivity of the models to the variables of the system was examined through the application of the predictive models to a series of different conditions. The interaction effects between each variable and the other were investigated while the other effects were fixed.

Slope Model

Figure 3-14 shows the interaction effects of the slope model parameters on the predicted slope values. The predicted slope values are directly proportional with the interaction effects between λ & K and K & P_b, whereas they are inversely proportional with the interaction effects between λ & GA, λ & TX, and GA & P_b.

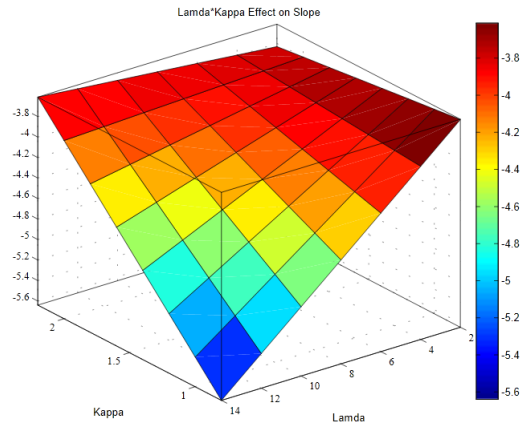

(a) λ and K Effect on Slope

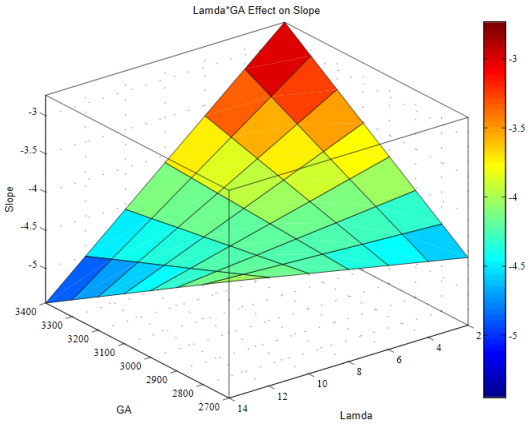

(b) λ and GA Effect on Slope

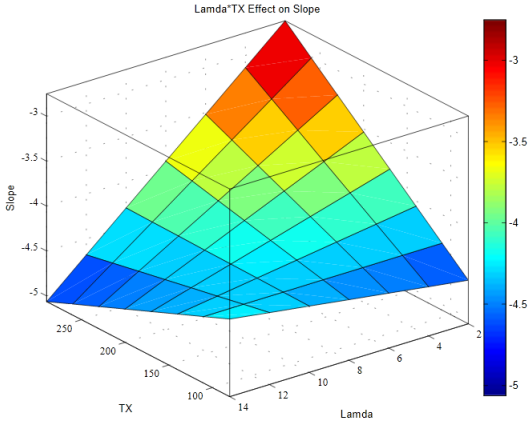

(c) λ and TX Effect on Slope

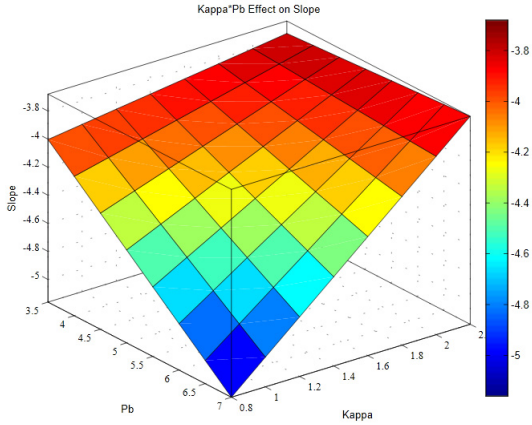

(d) K and P_b Effect on Slope

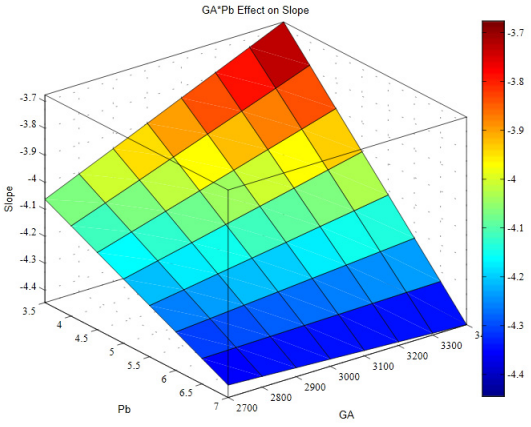

(e) GA and P_b Effect on Slope

Figure 3-15. The Interaction Effect on the Predicted Slope Values

Intercept Model

Figure 3-15 shows the interaction effects of the intercept model parameters on the predicted intercept values. The predicted intercept values are directly proportional with the interaction effects between λ & η, K & TX, and GA & $P_{b,}$, whereas they are inversely proportional with the interaction effects between λ & K, λ & GA, λ & TX, K & η, and GA & η.

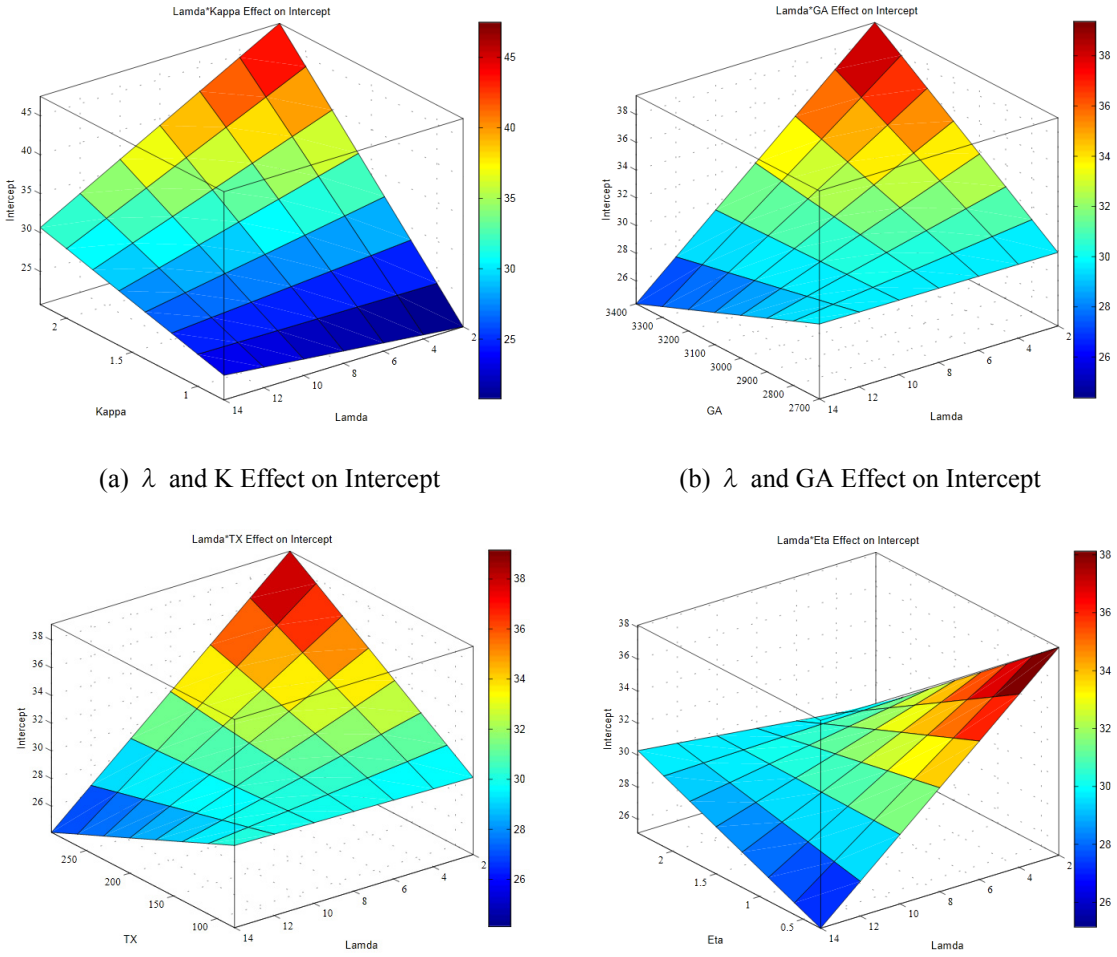

(a) λ and K Effect on Intercept

(b) λ and GA Effect on Intercept

(c) λ and TX Effect on Intercept

(d) λ and η Effect on Intercept

Figure 3-16. The Interaction Effect on the Predicted Intercept Values

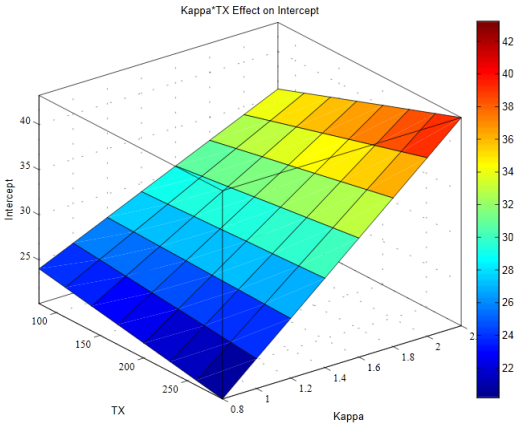

(e) K and TX Effect on Intercept

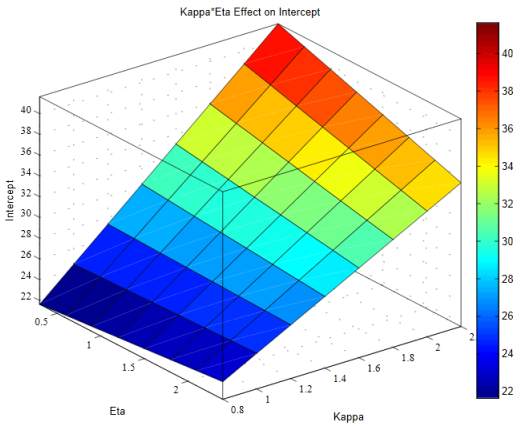

(f) K and η Effect on Intercept

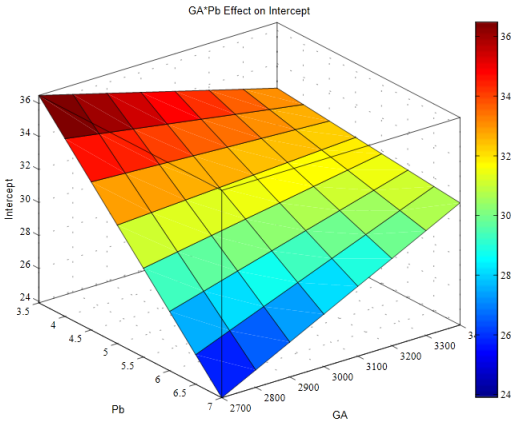

(g) GA and P_b Effect on Intercept

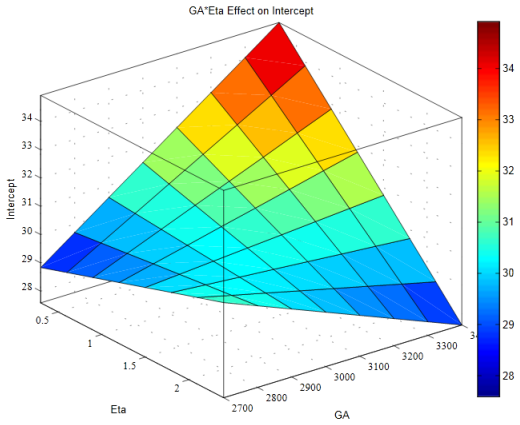

(h) GA and η Effect on Intercept

Figure 3-17. The Interaction Effect on the Predicted Intercept Values (Continued)

The gradation parameters (λ and k) were found to have a significant impact on the slope and intercept values of the compaction curves. As presented in Figure 3-6, the Type C mixtures with low values of gradation parameters λ and k had the highest slope value with the lowest intercept value, while the PFC mixtures with high values of gradation parameters λ and k had the lowest slope value with the highest intercept value. In addition, the binder content showed a significant effect on the slope and intercept values of the compaction curves. As shown in Figure 3-8, at a certain gradation, the higher binder the content, the higher the slope and the lower the intercept values. The increase in texture and angularity of aggregates was found to reduce the slope values and increase the intercept values of the compaction curves. In addition, the viscosity of the binder showed some effect on the intercept values of the compaction curves.

CONCLUSIONS AND RECOMMENDATIONS

This part of the research study investigated the ability of predicting slope and intercept of the laboratory compaction curves of asphalt mixtures. Two statistical linear mixed models were used to predict slope and intercept based on parameters that describe aggregate shape characteristics, aggregate gradation, binder content, and binder viscosity at compaction temperatures. The results showed clearly that a strong correlation was found between the measured intercept and slope and the predicted ones. These models can be used to assess the compactability of asphalt mixture in the laboratory. These methods provide the potential of predicting field compaction based on the mix design and aggregate and binder characteristics. Kassem et al. (2012) correlated the field compaction to the intercept and slope of laboratory curves. The models developed herein predict the slope and intercept of the compaction curves. These values can be used as inputs in the methods developed by Kassem et al. (2012) to predict the number of passes needed to compact a given mixture in the field. Engineers can also use this method as a preliminary check on the compactability of an asphalt mixture based on its characteristics that include aggregate angularity and texture, aggregate gradation, binder content, and binder viscosity at compaction temperatures. Engineers can also modify the type of aggregates, binder, or mix design to design a mix that doesn't require many number of roller passes to reach the target density in the field. The authors recommend validating both models of intercept and slope for mixes with different aggregate sources, different mix types, different binder types, and content.

CHAPTER 4: EFFECT OF COMPACTION ON SKID RESISTANCE OF ASPHALT PAVEMENTS

INTRODUCTION

Chapters 2 and 3 presented an introduction and literature search on skid resistance and compaction of asphalt mixtures, respectively. This part of the study examined the effect of compaction method and level of compaction on skid resistance of asphalt pavements. In addition, the researchers evaluated the influence of compaction on the internal structure of asphalt mixtures. Recently, researchers at the Texas Transportation Institute constructed several test sections at the Riverside Campus of Texas A&M University as a part of TxDOT Research Project 0-6692, where they evaluated several factors that affect the compaction of asphalt mixtures (Kassem et al. 2012). The test sections included HMA and WMA. These test sections were compacted using different compaction rollers: static and vibratory steel-wheel rollers with a varying number of roller passes. In this part of the research project, the researchers studied the frictional characteristics of some of these test sections in order to evaluate the effect of compaction on skid resistance of asphalt pavements. In addition, they utilized the X-ray Computed Tomography (CT) to study the influence of compaction method and level of compaction on the internal structure of asphalt mixtures.

OBJECTIVES

The objectives of this part of the study were as follows:

1. Study the effect of compaction method and level of compaction on skid resistance of asphalt pavement.
2. Evaluate the effect of mixture type (coarse vs. fine) and technology (HMA vs. WMA) on skid resistance of asphalt pavement.
3. Study the effect of compaction method and level of compaction on the internal structure of asphalt mixtures.

RESEARCH TASKS

The researchers carried out the following tasks in order to achieve the aforementioned objectives:

1. Identified three test sections that were compacted using different compaction rollers.

2. Measured the frictional characteristics of the test sections using DFT and CTMeter.
3. Calculated the IFI for each test section.
4. Extracted field cores from strips that were compacted using a different number of roller passes.
5. Utilized the X-ray Computed Tomography to study the air void distribution of the extracted field cores.

DESCRIPTION OF THE TEST SECTIONS

Several test sections were constructed at the Riverside Campus of Texas A&M University as part of TxDOT Research Project 0-6992. These test sections were constructed to evaluate the effect of the compaction method, asphalt mixture type, base type, compaction temperature, and joint conditions on the compactability of asphalt mixtures and uniformity of the compaction across the mat. Each test section was divided into sub-test sections that were compacted using different compaction methods. In the study herein, the researchers measured the frictional characteristics on selected sub-test sections. Figure 4-1 shows examples of the schematic layouts and the rolling patterns for the selected sub-test sections. Each sub-test section was compacted using a steel-wheel roller that operated at a different mode: static or vibratory (Figure 4-2). Each sub-test section was 9 ft wide and 120 ft long. Each sub-test section was then divided into several smaller strips (approximately 30 ft long), which were compacted using a varying number of roller passes. The researchers selected three test sections: Test Section No. 1 was constructed using Type C mix with binder PG 76-22, Test Section No. 2 was constructed using Type D mix with binder PG 64-22, and Test Section No. 3 was Type D mix with PG 64-22 and warm mix additive. TxDOT Type C is a relatively coarse mix with a nominal maximum size of 0.5 inch. Type D is one size finer than Type C (TxDOT 2004).

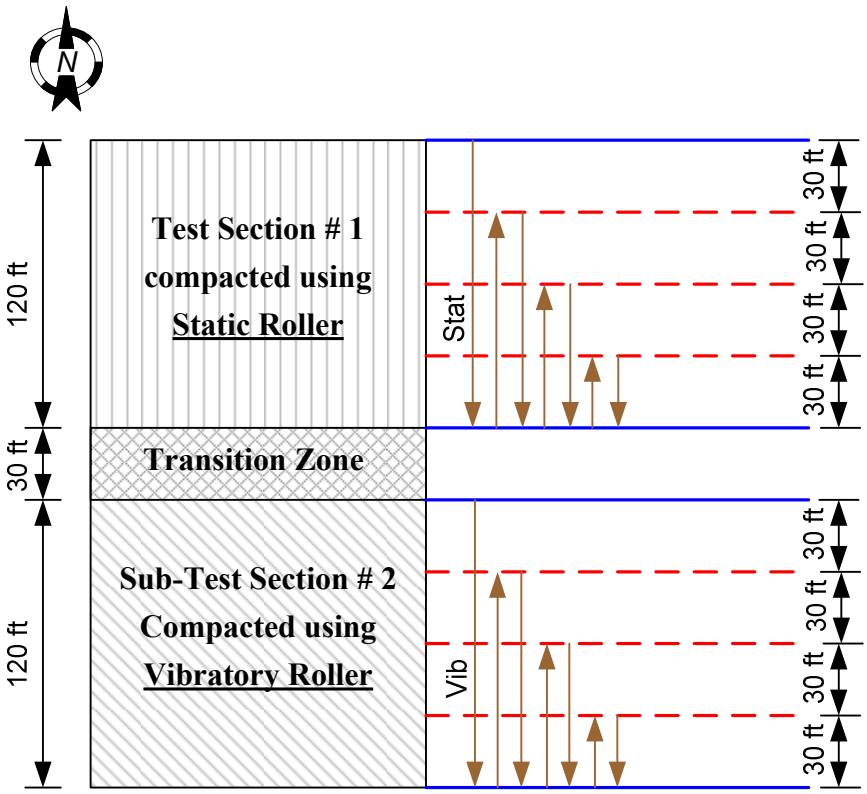

Figure 4-1. Schematic of Selected Sub-Test Sections and the Rolling Patterns

Figure 4-2. Steel-Wheel Roller

FRICTIONAL CHARACTERISTIC MEASUREMENTS

The researchers studied the frictional characteristics of the test section using the CTMeter and DFT (Figure 4-3). The CTMeter and DFT were used to measure the MPD and coefficient of friction of the surface of the test sections, respectively. The researchers measured the coefficient of friction and MPD at two different locations on each test strip. Table 4-1 presents the MPD and DFT_{20} measurements. The IFI was calculated for different test sections using Equation (2-2).

(a) CTMeter Setup (b) DFT Setup

Figure 4-3. Field Frictional Characteristic Measurements Using CTMeter and DFT

Figures 4-4 through 4-6 show the MPD values versus the number of passes for the evaluated test sections. The MPD decreased with the number of passes for the test sections compacted using both static and vibratory rollers. However, the change in the MPD for the test sections compacted using the vibratory roller was steeper compared to the corresponding test sections compacted using the static roller. The MPD is a measure of the macrotexture of pavement surface. A smooth surface yields a low MPD, while a rough surface yields a high MPD. The vibratory roller was found to yield a smoother surface than the static roller. In addition, it was found that the compaction process had less impact on the coefficient of friction at 20 km/hr (DFT_{20}) for a given asphalt mixture, as shown in Table 4-1. The DFT_{20} is considered an indication of the pavement microtexture, so it was not expected that the microtexture would change for a given mixture as a result of different compaction levels. The compaction is

significant at the macrotexture level and not at the microtexture level. However, the researchers found a fair relationship between the MPD and the coefficients of friction at 80 km/h, as Figure 4-7 shows.

Table 4-1. Coefficient of Friction and MPD Measurements

Test Section #	Compaction Method	No. of Passes	MPD	S_p	DFT_{20}	IFI
1	Static	1	0.62	69.37	0.655	0.3503
		3	0.60	68.02	0.652	0.3459
		5	0.48	57.26	0.668	0.3240
		7	0.49	58.15	0.678	0.3305
	Vibratory	1	0.59	66.67	0.639	0.3377
		3	0.47	55.91	0.620	0.3029
		5	0.46	55.01	0.601	0.2934
		7	0.37	47.61	0.583	0.2651
2	Static	1	0.40	50.30	0.593	0.2768
		3	0.40	49.86	0.593	0.2756
		5	0.39	49.41	0.591	0.2735
		7	0.34	44.47	0.554	0.2458
	Vibratory	1	0.56	64.66	0.617	0.3241
		3	0.42	51.65	0.591	0.2802
		5	0.34	44.70	0.599	0.2602
		7	0.28	39.32	0.569	0.2314
3	Static	1	0.61	69.14	0.675	0.3578
		3	0.48	57.48	0.700	0.3365
		5	0.46	55.46	0.698	0.3294
		7	0.47	56.58	0.691	0.3304
	Vibratory	1	0.54	62.19	0.694	0.3478
		3	0.48	57.48	0.670	0.3254
		5	0.35	45.60	0.692	0.2917
		7	0.27	37.97	0.620	0.2393

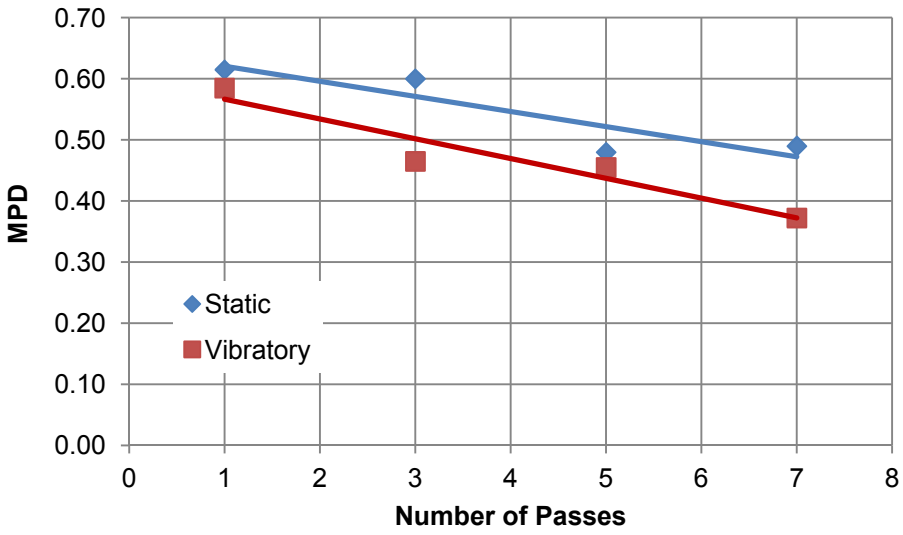

Figure 4-4. MPD vs. Number of Passes for Test Section 1

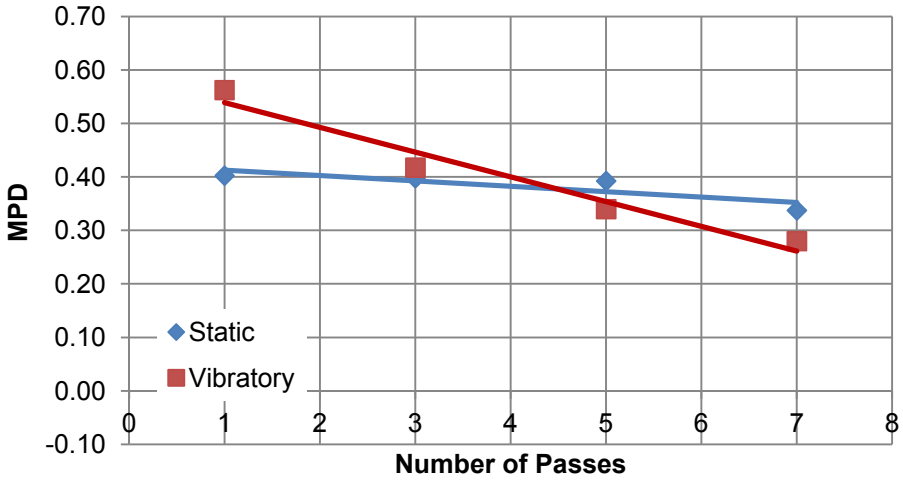

Figure 4-5. MPD vs. Number of Passes for Test Section 2

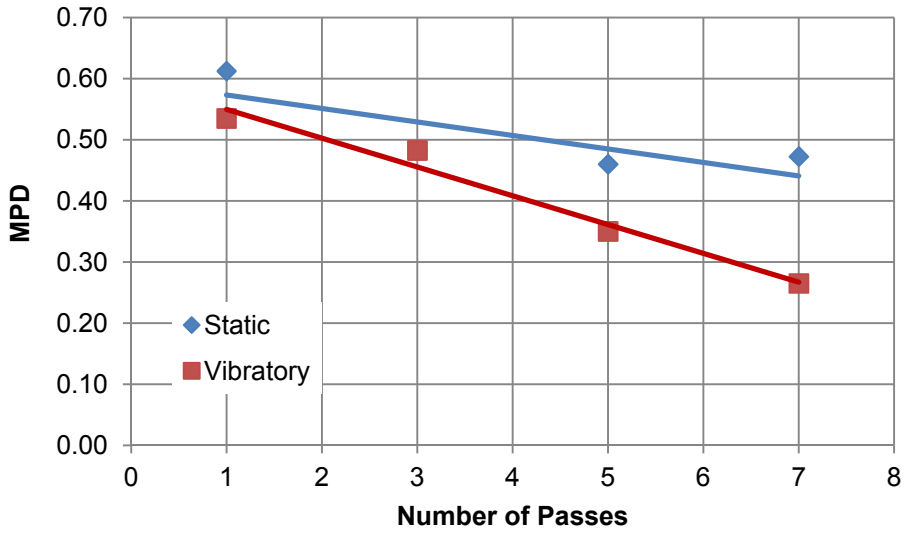

Figure 4-6. MPD vs. Number of Passes for Test Section 3

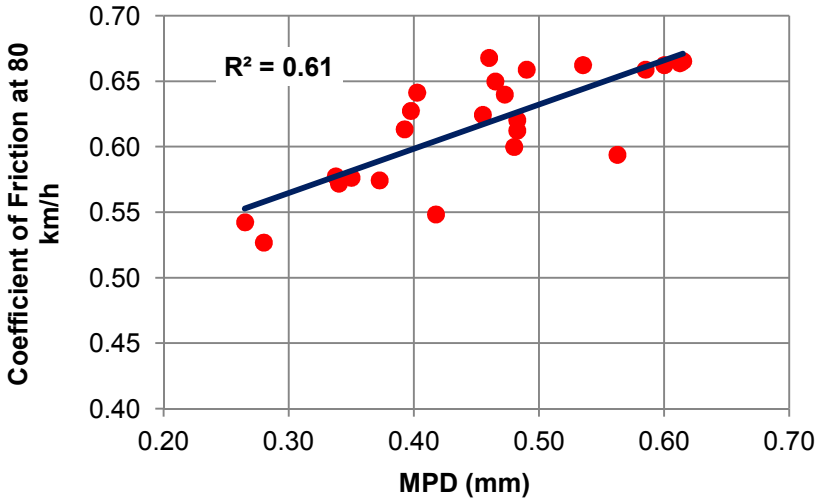

Figure 4-7. Coefficient of Friction at 80 km/h vs. MPD

The IFI calculated at the different number of passes is shown in Figure 4-8. The IFI decreased with the number of passes for all the test sections; however, the change in the IFI values were higher for the sub-test sections compacted using the static roller compared to the ones compacted using the vibratory roller in each test section. The vibratory roller was found to yield a smoother surface than the static roller. It was interesting to notice that the WMA test section had higher IFI values compared to the HMA test section. The HMA Type C test section had higher IFI compared to the HMA Type D. Type C is a coarser mixture than Type D.

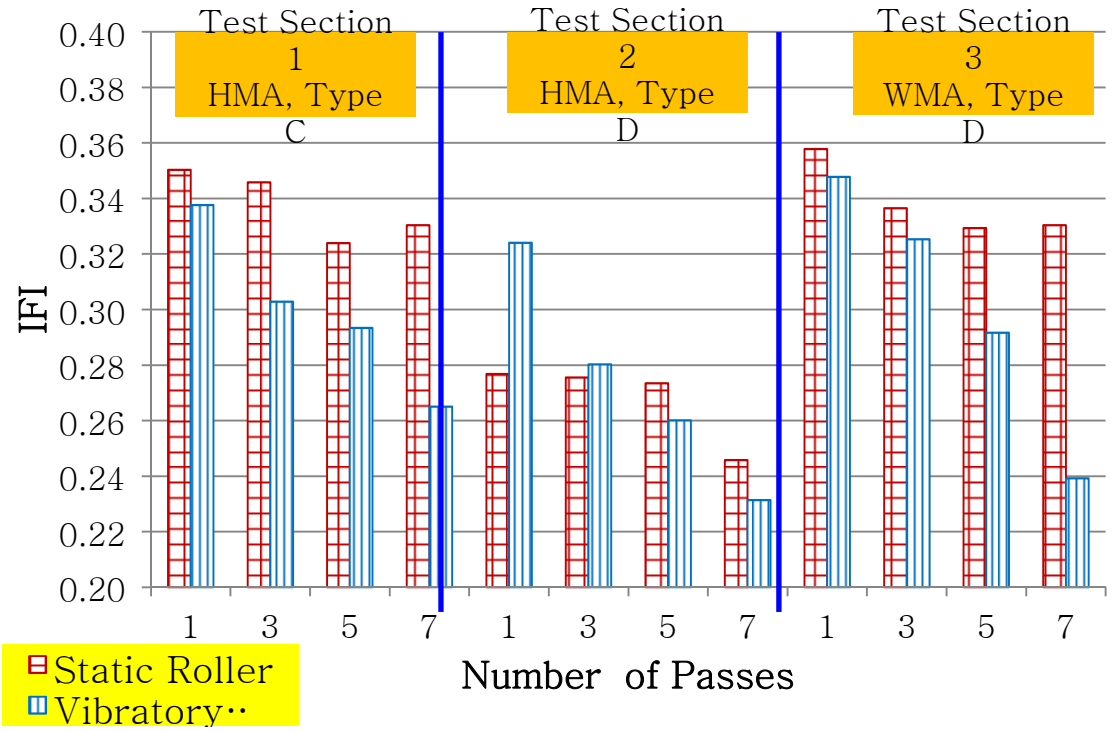

Figure 4-8. IFI vs. Number of Passes for the Test Sections

INTERNAL STRUCTURE ANALYSIS

In TxDOT Research Project 0-6692 (Kassem et al. 2012), the researchers recovered 14 field cores from each strip for density measurements and mechanical testing. Figure 4-9 shows an example of the coring layout across the width of the testing strips (7 ft wide). In this study, the researchers used the X-ray CT to examine the air void distribution across the depth. Two field cores were scanned using the X-ray CT. These cores were taken from the middle of the mat from test strips that were compacted using different numbers of roller passes (one pass, three passes, and seven passes). All the X-ray CT testing in this study was conducted using the X-ray CT system at the Advanced Characterization of Infrastructure Materials (ACIM) laboratory at Texas A&M University. The X-ray CT is a nondestructive technique used to visualize the internal structure of opaque objects. In this test, the test specimen is placed between the X-ray source and linear detector (Figure 4-10). The source sends out X-rays that penetrate the test specimen and reach the detector on the opposite side. An X-ray CT image is obtained after the test specimen completes a full rotation with respect to its center. The test specimen moves upward to take images at different locations across the depth. The researchers used Image-Pro® Plus software to

process the images and analyze the air void distribution. They developed macros to calculate the percent of air voids and the average radius of air voids across the depth of a specimen. For more information on the X-ray system, the reader is referred to Masad (2004) and Kassem, Walubita, et al. (2008).

Figure 4-9. Coring Layout

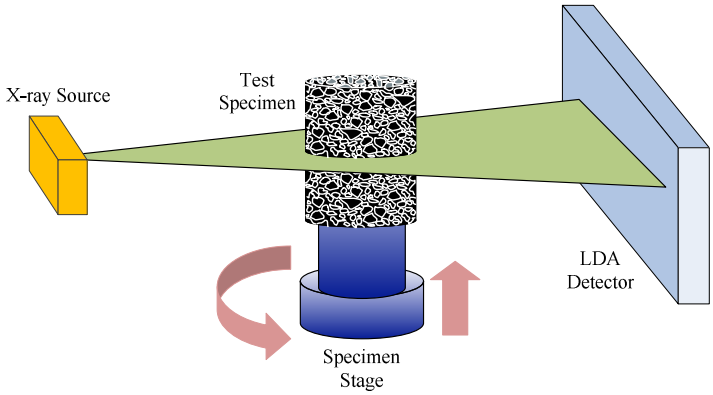

Figure 4-10. Schematic of X-Ray CT System

Figure 4-11 shows the air void distribution across the depth at different numbers of passes for the extracted field cores. The results showed clearly that the vibratory roller was more effective in reducing the air voids with the number of passes compared to the static roller. In addition, the percent air voids toward the top surface of the test sections compacted using the static roller didn't change with the number of passes but decreased significantly when the vibratory roller was used.

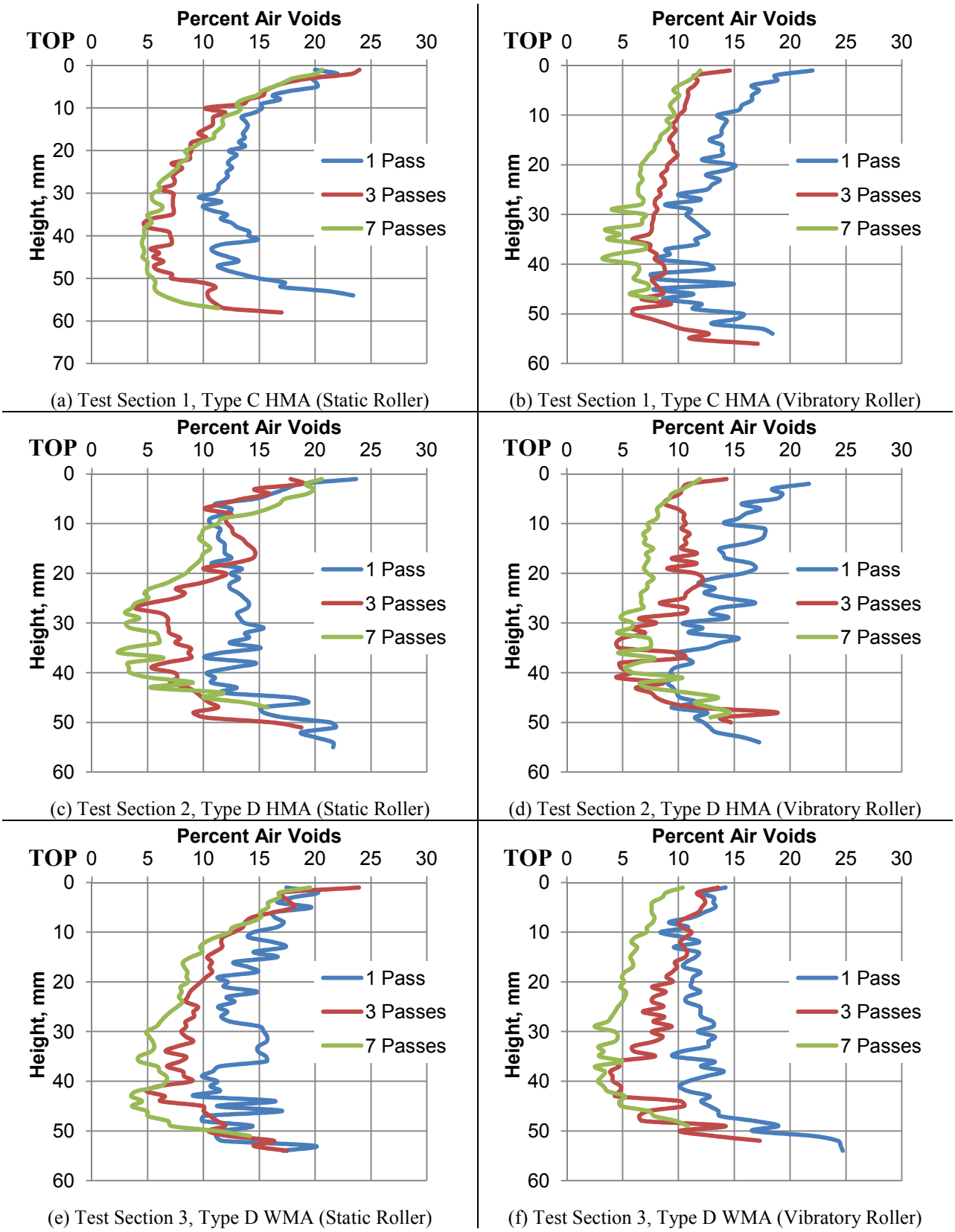

(a) Test Section 1, Type C HMA (Static Roller)

(b) Test Section 1, Type C HMA (Vibratory Roller)

(c) Test Section 2, Type D HMA (Static Roller)

(d) Test Section 2, Type D HMA (Vibratory Roller)

(e) Test Section 3, Type D WMA (Static Roller)

(f) Test Section 3, Type D WMA (Vibratory Roller)

Figure 4-11. Air Void Distribution across the Depth

Figure 4-12 shows an example of three-dimensional air void distributions with the number of passes in field cores extracted from test strips that were compacted using static and vibratory rollers. There was a higher percent air void at the top for the cores compacted using the static roller compared to the counterparts compacted using the vibratory roller. The higher percent air void toward the surface increases the MPD and hence yields higher IFI. This explains the reason that test sections compacted using the static roller had a higher IFI with less change with the number of passes than those compacted using the vibratory roller.

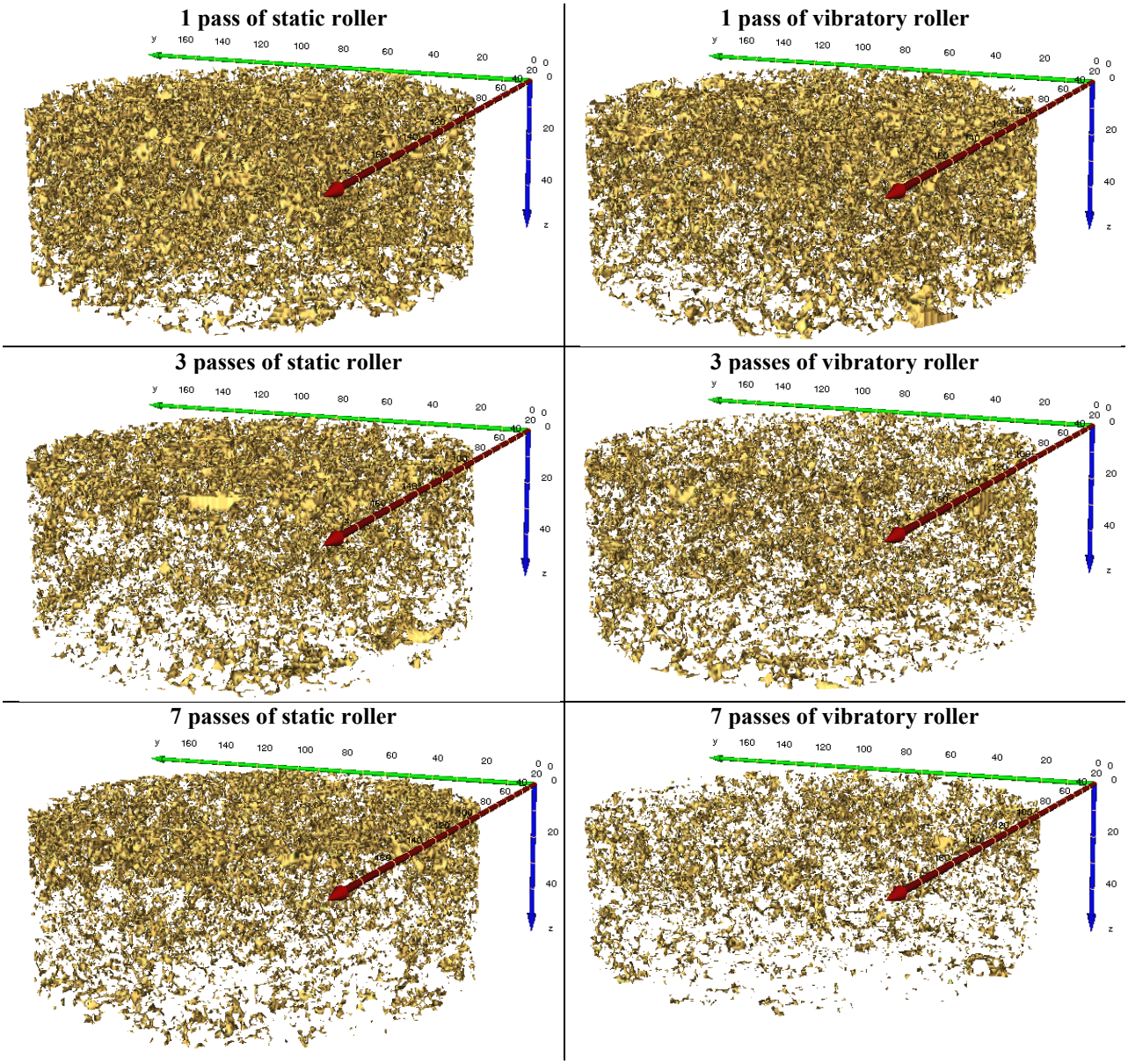

Figure 4-12. Three-Dimensional Air Void Distribution

The researchers studied the uniformity of the air void distribution in the top half of field cores by calculating an index called the uniformity index (UI). The UI is calculated using Equation (4-1), as follows:

1. Plot percent air voids *f(x)* against the core depth x.
2. Fit a fourth-order polynomial for *f(x)*.
3. Calculate the derivate $f'(x)$ of the function *f(x)*.
4. Calculate the UI using Equation (4-1).

$$UI = \frac{1}{b-a}\int_{a}^{b}[f'(x)]^2 dx \qquad (4\text{-}1)$$

Kassem, Masad, et al. (2008) found that the fourth-order polynomial to fit the percent air void functions very well. The UI is equal to zero for a straight-line function representing uniform distribution, and it increases with an increase in non-uniformity. The integration limits depend on the thickness over which the analysis is conducted for the top half (a = 0, b = h/2).

Figure 4-13 shows the UI for all test field cores. The UI for test sections compacted using the vibratory roller was less than the ones compacted using the static roller. This means that the air voids at the top half of the pavement were more uniform in the test section compacted using the vibratory roller compared to the static roller. Also, it is interesting to notice that the UI decreased with the number of the passes when the vibratory roller was used, while the UI increased with the number of passes when the static roller was employed, which means that the air void distribution at the top half of the pavement surface became more non-uniform. The findings of the X-ray analysis explained and correlated well with the skid results.

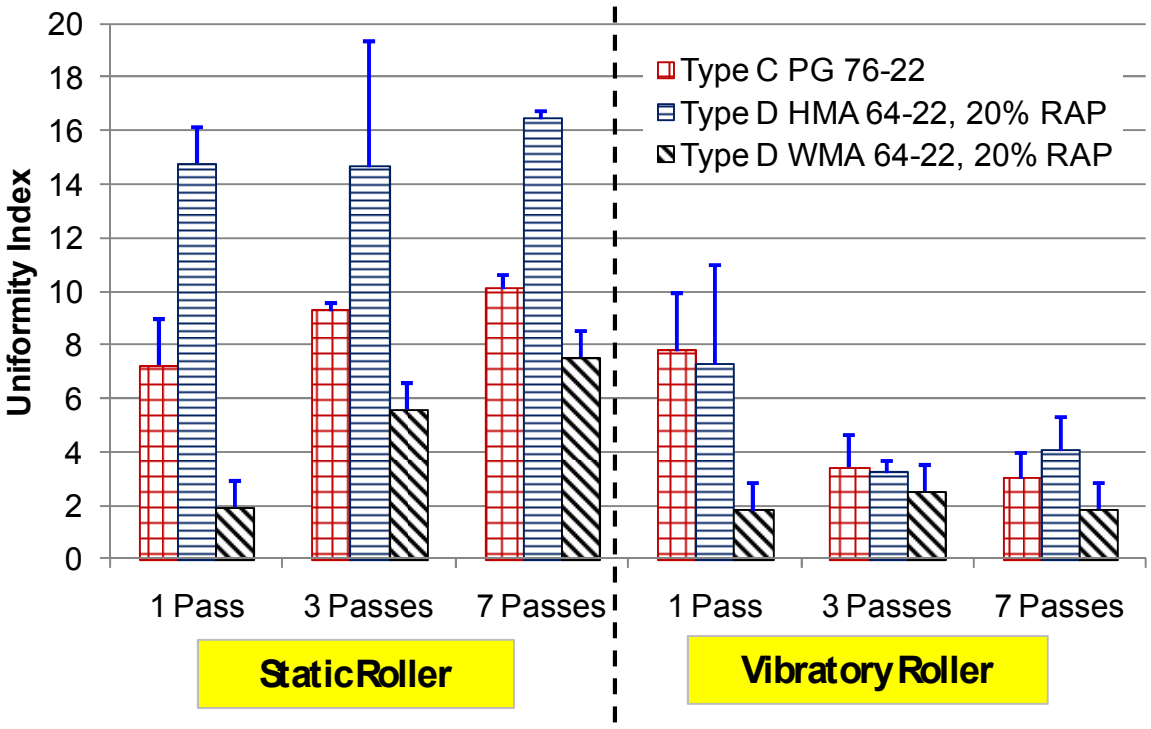

Figure 4-13. Uniformity Index at the Top Half of Field Cores

CONCLUSIONS

This part of the study evaluated the effect of compaction method and level of compaction on the skid resistance of asphalt pavements as well as the internal structure of the asphalt mixtures. The main findings for this part of the study are summarized as follows:

- The MPD, which is a measure of the macrotexture of pavement surface, decreased with the number of passes for the test sections compacted using both static and vibratory rollers.
- The change in the MPD for the test sections compacted using the vibratory roller was steeper compared to the corresponding test sections compacted using the static roller. The vibratory roller was found to yield a smoother surface than the static roller.
- The microtexture of pavement surface represented in the DFT_{20} measurements did not change with compaction levels as expected.
- A fair relationship between the MPD and the coefficients of friction at 80 km/h was found.

- The IFI decreased with the number of passes for all the test sections. However, the change in the IFI with the number of passes was higher for the sub-test sections compacted using the static roller compared to the ones compacted using the vibratory roller. Sub-test sections with low IFI were smoother than the ones with high IFI.
- Coarse mixtures had higher IFI compared to finer mixtures. In addition, WMA had higher IFI compared to HMA.
- The vibratory roller was more effective in reducing the air voids with the number of passes compared to the static roller.
- The percent air voids toward the top surface of the test sections compacted using the static roller didn't change with the number of passes but decreased significantly when the vibratory roller was used.
- Test sections compacted using the vibratory roller had more uniform air void distribution compared to test sections compacted using the static roller.

CHAPTER 5: CONCLUSIONS

This study aimed to develop prediction models for friction loss and laboratory compaction of asphalt mixtures. Chapter 1 presented the objectives and detailed work plan of this study. The study had three phases and eight main tasks. In the first phase, fundamental properties of the asphalt mixture constituents were evaluated. The AIMS was used to measure characteristics of the aggregates (texture, angularity) before and after the Micro-Deval abrasion test. In addition, the viscosity of the binders was determined at the compaction temperatures. In the second phase, the researchers conducted intensive laboratory experiments. They prepared and polished test slabs and measured the friction at the surface. In addition, they prepared laboratory SGC specimens and obtained compaction curves. They also took friction measurements on field test sections. In the third phase, the researchers developed predictive models for skid resistance and compactability based on the measured fundamental properties in the first phase and the collected experimental data in the second phase. In addition, they evaluated the effect of field compaction on skid resistance and internal structure of asphalt mixtures.

Chapter 2 discussed the preparation of the asphalt mixture slabs, the polishing procedure, and the development of friction loss model. The researchers prepared square-shaped laboratory asphalt mixture slabs (20 inches by 20 inches) using a linear kneading compactor. They utilized a wheel-polishing device to polish the test slabs. The CTMeter and DFT were used to measure the MPD coefficient of friction after each application of polishing cycles. A predictive model was developed for friction loss of asphalt mixtures based on inputs that described aggregate texture and angularity before and after polishing, aggregate gradation, and polishing cycles in the laboratory. The researchers found that mixtures with coarser aggregate gradation (PFC and SMA) had higher IFI, better skid resistance, than those with finer aggregate gradation (Type C and Type F). Aggregates with good resistance to abrasion and polishing had better skid resistance compared to aggregates with poor resistance to abrasion and polishing. The predictive model was found to correlate very well with the experimental measurements in the laboratory.

Chapter 3 discussed the development of a predictive model for laboratory compaction of asphalt mixtures. This model was developed based on parameters that described aggregate shape characteristics, aggregate gradation, binder content, and binder properties at compaction temperatures. The researchers executed intensive laboratory experiments to quantify the effect of

these parameters on the compaction of asphalt mixture in the laboratory. Two models that described slope and intercept of the laboratory compaction curves of asphalt mixtures were developed. The developed models showed strong correlations between the predicted values and the measured ones. These methods provide essential inputs for the methods that were developed by Kassem et al. (2012) to quantify the needed compaction effort to compact asphalt mixtures. Engineers can use these methods as a preliminary check on the compactability of an asphalt mixture based on its characteristics that include aggregate angularity and texture, aggregate gradation, binder content, and binder viscosity at compaction temperatures. They can modify the mixture design and materials to produce asphalt mixtures that don't require many roller passes to reach the target density in the field. However, further research is needed to validate both models of intercept and slope using mixes with different aggregate sources, different mix types, different binder types, and content.

Chapter 4 presented the effort by the researchers to evaluate the effect of compaction level and compaction method on skid resistance of asphalt pavements. In addition, they utilized the X-ray CT to study the influence of compaction method and level of compaction on the internal structure of asphalt mixtures. The researchers found that the MPD decreased with the number of passes for the test sections compacted using both static and vibratory rollers. However, the change in the MPD for the test sections compacted using the vibratory roller was steeper compared to the corresponding test sections compacted using the static roller. Similarly, the calculated IFI decreased with the number of passes for all the test sections, with a steeper change for the test sections compacted using the vibratory roller. The vibratory roller was found to yield a smoother surface than the static roller. In addition, the vibratory roller was more effective in reducing the air voids with the number of passes compared to the static roller. Moreover, the test sections compacted using the vibratory roller had more uniform air void distribution compared to test sections compacted using the static roller.

REFERENCES

AASHTO (2002). AASHTO Designation TP 58-00: *Standard Test Method for Resistance of Coarse Aggregate to Degradation by Abrasion in the Micro-Deval Apparatus*. AASHTO Provisional Standards, American Association of State Highway and Transportation Officials, Washington, D.C.

AASHTO (2004). AASHTO Designation TP 69-04: *Standard Method of Test for Bulk Specific Gravity and Density of Compacted Asphalt Mixtures Using Automatic Vacuum Sealing Method*. AASHTO Provisional Standards, American Association of State Highway and Transportation Officials, Washington, D.C.

AASHTO (2006). AASHTO Designation TP48-97: *Standard Method of Test for Viscosity Determination of Asphalt Binder Using Rotational Viscometer.* AASHTO Provisional Standards, American Association of State Highway and Transportation Officials, Washington, D.C.

AASHTO (2009). AASHTO Designation PP 60-09: *Preparation of Cylindrical Performance Test Specimens Using the Superpave Gyratory Compactor (SGC).* AASHTO Provisional Standards, American Association of State Highway and Transportation Officials, Washington, D.C.

AASHTO (2010). AASHTO Designation PP64-10: *Standard Practice for Determining Aggregate Source Shape Values from Digital Image Analysis Shape Properties.* AASHTO Provisional Standards, American Association of State Highway and Transportation Officials, Washington, D.C.

Al-Rousan, T.M. (2004), Characterization of Aggregate Shape Properties Using a Computer Automated System, *Ph.D. Dissertation*, Texas A&M University, College Station, Texas.

ASCE (2009). 2009 *Report Card for America's Infrastructure*. American Society of Civil Engineers, Reston, VA.

Asphalt Institute (2007). *The Asphalt Handbook: MS-4*, *7th Ed*. The Asphalt Institute, Lexington, KY

ASTM (2009a). ASTM Designation E2157: *Standard Test Method for Measuring Pavement Macrotexture Properties Using the Circular Track Meter.* American Society for Testing and Materials, Philadelphia, Pa.

ASTM (2009b). ASTM Designation E1911: *Standard Test Method for Measuring Paved Surface Frictional Properties Using the Dynamic Friction Tester*. American Society for Testing and Materials, Philadelphia, Pa.

ASTM (2011). ASTM Designation D2041: *Standard Test Method for Theoretical Maximum Specific Gravity and Density of Bituminous Paving Mixtures*. American Society for Testing and Materials, Philadelphia, Pa.

Bahia, H. U., T. P. Friemel, P. A. Peterson, J. S. Russell, and B. Poehnelt (1998). *Optimization of Constructability and Resistance to Traffic: A New Design Approach for HMA Using the Superpave Compactor*. Journal of the Association of Asphalt Paving Technologists, AAPT, Vol. 67, pp. 189-232.

Bloem, D. (1971). *Skid Resistance—The Role of Aggregates and Other Factors*. National Sand and Gravel Association Circular 109, Silver Spring, MD, pp. 1-30.

Crouch, L., J. Gothard, G. Head, and W. Goodwin (1995). *Evaluation of Textural Retention of Pavement Surface Aggregates*. Transportation Research Record 1486, Transportation Research Board, pp. 124-129, Washington, D.C.

Dahir, S. H. (1979). *A Review of Aggregate Selection Criteria for Improved Wear Resistance and Skid Resistance of Bituminous Surfaces*. Journal of Testing and Evaluation, JTEVA, Vol. 7, No. 5, pp. 254-253.

Davis, R. M., G. W. Flintsch, I. L. K. Al-Qadi, and K. McGhee (2002). *Effect of Wearing Surface Characteristics on Measured Pavement Skid Resistance and Texture*. Presented at 81st Transportation Research Board Annual Meeting, Washington, D.C.

FHWA (1990). *Nationwide Personal Transportation Survey*. NPTS Databook, FHWA-Report FHWA-PL-94-010, Federal Highway Administration, U.S. Department of Transportation.

Henry, J. J. (2000). *NCHRP Synthesis of Highway Practice 291: Evaluation of Pavement Friction Characteristics*. Transportation Research Board, National Research Council, Washington, D.C.

Henry, J. J., H. Abe, S. Kameyama, A. Tamai, A. Kasahara, and K. Saito (2000). *Determination of the International Friction Index Using the Circular Track Meter and the Dynamic Friction Tester*. Proceedings of SURF 2000, the World Road Association. Paris, France.

Hogervorst, D. (1974). *Some Properties of Crushed Stone for Road Surfaces*. Bulletin of the International Association of Engineering Geology 10, pp. 59-64.

Ivey, D. L., D. L. Bullard, J. R. Lock, and L. I. Griffin III (1992). *Texas Skid Initiated Accident Reduction Program: Final Report*. Report 910-1F, TTI: 2-18-89/910, TX-92/910-1F, Texas Department of Transportation.

Kandhal, P. S., and F. Jr. Parker (1998). *Aggregate Tests Related to Asphalt Concrete Performance in Pavements.* NCHRP Report 405, National Cooperative Highway Research Program, National Academy Press, Washington, D.C.

Kassem, E., E. Masad, A. Chowdhury, and G. Claros (2008). *Influence of Field Compaction Pattern on Asphalt Pavement Uniformity*. Journal of the Association of Asphalt Paving Technologists*,* AAPT, Vol. 77, pp. 257-298.

Kassem, E., T. Scullion, E. Masad, A. Chowdhury, W. Liu, C. Estakhri, and S. Dessouky (2012). *Practical Field Guidelines for the Compaction of HMA or WMA*. Technical Report Number 0-6992-2, Texas Transportation Institute, Texas A&M University, College Station, TX.

Kassem, E., L. Walubita, T. Scullion, E. Masad, and A. Wimsatt (2008). *Evaluation of Full Depth Asphalt Pavement Construction Using X-ray Computed Tomography and Ground Penetrating Radar*. Journal of Performance of Constructed Facilities, ASCE, Vol. 22. No. 6, pp. 408-416.

Leiva, F., and R. C. West (2008). *Analysis of Hot-Mix Asphalt Lab Compactability Using Lab Compaction Parameters and Mix Characteristics*. Transportation Research Record: Journal of the Transportation Research Board, No. 2057, pp. 89-98. Washington, D.C.

Luce, A. D. (2006). *Analysis of Aggregate Imaging System (AIMS) Measurements and Their Relationship to Asphalt Pavement Skid Resistance*. M.S.C.E Thesis, Texas A&M University, College Station, TX.

Mahmoud, E.M. (2005). *Development of Experimental Methods for the Evaluation of Aggregate Resistance to Polishing, Abrasion, and Breakage.* M.S. Thesis, Texas A&M University, College Station, TX

Mahmoud, E., and E. Masad (2007). *Experimental Methods for the Evaluation of Aggregate Resistance to Polishing, Abrasion and Breakage*. Journal of Materials in Civil Engineering, ASCE, Vol. 19, No. 11, pp. 977-985.

Mahone, D. C. (1975). *An Evaluation of the Effects of Tread Depth, Pavement Texture, and Water Film Thickness on Skid Number-Speed Gradients*. Virginia Highway and Transportation Research Council, Charlottesville, VA.

Masad, E. (2004). *X-ray Computed Tomography of Aggregates and Asphalt Mixes*. Materials Evaluation, Vol. 62, No. 7, pp. 775-783.

Masad, E., T. Al-Rousan, J. Button, D. Little, and E. Tutumluer (2005). *Test Methods for Characterizing Aggregate Shape, Texture, and Angularity*. NCHRP Project 4-30A Final Report, National Cooperative Highway Research Program, Washington, D.C.

Masad, E., S. Koneru, T. Scarpas, E. Kassem, and K. R. Rajagopal (2010). *Modeling of Hot-Mix Asphalt Compaction: A Thermodynamics-Based Compressible Viscoelastic Model. McLean*. VA: U.S. Dept. of Transportation, Federal Highway Administration, Research, Development, and Technology, Turner-Fairbank Highway Research Center & Texas Transportation Institute.

Masad, E., A. Luce, and E. Mahmoud (2006). *Implementation of AIMS in Measuring Aggregate Resistance to Polishing Abrasion and Breakage*. Texas Transportation Institute, Research Report 5-1707-03-1, Texas A&M University, College Station, TX.

Masad, E., A. Rezaei, and A. Chowdhury (2010). *Field Evaluation of Asphalt Mixture Skid Resistance and Its Relationship to Aggregate Characteristics.* Texas Transportation Institute, Research Report 09/0-5627-3, Texas A&M University, College Station, TX.

Masad, E., A. Rezaei, A. Chowdhury, and P. Harris (2009). *Prediction Asphalt Mixture Skid Resistance Based on Aggregate Characteristics*. Texas Transportation Institute, Research Report 09/0-5627-1, Texas A&M University, College Station, TX.McDaniel, R. S., and B. J. Coree (2003). *Identification of Laboratory Techniques to Optimize Superpave HMA Surface Friction Characterization*. Phase I: Final Report SQDH 2003-6, North Central Superpave Center, Purdue University, West Lafayette, IN.

Muras, A. J. (2010). *Prediction of Asphalt Mixture Compactability from Mixture, Asphalt, and Aggregate Properties*. Texas A&M University, College Station, TX.

NCAT (2011). *Using Lab Data to Predict the Field Compactability*. Hot Mix Asphalt Technology (HMAT), Vol. 16, No. 1, pp. 57-58.

Noyce, D. A., H. U. Bahia, J. M. Yambó, and G. Kim (2005). *Incorporating Road Safety into Pavement Management: Maximizing Asphalt Pavement Surface Friction for Road Safety Improvements*. Midwest Regional University Transportation Center Traffic Operations and Safety (TOPS) Laboratory.

Pine Instrument Company. (2011). *Aggregate Image Measurement System: Operation Manual*. Model AFA2A. Test Equipment Division, Grove City, PA.

Pine, W. J. (2004). *The Bailey Method: Achieving Volumetrics and HMA Compactability*. Indianapolis, IN: Heritage Research Group.

Roberts, F., P. Kandhal, E. R. Brown, D. Lee, and T. Kennedy (1991). *Hot Mix Asphalt Materials, Mixture Design and Construction*. National Asphalt Pavement Association, Research and Education Foundation, Lanham, MD.

Smith, H. (1976). *Pavement Contributions to Wet-Weather Skidding Accident Reduction*. Transportation Research Record 622, Transportation Research Board, TRB, National Research Council, Washington, D.C.

Texas Department of Transportation (2004). *Standard Specifications for Construction and Maintenance of Highways, Streets, and Bridges.* TxDOT, Austin, TX.

U.S. Army Corps of Engineers (2000). *Hot-Mix Asphalt Paving Handbook.* Washington, DC.

Vollor, T.W., and D.I. Hanson (2006). *Development of Laboratory Procedure for Measuring Friction of HMA Mixtures – Phase I*. NCAT Report 06-06, National Center for Asphalt Technology, Auburn, Al.

Wambold, J. C., C. E. Antle, J. J. Henry, and Z. Rado (1995). *International PIARC Experiment to Compare and Harmonize Texture and Skid Resistance Measurement*. PIARC (Permanent International Association of Road Congress) Report, C-1 PIARC Technical Committee on Surface Characteristics, France.